2021

Evaluating The Efficacy Of Prone Position And Therapeutic Treatments In Ards Lungs Using Computed Tomography

Yi Xin
University of Pennsylvania

Evaluating The Efficacy Of Prone Position And Therapeutic Treatments In Ards Lungs Using Computed Tomography

Abstract

Acute respiratory distress syndrome (ARDS) is a condition of rapid onset hypoxemia, pulmonary edema and collapse resulting from inflammatory lung injury, often requiring mechanical ventilation to avoid immediate death. Yet ventilator-induced lung injury (VILI) can also worsen ARDS progression. Developing and refining strategies to reduce VILI requires a thorough understanding of its mechanisms of onset and propagation. The main objective of this project is to develop computed tomography (CT)-based markers capable of predicting injury progression in ARDS, and to use these markers to test the efficacy of prone position ventilation in combination with therapeutic treatment (Imatinib) in ameliorating this progression.Early ventilation in the prone position improves blood gases and decreases mortality in ARDS, but the efficacy of prone positioning may change between early and later stages of injury. Furthermore, baseline characteristics of the primary injury may influence therapeutic response. Understanding the interaction between injury progression and prone positioning's efficacy may help to target the patients who will benefit most from this therapy and could also help to refine both its timing and indications. Through a series of experiments porcine models of lung injury and patients with acute respiratory distress syndrome (ARDS), we found that the effects of prone positioning on lung aeration may depend on both the stage of lung injury and duration of prior ventilation—potentially limiting the clinical efficacy of this treatment if applied late. Restoring or protecting the endothelial barrier could minimize vascular damage in highly perfused tissue. Imatinib, a tyrosine kinase inhibitor used to treat chronic myelogenous leukemia, reduces injury severity in pre-clinical ARDS models as well as pulmonary leak index in clinical ARDS patients by inhibiting the Abl-related gene as well as related kinases and platelet-derived growth factor receptor (PDGFR), which are important in maintaining endothelial integrity. Our results using sequential CT scans showed that Imatinib mitigated lung injury in mechanically ventilated rats and reduced mortality while delaying functional and radiological injury progression. Imatinib also attenuated edema (lung tissue mass on CT) and capillary leak (BAL protein concentration), and treated animals displayed fewer histological and biological markers of inflammatory lung injury.

Degree Type

Dissertation

Degree Name

Doctor of Philosophy (PhD)

Graduate Group

Bioengineering

First Advisor

Rahim R. Rizi

Second Advisor

Maurizio Cereda

Keywords

ARDS, CT, Lung Imaging, Lung Injury

EVALUATING THE EFFICACY OF PRONE POSITION AND THERAPEUTIC TREATMENTS IN ARDS LUNGS USING COMPUTED TOMOGRAPHY

Yi Xin

A DISSERTATION

in

Bioengineering

Presented to the Faculties of the University of Pennsylvania

in

Partial Fulfillment of the Requirements for the

Degree of Doctor of Philosophy

2021

Supervisor of Dissertation

_____

Rahim R. Rizi, Ph.D. Professor of Radiology

Graduate Group Chairperson

_____

Yale E. Cohen, Ph.D. Professor of Bioengineering

Dissertation Committee

_____

Maurizio Cereda, M.D. Associate Professor of Anesthesiology and Critical Care
Associate Professor of Radiology

Jason D. Christie, M.D. Professor of Medicine

Stephen Kadlecek, Ph.D. Associate Professor of Radiology

EVALUATING THE EFFICACY OF PRONE POSITION AND THERAPEUTIC TREATMENTS IN ARDS LUNGS USING COMPUTED TOMOGRAPHY

ACKNOWLEDGMENTS

First and foremost, I wish to thank my advisor, Dr. Rahim Rizi, for his mentorship and continued support throughout my graduate studies; his guidance was invaluable in helping me to realize the goals of this research project, and he served as a great source of inspiration and enthusiasm.

I am also truly indebted to Dr. Maurizio Cereda for his willingness to patiently share his knowledge and experience with me, and for all the effort he spent revising my papers. I would additionally like to thank Dr. Stephen Kadlecek for his guidance and support over the past decade.

I am grateful to all of my colleagues in the Functional and Metabolic Imaging Group, whose camaraderie and support during my graduate studies were invaluable: Mr. Hooman Hamedani, Dr. Kiarash Emami, Dr. Mehrdad Pourfathi, Dr. Sarmad Siddiqui, Mr. Harrilla Profka, Dr. Paolo Delvecchio, Dr. Kai Ruppert, Dr. Xiaoling Jin, Mr. Faraz Amzajerdian, Dr. Ian Duncan, and many other colleagues and undergraduate students I have worked with.

I would of course like to thank my thesis committee member—Dr. Jason Christie—for taking the time to provide me with insightful feedback that challenged my thinking and greatly improved the quality of this project.

Lastly, I would like to express my deepest gratitude to my wife, Wenli Sun, and my sons, Daniel and Tyson Xin, for giving me unlimited happiness, as well as my parents, my grandmother and the rest of my family and friends. Their love, support and patience through the years allowed me to focus on and complete my graduate studies.

ABSTRACT

EVALUATING THE EFFICACY OF PRONE POSITION AND THERAPEUTIC TREATMENTS IN ARDS LUNGS USING COMPUTED TOMOGRAPHY

Yi Xin

Rahim R. Rizi

Acute respiratory distress syndrome (ARDS) is a condition of rapid onset hypoxemia, pulmonary edema and collapse resulting from inflammatory lung injury, often requiring mechanical ventilation to avoid immediate death. Yet ventilator-induced lung injury (VILI) can also worsen ARDS progression. Developing and refining strategies to reduce VILI requires a thorough understanding of its mechanisms of onset and propagation. The main objective of this project is to develop computed tomography (CT)-based markers capable of predicting injury progression in ARDS, and to use these markers to test the efficacy of prone position ventilation in combination with therapeutic treatment (Imatinib) in ameliorating this progression.

Early ventilation in the prone position improves blood gases and decreases mortality in ARDS, but the efficacy of prone positioning may change between early and later stages of injury. Furthermore, baseline characteristics of the primary injury may influence therapeutic response. Understanding the interaction between injury progression and prone positioning's efficacy may help to target the patients who will benefit most from this therapy and could also help to refine both its timing and indications. Through a series of experiments porcine models of lung injury and patients with acute respiratory distress syndrome (ARDS), we found that the effects of prone positioning on lung aeration may

depend on both the stage of lung injury and duration of prior ventilation—potentially limiting the clinical efficacy of this treatment if applied late.

Restoring or protecting the endothelial barrier could minimize vascular damage in highly perfused tissue. Imatinib, a tyrosine kinase inhibitor used to treat chronic myelogenous leukemia, reduces injury severity in pre-clinical ARDS models as well as pulmonary leak index in clinical ARDS patients by inhibiting the Abl-related gene as well as related kinases and platelet-derived growth factor receptor (PDGFR), which are important in maintaining endothelial integrity. Our results using sequential CT scans showed that imatinib mitigated lung injury in mechanically ventilated rats and reduced mortality while delaying functional and radiological injury progression. Imatinib also attenuated edema (lung tissue mass on CT) and capillary leak (BAL protein concentration), and treated animals displayed fewer histological and biological markers of inflammatory lung injury.

TABLE OF CONTENTS

LIST OF TABLES

LIST OF FIGURES

LIST OF ABBREVIATIONS

ARDS	Acute respiratory distress syndrome
CT	Computed tomography
VILI	Ventilator induced lung injury
HU	Hounsfield units
EI	End-inspiratory
EE	End-expiratory
PRM	Parametric response map
V_T	Tidal volume
PEEP	Positive end-expiratory pressure
C_{dyn}	Dynamic compliance
PaO_2	Partial pressure of oxygen
$PaCO_2$	Partial pressure of carbon dioxide
FiO_2	Fraction of inspired oxygen
PIP	Peak inspiratory pressure

CHAPTER 1: INTRODUCTION

1.1. Acute Respiratory Distress Syndrome (ARDS)

Acute respiratory distress syndrome (ARDS) is characterized by widespread inflammation with heterogeneous inflation of the lungs, subsequent development of edema, and impaired gas exchange[1]. ARDS is a serious public health problem which, according to the most recent epidemiologic report, accounts for more than 75,000 deaths annually in the United States[2]. Mortality of severe ARDS is over 40%[3] and drives mortality in SARS-COV2 pneumonia[4]; its incidence is about 10% in patients admitted to the intensive care unit, and it can be triggered by several common disorders such as pneumonia, acid aspiration, sepsis, trauma and ventilator induced lung injury[3]. Since it was first described and characterized exactly fifty years ago[5], the lack of a standardized definition of ARDS[6] has posed arguably the biggest obstacle to its treatment. While the largely accepted Berlin definition defines the syndrome as presenting with impaired oxygenation and bilateral infiltration on chest x-ray, it has also been extensively criticized. The two main objections are that: 1) the measurement of hypoxemia is treatment dependent, so that patients with different ventilation settings can fulfill different oxygenation criteria[7]; 2) the chest radiograph is subjective, inaccurate, and unreliable due to variability in readers' knowledge[8]. Unfortunately, these shortcomings hamper personalized patient management and informed enrollment into clinical trials[9].

1.2. Ventilator Induced Lung Injury

In order to prevent immediate death, ARDS patients often require prolonged mechanical ventilation. Yet ventilator-induced lung injury (VILI) can worsen injury progression[10,11],

as injured lungs are particularly sensitive to ventilator-induced stretch[10]. Developing and refining strategies to reduce VILI requires a thorough understanding of the mechanisms through which VILI develops.

1.3. Prone Position Ventilation

Prone ventilation improves oxygenation and decreases mortality in severe ARDS when implemented within 72 hours of disease onset[12,13]. Imaging studies suggest that redistribution of lung inflation along the gravitational axis may explain these beneficial effects. In fact, pulmonary aeration[14], pleural pressures[15] and regional strain[16,17] are all more homogeneous when subjects are prone rather than supine due to the apparent attenuation of the gravity-related forces that compress and deform the lungs[18]. Yet clinicians often defer positional therapy and attempt other strategies—e.g. higher PEEP or inhaled vasodilators to improve oxygenation—neither of which consistently improve long-term survival in ARDS patients[19,20]. Prioritizing oxygenation therapies and neglecting protective ventilation strategies may delay the initiation of positional therapy and hasten disease progression, thus losing the beneficial effects of early pronation. Understanding the interaction between injury progression and prone positioning's efficacy may help to refine the timing and indications of this therapy, as well as to target those patients most likely to benefit from it.

1.4. Pharmacological Treatments of ARDS

Drug treatments that address the pathogenesis of the primary injury process in ARDS, such as steroids[21], statins[22] and a variety of anti-inflammatory agents, have failed to show clear outcome benefits when tested in clinical trials. Our inability to find effective ARDS

treatments is likely related to the diverse mechanisms of injury and the heterogeneity of therapeutic responses that are common in this syndrome. Restoring or protecting the endothelial barrier could minimize vascular damage in highly perfused tissue. Imatinib, a tyrosine kinase inhibitor used to treat chronic myelogenous leukemia, reduces injury severity in pre-clinical ARDS models[23,24] as well as pulmonary leak index in patients[25]. Imatinib inhibits the Abl-related gene as well as related kinases and platelet-derived growth factor receptor (PDGFR), which are important in endothelial integrity[24,26].

1.5. Quantitative Computed Tomography

Computed tomography represents thoracic structures in three dimensions; it refines the morphologic assessment of lung aeration in ARDS and, combined with quantitative analysis of regional tissue density, accurately measures the severity of lung injury[27]. Recent advances in image processing yield spatial resolution approaching the acinar level and provide detailed maps of regional ventilation and lung stretch[28]. Quantitative analysis of CT (qCT) images can serve as a valuable method for assessing ARDS, as qCT can quantify various aspects of ARDS pathophysiology—including injury severity, degree of atelectasis and over-distension, and regional heterogeneity of lung mechanics.

1.6. Objective and Specific Aims

The overall goal of this project is to develop and implement longitudinal quantitative CT markers to

1. Visualize and predict the propagation of acute lung injury in rats

2. Evaluate the effect of prone ventilation on lung inflation and recruitment in late vs. early stages of lung injury
3. Test the efficacy of imatinib in preventing dissemination of edema after initial lung injury

1.7. Thesis Organization

The remainder of this dissertation is organized as follows:

Chapter 2 provides visual evidence of the spatial propagation of VILI using sequential CT. In the presence of pre-existing injury, propagation begins in regions of primary injury and spreads concentrically. Injury propagation is predicted by lung strain, which could help quantify the risk of ARDS progression.

Chapter 3 develops a set of super superimposed inspiratory–expiratory CT scans using deformable image registration to predict lung injury progression and outcome in both preclinical and human ARDS.

Chapter 4 shows that prone positioning limits the radiologic progression of early lung injury. Minimizing unstable inflation (developed from Chapter 3) in this setting may alleviate the burden of acute respiratory distress syndrome.

Chapter 5 further improves our registration pipeline to accurately align supine and prone images at the voxel level. The evidence shows that lung reinflation and recruitment by prone positioning were primarily localized in the dorso-caudal lung. The local effects of positioning in this lung region may determine its clinical efficacy.

Chapter 6 tests the efficacy of prone position ventilation in early vs. late injury. Results support the hypothesis that evolving lung injury is characterized by a time-dependent loss of aeration response to prone positioning in the posterior lung. This deterioration probably contributes to variability in responses to positional therapy, and might undermine the clinical outcome benefits of this treatment.

Chapter 7 tests the hypothesis that imatinib mitigates lung injury in mechanically ventilated rats. Results support this hypothesis and show that: 1) Imatinib reduced mortality while delaying functional and radiological injury progression; 2) Imatinib attenuated edema (increase of lung tissue mass on CT) and capillary leak (BAL protein concentration); 3) Treated animals had fewer histological and biological markers of inflammatory lung injury.

Finally, *Chapter 8* summarizes the key findings of this project. A number of planned future studies are outlined, including imaging lung perfusion using dual energy CT for a more comprehensive evaluation of lung function. We also plan to test imatinib's efficacy in preventing ischemia reperfusion injury after lung transplant in rats.

CHAPTER 2: VISUALIZING THE PROPAGATION OF ACUTE LUNG INJURY

This chapter has been adapted from the published article, Cereda M, Xin Y, Meeder N, Zeng J, Jiang Y, Hamedani H, Profka H, Kadlecek S, Clapp J, Deshpande CG, Wu J, Gee JC, Kavanagh BP, Rizi RR. Visualizing the Propagation of Acute Lung Injury. Anesthesiology 2016;124:121–31. https://doi.org/10.1097/ALN.0000000000000916.

2.1. Introduction

Mechanical ventilation at lower tidal volume (V_T) has been shown to improve survival in acute respiratory distress syndrome (ARDS)[7], suggesting that V_T reduction protects against ventilator induced lung injury (VILI) by reducing inspiratory strain. To best limit damage, it might be important to detect early changes in vulnerable lung and to accurately determine the propensity for VILI. However, the onset of VILI is poorly characterized in the clinical setting, and it is almost always superimposed upon an underlying primary pulmonary lesion (e.g. aspiration, pneumonia, contusion)[29].

Computed tomography (CT) suggested that ARDS lung is composed of an atelectatic (dependent) region and a normally aerated (non-dependent) region[30]. In this two-compartment model, the aerated 'baby' lung preferentially receives the bulk of each V_T, but comprises a significantly smaller available volume than the lungs in a healthy subject. Because inflammation predominates in this 'aerated' region[31,32], measuring strain and visualizing the propagation of lung injury in the aerated lung could predict and characterize the trajectory of VILI.

In this study, we used sequential CT to investigate the relationship between the spatial distribution of aerated/non-aerated lung vs. the tendency of injury to propagate during mechanical ventilation. In an in-vivo rat model of acid aspiration with variable injury

trajectory, we sought predictors of its propagation. We hypothesized that secondary VILI originates adjacent to the primary lesions—due to the local diffuse intermingling of aerated and collapsed tissue—and propagates concentrically and in proportion to strain. Such a pattern was contrasted with observations in lungs that were free of pre-existing injury, where VILI has been shown to originate in the lung periphery[33] and, in the setting of the 'baby lung' appears to become generalized across the normally aerated lung tissue.

2.2. Methods

We studied 20 ventilated rats (353±26 g) after hydrochlocic acid (HCl 2.5 ml/kg, pH 1.25) intratracheal. Rats were immediately returned to the supine position after acid induction and allowed to stabilize while ventilated with PEEP 10 cm H_2O and V_T 6 ml/kg for 1 h. After stabilization, ventilation continued for 3 h with moderate V_T (12 ml/kg, PEEP 3 cmH_2O, FiO_2 1.0, f 53 min^{-1}).

High-resolution whole-lung CT scans were acquired and reconstructed to three-dimensional whole lung maps with 200 μm isotropic resolution. Imaging was ventilator-gated and performed during 500-ms breath-holds. For quantitative CT analysis, 3-D whole-lung regions of interest were obtained by semi-automated, multi-landmark, registration-based lung segmentation methodology (the delineation of lung borders from surrounding structures) developed by the authors[34]. Using established methods 15 of CT density analysis, each voxel was partitioned in air and tissue, allowing to quantify lung weight, end-inspiratory, and end-expiratory lung gas volumes (EILV, EELV); lung strain was defined as V_T/EELV.

2.3. Results

In the 15 rats that survived longer than 2h, baseline (i.e. post-aspiration) CT demonstrated circumscribed lesions in the dorsal lung. Two radiological patterns of injury were observed in this cohort: 'diffuse' (Propagated; Figure 2.1, A), and Contained (Figure 2.1, B).

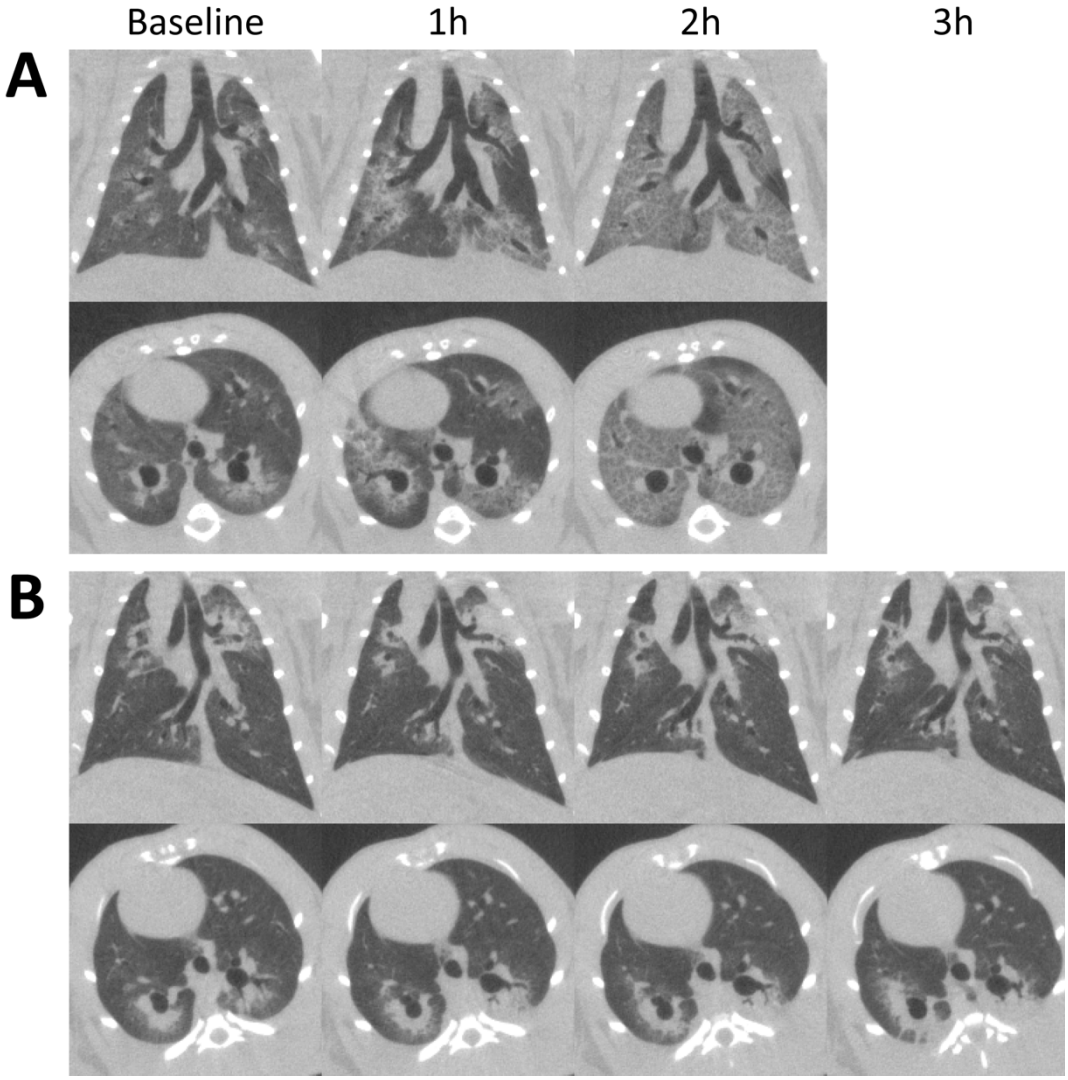

Figure 2.1 Radiological injury propagation in two representative rats. Images were obtained after acid aspiration (following a period of stabilization of one hour) and were repeated hourly. Coronal (A) and axial (B) images are shown. One animal (top panel) showed rapidly spreading

radiological infiltrates and died after two hours of ventilation. The second animal (bottom panel) had limited injury propagation and survived until the end of the experiment.

Propagation vs. Containment — Five animals (5/6) died in the Propagation subgroup vs. none (0/9) in the Containment subgroup. While the overall injury scores were similar in both groups at baseline, the injury was considerably increased (≈4-fold) in the Propagation group at 2 h and minimally increased in the Containment group EELV was significantly lower in the propagation cohort. At baseline, there was no overlap of the individual lung strain values between the two groups, but there was considerable overlap in PaO_2 and compliance (Figure 2.2., A-C).

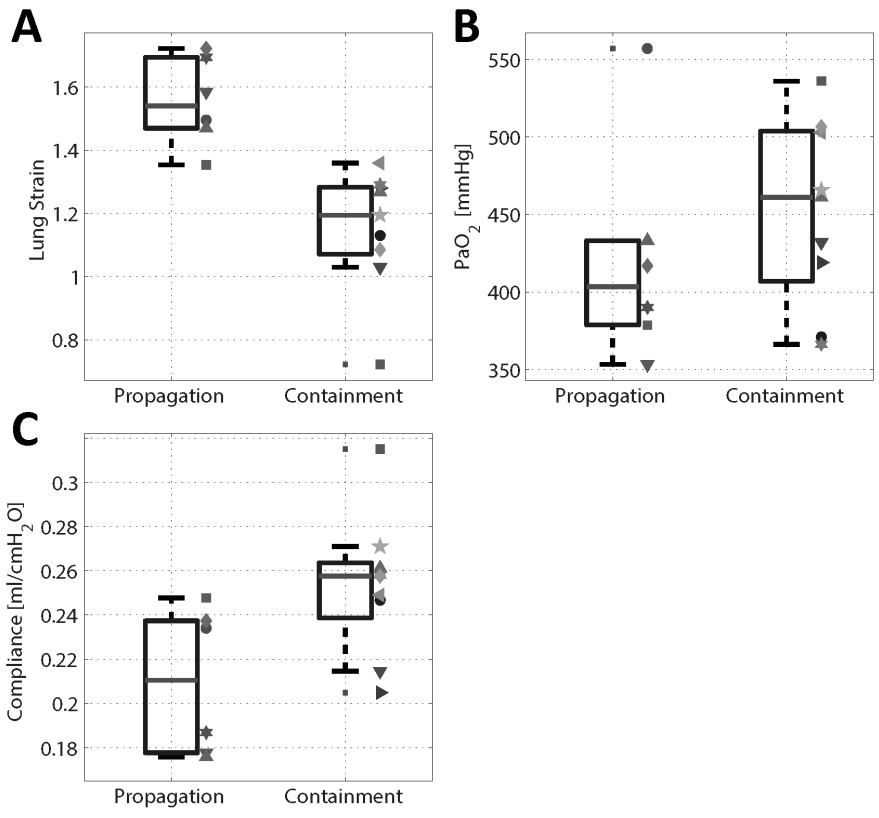

Figure 2.2 Individual baseline values and summary statistics (median, interquartile range, and extremes of the distribution) of: a) Lung Strain, b) Compliance, and c) PaO_2 in rats that had progression vs. containment of lung injury while receiving moderate volume ventilation following acid aspiration.

2.4. Discussion

Our key finding is the nature of VILI propagation in the presence or absence of an underlying (primary) lesion. When VILI complicated a pre-existing lesion, it started at that lesion and was propagated concentrically toward the rest of the lung. Furthermore, we found that while impaired oxygenation was not a predictor of injury propagation in pre-injured animals, strain predicted propagation in both cohorts. These findings suggest that it may ultimately be possible to predict (and perhaps prevent) propagation of injury and thereby minimize its generalization.

The results of this study have two potential implications for the eventual management of patients with early lung injury. First, studying the spatial propagation of lung injury might facilitate the investigation of containment strategies. In contrast, studying established ARDS clouds understanding about the condition's initial evolution. Moreover, clinical definitions[35] omit the evolving distribution of injury which may be especially important in ARDS that presents with non-diffuse injury[36]. Second, our work is consistent with other studies emphasizing that protecting injured lungs from excessive strain is essential to mitigating ARDS[37]. To reduce strain, clinicians prescribe V_T according to a patient's predicted body weight. However, recent studies have highlighted that severely ill patients have smaller lung capacities[38] and are at risk of VILI even with smaller V_T[39]. Global lung

strain can be measured at bedside with non-radiological instruments[40], although regional stress distribution is missed[41]. Our work extends the relevance of strain to less severe injury, where lung capacity is preserved. This may be relevant in low-VT ventilation in patients without established ARDS[42], though we note that generalized use of low VT can have undesired consequences such as atelectasis[43] and patient discomfort[44].

Risk of propagation after HCl was not related to oxygenation. This suggests that baseline PaO_2/FiO_2 measurement has only a limited ability to characterize early lung injury and to predict its evolution. The hypoxemia that reflects severity in ARDS[35] is perhaps the end-result of complex maldistributions of ventilation and blood flow rather than a marker of injury progression. Within this context, pulmonary strain may be a more pertinent measurement for characterizing individual risk of ARDS progression.

CHAPTER 3: TIDAL CHANGES ON CT AND PROGRESSION OF ARDS

This chapter has been adapted from the published article, Cereda M, Xin Y, Hamedani H, Bellani G, Kadlecek S, Clapp J, Guerra L, Meeder N, Rajaei J, Tustison NJ, Gee JC, Kavanagh BP, Rizi RR. Tidal changes on CT and progression of ARDS. *Thorax* 2017;**72**:981–9. https://doi.org/10.1136/thoraxjnl-2016-209833.

3.1. Introduction

Secondary lung injury initiated by tidal inflation worsens outcome of acute respiratory distress syndrome (ARDS)[7]. However, because consensus criteria for ARDS select populations of patients with heterogeneous characteristics, predicting the effect of mechanical ventilation on injury trajectory is difficult[45].

Diagnosis of ARDS[35] is largely based on plain (2-dimensional) chest radiography. A major advance came with the characterization by computed tomography (CT), of the ventral "baby lung"[46], which provided the rationale for use of low tidal volume[7] and prone positioning[12]. Quantitative study of ARDS using CT has been mostly limited to large regions of lung[47], with limited analysis of inflation at very high resolution[41].

An alternative approach to pulmonary CT analysis pairs individual voxels in end-inspiratory (EI) and end-expiratory (EE) images, and images are warped in order to superimpose anatomical structures which may be distorted by respiration or disease progression[34,48]. This approach permits detection of hyperinflation (low EI density) and air trapping (low EE density) in emphysematous lungs that is not otherwise detectable[49]. We previously reported that the spatial propagation of experimental lung injury was driven by tidal inflation[50], and therefore hypothesized that in early acute lung injury, areas of lung

with unstable inflation (detected by superimposed EI and EE CT scans) are 'at risk' for injury progression.

We first characterized the analysis of paired EI-EE CT scans in laboratory experiments (anesthetized rats). We then used serial CT scans in rats and confirmed that areas of lung with the greatest differences in paired EI-EE aeration at baseline (potentially representing atelectrauma and local strain) corresponded to the areas of maximum progression of injury. Finally, we used paired EI-EE CT images from a small group (n=9) of patients with ARDS who were studied early in their disease, and found that EI-EE aeration was associated with survival.

3.2. Methods

Animal Preparation: The experiments were performed on male Sprague-Dawley rats (n=73) following a protocol approved by the local Institutional Animal Care and Use Committee, fully described in our previous work[50]. Following general anesthesia and intubation, hydrochloric acid (HCl, pH 1.25) was injected into the trachea, followed by stabilization for one hour and mechanical ventilation for up to four hours (or until death). To increase variability of injury progression, animals received ranges of HCl doses (1-4 ml/kg), and were ventilated with one of several options (not randomized) of positive end-expiratory pressure (PEEP, 3-10 cmH_2O), and tidal volume (V_T, 6-12 ml/kg). In a preliminary analysis, these strategies were aggregated for overall comparison into two groups with higher vs. lower propensity to injury progression: one group ventilated non-protective settings and one receiving protective ventilation. Gas exchange, peak inspiratory

pressure (PIP), driving pressure, mechanical power of inspiration, and dynamic compliance (C_{dyn}) were monitored.

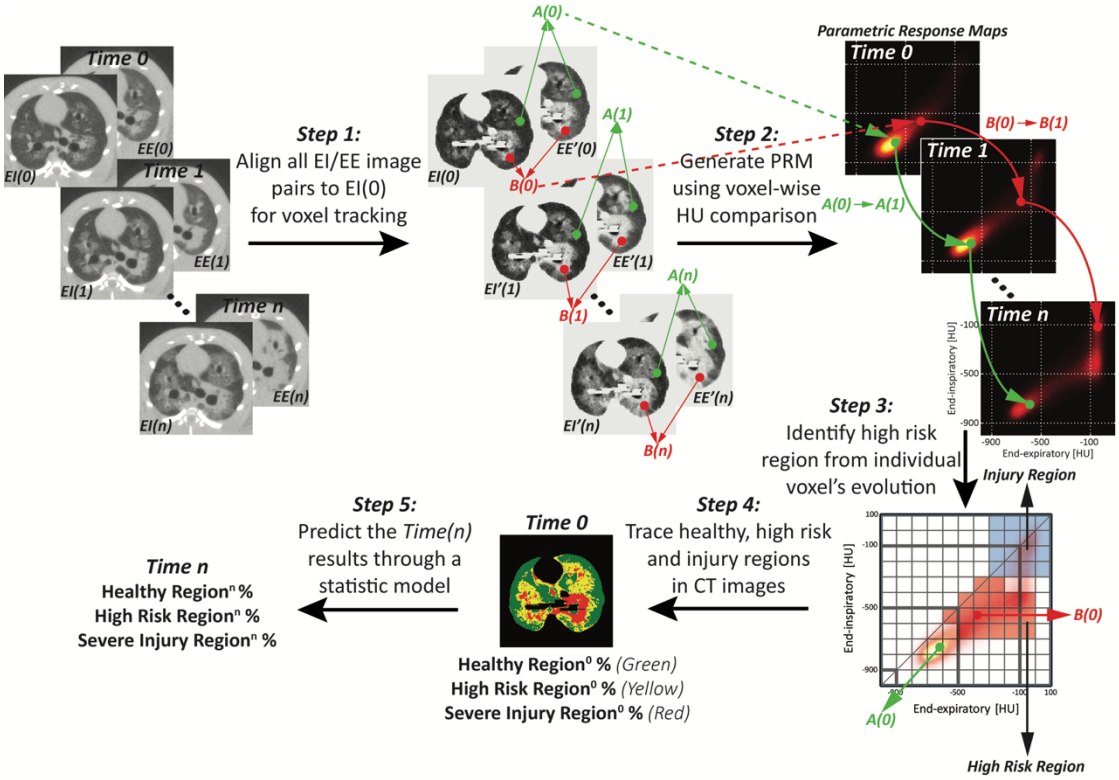

Figure 3.1 General workflow of the methodology used to spatially correlate unstable inflation with later injury progression in rats ventilated after acid aspiration. *Step 1:* all EI and EE image pairs are superimposed on each other and aligned to the first EI image (time 0) following acid aspiration: EI(0). Then, the outline of the lungs is separated from surrounding non-pulmonary tissue. Because all images are superimposed, each individual voxel (see points A and B as an example) can be tracked in EI/EE image pairs and longitudinally over time. *Step 2:* plotting EI and EE densities against each other, each pair of EI/EE images generates one PRM: points in the PRM indicate the densities at EI and EE of the corresponding voxels, unmasking unstable inflation; the relative frequency of voxels in the PRM is displayed by the colour scale. Individual voxels A and B are now traceable in the consecutive PRMs: as the density of voxel B increases over time, its position in the PRM changes, while voxel A is more stable. *Step 3:* tracking all points of each PRM, we identified a high-risk density range (in red) where voxels had the highest

probability of further increasing their density between consecutive PRMs, reaching a predefined severe injury range (blue area). Here, time 0 PRM is gridded, showing that point B(0) is located in the high-risk range, while A(0) is not. *Step 4:* the voxels in the high-risk and severe injury ranges of the PRM are now back-tracked to the corresponding baseline CT image. Step 5: a statistical model is created to predict the distribution of lung CT densities after 4 hours, starting from the density distributions at time 0. EE, end-expiratory; EI, end-inspiratory; PRM, parametric response map.

Animal Imaging: CT scans were acquired every hour at EI and EE, without changing ventilator settings. Image analysis (summarized in Figure 3.1) identified regions in which injury subsequently progressed. To achieve this, all EI and EE images were superimposed on each other and all voxels were aligned upon the first image after HCl (with high anatomical accuracy using a method developed by our group[34]). Lung outlines were semi-automatically separated from surrounding tissue, and the image alignment did not distort major anatomic landmarks, preserved lung density distributions, and accurately reproduced tidal lung deformation.

Parametric Response Mapping: Lung inflation was analyzed in parametric response maps (PRM)[49] created by plotting EI and EE densities of all paired CT voxels against each other on a bi-dimensional matrix with range between -1000 and 100 Hounsfield Units (HU) (Figure 3.1). The position of each point in the PRM describes EI and EE aeration of the corresponding voxel, showing normal vs. abnormal inflation patterns.

Risk Quantification: After superimposing all sequential images, evolving density of individual voxels was tracked over time. Injury progression was a binary outcome and was defined by an increase of both EI and EE densities to above the -300 HU cut point (‘severe

injury') in subsequent images (Figure 3.1). In the earlier images, voxels with higher probability of later progression were considered 'high-risk'. We measured such probability by analyzing range-wise receiver operating characteristic (ROC) between consecutive PRMs: values of sensitivity and specificity for observed progression were calculated for voxels of each bin. Using multivariate linear regression in a two-stage approach, we created a statistical model to predict the future distribution of lung CT densities and the worsening of C_{dyn}, starting from the percentage of voxels which, in earlier images, fell into the high-risk and the 'severe injury' density ranges.

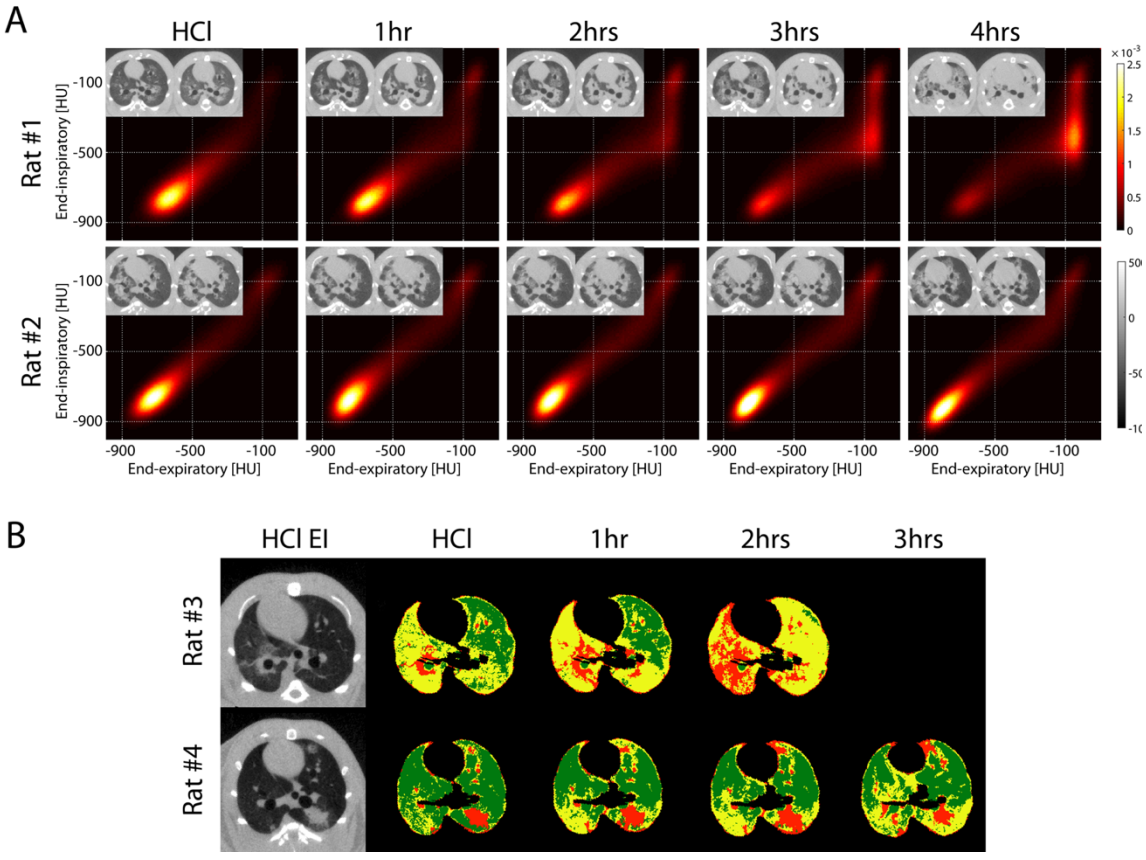

Figure 3.2 (A) PRM obtained at baseline after HCl aspiration and hourly until the end of the experiment in two rats ventilated with non-protective ventilation (top: V_T 12 ml/kg, PEEP 5

cmH_2O) versus protective ventilation (bottom: V_T 6 mL/kg, PEEP 10 cmH_2O). The corresponding EI and warped EE images are shown in the inserts for each PRM and show more severe propagation in the animal with non-protective ventilation versus more contained injury in the rat with protective ventilation settings. In the rat with more propagation (top), the distribution of paired EI and EE density values in the PRM evolved over time, with increased fraction of voxels in the high EI and EE density range (>−300 HU), indicating oedema and/ or non-reversible atelectasis (severe injury). In the rat with less propagation, voxel distributions were more stable over time. (B) Voxels that fell in the high-risk (yellow) and in the severe injury (red) domains of the PRMs were plotted in the corresponding EI images for each time point of the experiment in two rats, both ventilated with non-protective ventilation. Areas in green indicate voxels that fell in all remaining areas of the PRM. The inserts show the original baseline (after HCl) EI images. Severely injured regions progressively replaced the regions at risk. The rat with more propagation had a larger fraction of high-risk tissue at baseline and died before the 3-hour time point. EE, end-expiratory; EI, end-inspiratory; HCl, hydrochloric acid; PEEP, positive end-expiratory pressure; PRM, parametric response map; V_T, tidal volume.

Human Imaging: We used EI and EE CT images from patients who were included in a previously published study[31]. Of 13 patients in the study, we included a priori the nine subjects with early ARDS, i.e. who were imaged within seven days following intubation. EI and EE images were aligned as for the animal scans and, after confirming stability of anatomical landmarks, were analyzed with PRM. CT densitometry was also used as described in the original publication[31].

3.3. Results

Identification of ‘At-Risk’ Tissue: Concentric propagation of radiological opacities developed from the sites of initial injury; this was apparent from serial CT images, as well as from the parametric response maps (Figure 3.2 A). In the parametric response maps, the

distribution of paired EI and EE density values evolved, with more voxels developing in the severe injury domain. In contrast, where injury progression was limited, the voxel distribution was more stable (Figure 3.2 A).

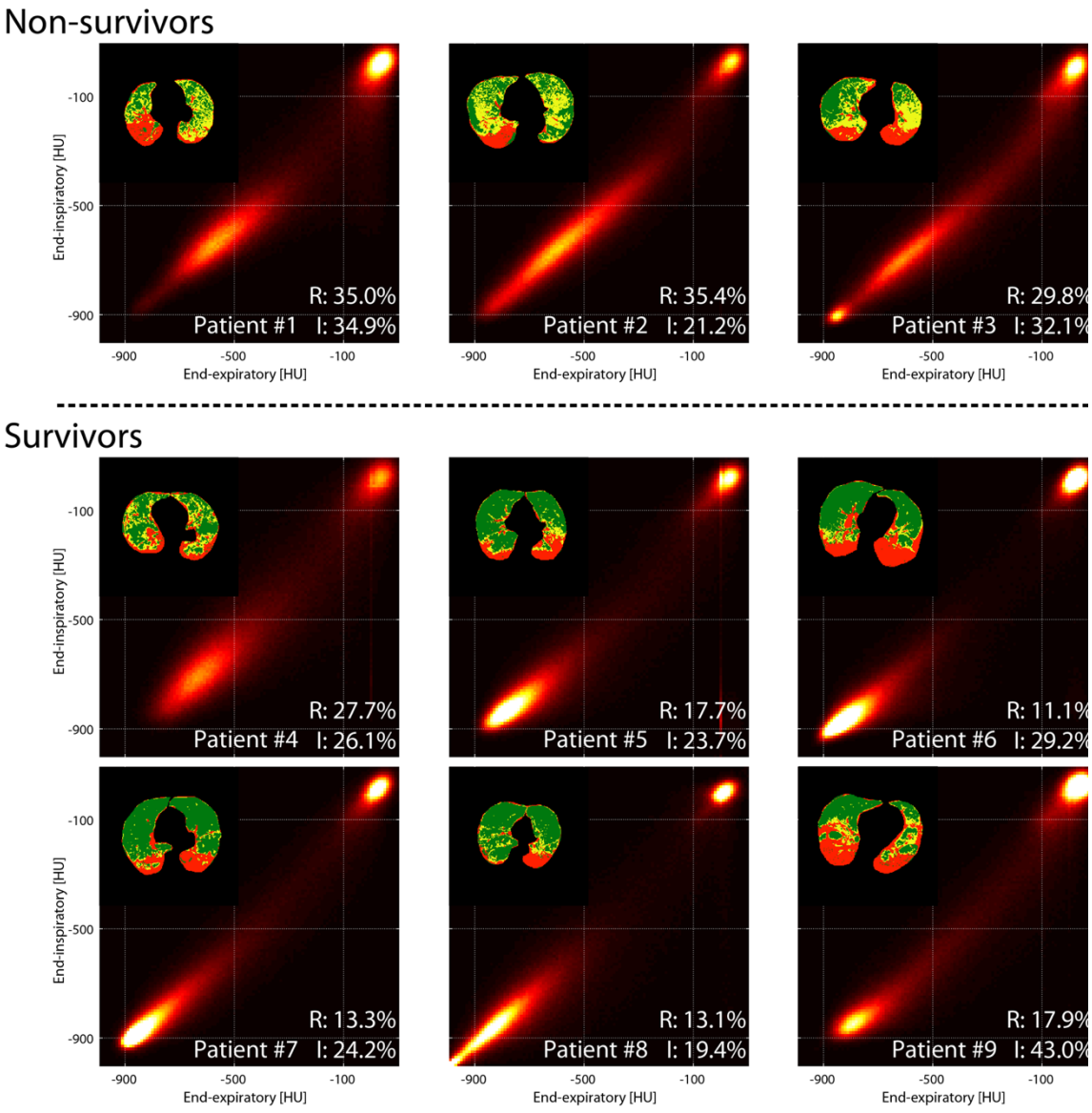

Figure 3.3 PRM maps on nine patients with ARDS imaged within 7 days from injury. The three patients who died in ICU or within 28 days from onset are shown on top. Voxels in the high-risk

(yellow), severely injured (red) and normal density (green) domains are plotted in the corresponding images. Individual amounts of severely injured (I) and high-risk (R) tissue are shown for each patient as percent of total parenchyma. ARDS, acute respiratory distress syndrome; ICU, intensive care unit; PRM, parametric response map.

Human Data: Parametric response maps of human subjects are shown (Figure 3.3). In the three non-survivors, voxel distribution was skewed towards intermediate density. By contrast, in the six survivors, there was higher representation of low-density regions. 'High-risk' and 'severe injury' voxels in patient images were identified by applying the density domains from the experimental images.

3.4. Discussion

These data suggest that a novel analysis of CT images may identify lung tissue at risk of further damage in experimental injury and might potentially predict outcome in patients with ARDS. Superimposing EI and EE images across the whole lung identified areas of unstable inflation that appear to represent lung at increased risk of local strain (possibly atelectrauma) when ventilator settings are injurious; such areas are foci for the propagation of lung injury. This three-dimensional approach covers the whole lung, and because it involves voxel-wise assessment, provides very high resolution (e.g. 1 mm^3 in humans). These features are in contrast to conventional plain radiography (two-dimensional)[35] and standard CT (three-dimensional), which are used to generate single inflation images and with focus restricted to large lung regions.

Parameters for identifying severity of ARDS include oxygenation (PaO_2/FiO_2 ratio), plain chest radiography, compliance, and 'driving pressure' (the difference between plateau and

end-expiratory pressure). The presence of unstable inflation may quantify risk of regional disease progression in experimental injury; and, the current patient data suggests it may potentially also predict outcome in ARDS. In animals, unstable inflation accurately mirrored the topographic/spatial development of secondary lung injury (Figure 3.2); and, in the retrospective patient series, a larger proportion (high-risk fraction >28%) of high-risk tissue at baseline was associated with mortality in ARDS (Figure 3.3).

Beyond higher resolution, the imaging approach implemented here offers important potential advantages over previous CT approaches. In experimental injury, we used repeat CT to identify the imaging characteristics that mirror the trajectory of lung injury; this was enabled by image alignment[34] which allowed tracking of individual voxels as sequential, superimposed EI-EE images over time. We thereby co-localized baseline unstable inflation with subsequent injury progression. This approach to scanning differs from a recently introduced method correlating ARDS survival with inflation heterogeneity in static CT images, but without EI-EE analysis[41]. Others have found correlations between CT imaging and ARDS outcomes, measuring the quota of tissue with recruitable atelectasis[47], percent diseased lung[51], and evidence suggesting early fibroproliferative changes[52]. However, our methodology is unique in that it builds outcome prediction on the quantitative correlation between imaging and later injury progression, this allowed us to detect “high risk” tissue in areas of the lung with unstable inflation vs. other states of aeration. Furthermore, this approach may unmask subtle inflation patterns that would not be noticed on conventional CT images.

In conclusion, we have developed a method that topographically links unstable inflation, regional trajectory of lung injury, and outcome. If validated by others as an independent predictor in larger populations, a single set of paired EI-EE CT images in early ARDS may predict outcome and responses to mechanical ventilation, may enable enrichment of clinical trials, and may facilitate personalized care.

CHAPTER 4: UNSTABLE INFLATION CAUSING INJURY — INSIGHT FROM PRONE POSITION AND PAIRED COMPUTED TOMOGRAPHY SCANS

This chapter has been adapted from the published article, in Xin Y, Cereda M, Hamedani H, Pourfathi M, Siddiqui S, Meeder N, Kadlecek S, Duncan I, Profka H, Rajaei J, Tustison NJ, Gee JC, Kavanagh BP, Rizi RR. Unstable Inflation Causing Injury. Insight from Prone Position and Paired Computed Tomography Scans. Am J Respir Crit Care Med 2018;198:197–207. https://doi.org/10.1164/rccm.201708-1728OC.

4.1. Introduction

Secondary lung injury caused by mechanical ventilation increases mortality in acute respiratory distress syndrome (ARDS)[2–4]. Because clinical trials of ventilator strategy in ARDS over the last 15 years have not substantially improved on mortality, new strategies for reducing ventilator-associated lung injury (VALI) are needed.

While ventilating patients in the prone position increases survival[12], the improved gas exchange associated with this strategy[54] does not explain the survival benefit[55]. Imaging studies using quantitative computed tomography (CT)[56] and positron emission tomography[57] report that prone positioning attenuates vertical gradients of aeration observed while supine. Such recruitment of atelectatic lung might lessen secondary VALI by reducing regional strain during inspiration[58]. However, it is not known if the homogeneity of inflation in the prone position is responsible for attenuating the progression of lung injury; this is potentially important for clinical management, as attenuation in the early stages might lessen the burden of established ARDS.

In our previous studies of experimental ARDS, we used sequential CT imaging to show that regional lung strain drives the propagation of early lung injury[59]. Tidal inflation was

imaged after primary injury, and the resultant parametric response maps of paired CT scans (*i.e*. paired scans at end-inspiration and at end-expiration) showed areas with partially aerated voxels and large tidal swings in tissue density. We termed this 'unstable inflation', and it was associated with the radiological propagation of secondary lung injury. Moreover, in both experimental lung injury and in patients with ARDS, the proportion of (voxels with) unstable inflation was directly related to the extent of injury progression[59].

In the current study, we used these insights to explore the mechanisms of protection afforded by prone (*vs*. supine) positioning in early lung injury. By linking the regional distribution of inflation with the subsequent trajectory of injury, we were able to successfully test two hypotheses. *First*, ventilation in the prone position limits the early progression of secondary lung injury following a primary insult; *second*, this effect is related to a reduction of the vertical gradients of unstable inflation associated with supine positioning. In an additional series of ventilated pigs, we verified the effects of prone position on unstable inflation in a large animal model. Some of these results have been presented in abstract form[60,61].

4.2. Methods

Animal Preparation: 24 Male Sprague-Dawley rats (365±21 g) were anesthetized with intraperitoneal pentobarbital, orally intubated, and paralyzed with pancuronium bromide. The carotid artery was catheterized. Heart rate and oxygen saturation (SpO_2) were monitored by pulse-oximetry.

Mechanical Ventilation: Animals were ventilated with tidal volume (V_T; 6 ml/kg) and positive end-expiratory pressure (PEEP; 10 cmH_2O) using a custom built ventilator[62]. Peak

inspiratory airway pressure (PIP) and PEEP were recorded, and dynamic compliance was calculated as $C_{dyn} = V_T/(PIP-PEEP)$.

Lung Injury: All rats received 2.5 ml/kg hydrochloric acid (HCl, pH 1.25) through the endotracheal tube in two aliquots[50,59], while in the right and left lateral decubitus. After one hour of supine stabilization (V_T 6 ml/kg, PEEP 10 cmH_2O), rats were randomized to ventilation in supine or prone position (12 rats in each group) for up to 3 hours, using settings known to induce secondary VALI[50,59]: V_T 12 ml/kg, PEEP 3 cmH_2O, FiO_2 1.0, and frequency 53 min^{-1}.

Small Animal Imaging: Whole lung computed tomography (CT) was performed at baseline (when stabilized after HCl) and hourly thereafter. Imaging was performed at end inspiration (EI) and end-expiration (EE). In the prone group, additional supine images were obtained at baseline to allow between-group comparisons of primary injury severity.

Image Analysis: The lung boundaries were semi-automatically delineated using a previously developed algorithm[34], yielding whole-lung 'Regions of Interest'. EI and EE images were registered (aligned) to each other using methodology to superimpose anatomical features when distorted by respiration[59]. To assess the effect of gravity and position on regional inflation (and on lung injury progression), lungs were partitioned into three coronal bins of equal thickness (ventral, middle and dorsal). Parametric response maps were then generated for the whole lung, as well as for each bin by matching individual voxels in each set of paired EI and EE images[28,49,59,63,64]. Voxels were categorized as *severe injury* if both EI and EE densities were >-300 HU, indicating pulmonary edema and stable atelectasis, and as *unstable inflation* if densities fell in the

range (EE: 0 to -600 HU, EI: −300 to −700 HU) that we previously found to indicate a high probability of injury progression[59].

Large Animals: Five Yorkshire pigs (32.4±2.7 kg) were anesthetized, intubated, ventilated with V_T 8 ml/kg, and received tracheal HCl (pH 1.25, 1 ml/kg into each lung). EI and EE CT scans were obtained at baseline and one hour after HCl, during ventilation in prone and supine position and with PEEP 5 and 10 cmH_2O. All images were analyzed as described for the rats.

Statistical Analysis: Image analysis was performed using Matlab 2016b software applications developed in the authors' laboratory. Statistical analysis was performed using 'R' (R Foundation for Statistical Computing, Vienna, Austria). Group mean and standard deviation of all the computed quantities were calculated. *Post hoc t*-tests were used to identify differences among means, and Bonferroni adjustment was performed. The Fisher exact test was used for proportions. $P<0.05$ was considered statistically significant.

4.3. Results

Survival: Ventilation in the prone position significantly improved survival; five rats in the supine group died between 2 and 3 hours of ventilation, compared to one in the prone group (Fisher, P=0.013).

Respiratory and Vital Parameters: Compliance and driving pressure (Table 4.1) were comparable between groups at baseline. In the supine group, compliance decreased at one hour and again at two hours of ventilation ($P<0.01$ vs. baseline), reaching lower values than in the prone group ($P<0.01$ at both times).

Baseline oxygenation was similar between groups (Table 4.1), but PaO_2 was lower in the supine than in the prone group after one hour of ventilation ($P<0.01$), and further decreased in the supine group over time. No significant effect of time or body position on $PaCO_2$ was detected. Oxygen saturation followed a similar trend to PaO_2 (Table 4.1). Blood pH was lower in the supine group than in the prone group after one hour of ventilation ($P<0.05$) due to higher lactic acid concentration in the former group (Table 4.1).

	Supine			**Prone**		
	Baseline	**1 hr**	**2 hrs**	**Baseline**	**1 hr**	**2 hrs***
Arterial Blood Pressure (mmHg)	113.8±12.3	108.9±19.9	82.9±41.9 §	126.0±8.4	118.2±23.1	104.8±28.5 §
Driving Pressure (cmH_2O)	19.1±2.9	23.3±5.6 §	28.7±6.6 §	19.9±2.2	20.7±3.3	21.8±4.0 †
pO_2 (mmHg)	396.3±79.7	107.5±56.5 §	43.6±7.5 §	388.8±65.9	217.0±109.3 †§	142.9±108.1
pCO_2 (mmHg)	45.9±8.2	50.0±11.2	50.6±10.2	46.4±6.7	44.8±7.8	48.7±11.1
pH	7.34±0.06	7.26±0.06 §	7.19±0.04 §	7.32±0.07	7.29±0.01	7.30±0.06
SpO_2 (%)	99.9±0.1	94.5±4.9 §	65.9±11.7 §	99.9±0.1	99.0±0.8	94.4±7.5 †§
Blood Lactate ($mmol \cdot L^{-1}$)	1.28±0.40	2.50±1.29 §	4.82±3.26 §	1.54±0.72	1.89±1.38	1.49±0.08

Table 4.1 Physiological characteristics of two groups of rats ventilated in the prone vs. supine position after hydrochloric acid instillation in the trachea. †: $P<0.05$ between cohorts; §: $P<0.05$ vs. baseline in the same group. *: In the prone group, arterial blood gases were available at two hours in only 3 rats due to positional difficulties drawing blood through the carotid catheter after one hour of prone ventilation.

Arterial blood pressure decreased from baseline after two hours of ventilation in both groups ($P<0.01$), although it was higher in prone than in supine rats at this time (Table 4.1).

Distribution & Progression of Lung Injury: Baseline CT scans, obtained supine in both groups, confirmed that the distribution of primary injury was similar and that primary lesions were dorsal, irrespective of group assignment.

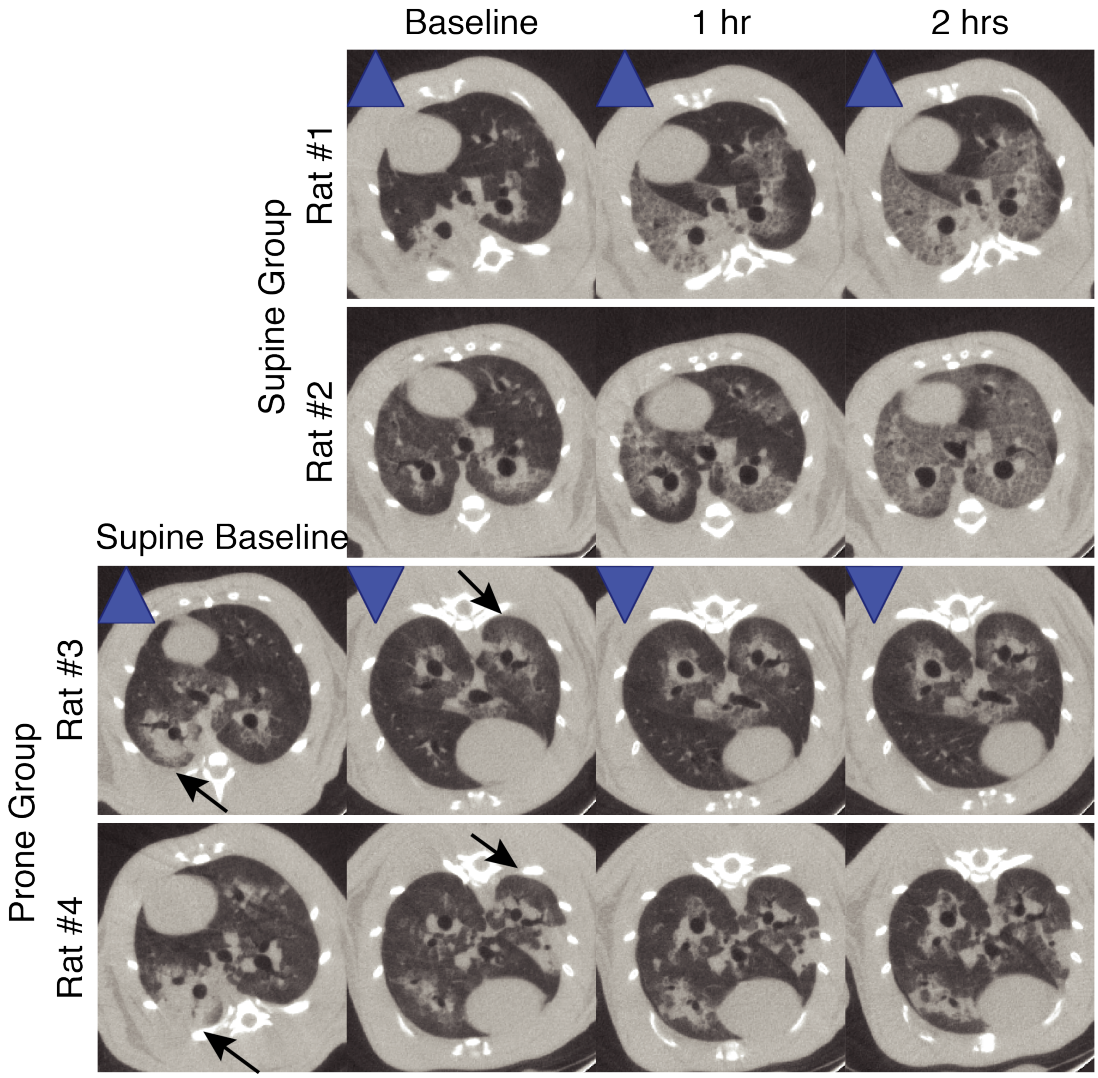

Figure 4.1 Radiological injury propagation in four representative rats ventilated in prone vs. supine position (two rats in each group) and imaged at end-inspiration. Baseline (after HCl) supine images are also shown for the two prone rats (#3 and #4). In all rats, primary injury was initially localized in the dorsal lung regions. In the rats ventilated supine (#1 and #2), injury

rapidly spread over the entire lung. In the prone rats, position change improved aeration in the dorsal lung regions (black arrows) and subsequent injury propagation was more contained. The blue triangles indicate body position (up-pointing: supine, down-pointing: prone)

In supine animals, injury propagated rapidly over the entire lung, as previously described. Changing from supine to prone position resulted in the attenuation of dorsal hyperdensities, which remained stable thereafter for the duration of the experiment.

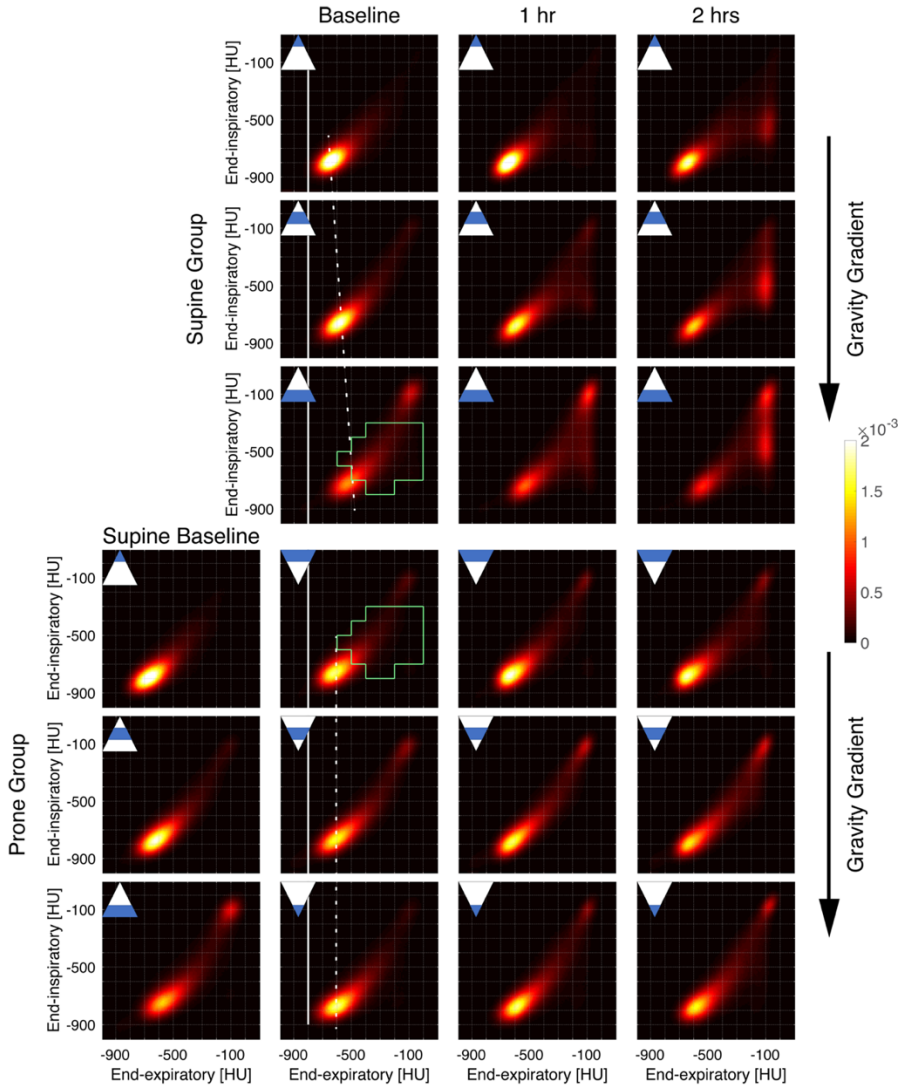

Figure 4.2 Cumulative parametric response maps of EI-EE voxels partitioned in non-dependent, mid-level, and dependent regions of the lungs (indicated by the solid blue color in the triangle) in the prone and supine position (indicated by the tip of the triangle). In the supine position at baseline, the centroid of the voxel distribution shifted towards higher density following the gravitational gradient. Over time, changes in the voxel distributions were more evident in the dependent lung regions than in the non-dependent ones. In the prone position, the centroid and the voxel distribution changed minimally in the tree regions at baseline (minimal deviation from white vertical reference line); evolution in the dorsal lung regions was less than in the supine rats. The area including voxels with unstable inflation is highlighted (green border) in the dorsal maps.

Categorization of voxel distribution at baseline showed that 'unstable inflation' and 'severely injured' voxels were significantly affected by gravity in the supine position, but not in the prone position (Figure 4.3 A). In supine animals, significantly higher fractions of 'unstable inflation' and severe injury tissue voxels were present in the dependent (dorsal) regions of the lungs compared to the other regions.

Finally, the baseline fraction of 'unstable inflation' voxels in the dorsal bins (dependent in supine, non-dependent in prone) was positively correlated with the decrease in respiratory system compliance (R=0.71; Figure 4.3 B), but not with 'severe injury'.

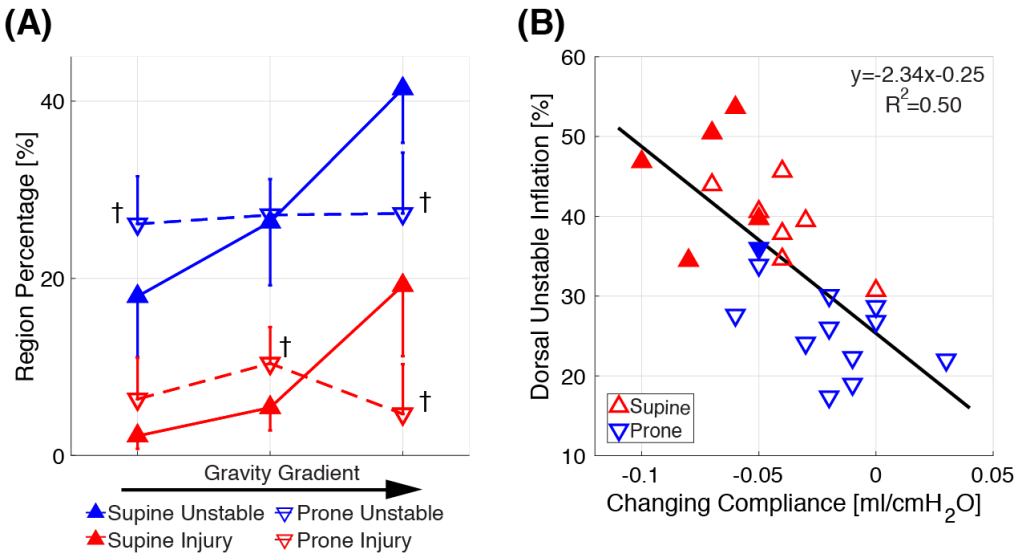

Figure 4.3 (A) Unstable inflation and severely injured voxels are shown (as a percent of total) in the non-dependent, mid-level, and dependent lung regions of the baseline images obtained in supine and prone rats. (B) Correlation between change in compliance (between baseline and the end of the experiment) and baseline percent fraction of unstable inflation voxels in the dependent lung regions. Solid dots indicate rats that died before two hours of ventilation. †: $P<0.05$ between cohorts.

4.4. Discussion and Conclusion

In this study, prone positioning limited the early propagation of radiological abnormalities after experimental lung injury and improved survival during mechanical ventilation. The effect of prone positioning was likely related to its ability to decrease areas of unstable inflation in the dependent regions of the lungs. Thus, prone positioning could prevent severe ARDS by protecting the lungs from the progression of injury in its early stages.

While prone positioning has been introduced as a rescue therapy for severely hypoxemic ARDS[65–67], the improved oxygenation which it produces does not explain the observed

improvement in survival among patients with severe ARDS[55]. Using serial CT, our study showed that prone positioning reduced the regional propagation of CT densities compared to supine positioning, while also attenuating the deterioration of respiratory mechanics and development of pulmonary edema (estimated from tissue weight). These results suggest that prone positioning may improve ARDS outcomes by alleviating the early evolution of 'secondary' (ventilator-associated) lung injury, before it becomes severe.

In a previous study of mechanical ventilation with non-protective settings in experimental ARDS[50], we reported that radiological propagation is the visual manifestation of evolving lung injury. Using analysis of longitudinal CT scans in a similar model[59], we then observed that this secondary propagation was more severe in lungs that displayed larger areas of tissue with unstable inflation. In that same study, unstable inflation was also found to be associated with higher mortality in a small group of patients with early ARDS[59]. Partial inflation includes areas with stable poor aeration, but it is dominated by large tidal density changes within partially aerated tissue. Studies using diffusion MRI suggest that this pattern of inflation indicates overstretched airspaces embedded in voxels with reduced (but not abolished) gas content[62,68,69]. While unstable inflation may be simply a marker of heterogeneous gas distribution, such stress concentration can regionally increases the risk of VALI. Unstable inflation is distinct from cyclic recruitment of atelectasis, which is defined as complete but reversible loss of aeration[70]. As with unstable inflation, cyclic recruitment was not correlated with propagation of injury after acid aspiration[50].

In the current study, regional analysis revealed a vertical gradient of abnormal inflation in supine rats that was not present in prone rats. Voxels with unstable inflation were more

abundant in the dependent (dorsal) lung of supine rats, where the radiological signs of both primary injury and its progression were more visible. We also observed that, irrespective of body position, the baseline fraction of unstable inflation in the dorsal lung predicted worsening mechanics (Figure 4.3B). Overall, the findings of this study suggest that prone positioning reduced the harmful effects of mechanical ventilation in dependent regions of tissue with unstable inflation, thereby mitigating the radiological propagation of the injury to the rest of the lung. Further studies will be needed to confirm that tissue inflammation is attenuated by this strategy.

Other authors have studied the effects of the prone position on regional lung mechanics and VALI, finding that prone position attenuated vertical gradients of pleural pressure and regional strain, in addition to improving dorsal atelectasis[14,15] and ventral hyperinflation[71]. Using CT in established ARDS, prone position was shown to augment recruitment by PEEP [58]. Nuclear medicine studies have shown less heterogeneity of both lung aeration and perfusion in prone vs. supine sheep with surfactant depletion[72]. Another study showed that prone position delayed the progression of lung injury in previously healthy lungs receiving high stretch ventilation[73], supporting a causal relation between improved mechanics and milder injury. Finally, in a study of pre-injured lungs (oleic acid) receiving ventilation with elevated inflation pressure, prone positioning attenuated injury in the dorsal lung[74], suggesting that attenuation of airspace collapse in dependent regions may be crucial to the success of positional therapy.

Our work differs from these previous studies[14,15,17,58,71–73] in that it is the first to demonstrate that prone positioning can attenuate the radiological and functional

progression of lung injury, before it becomes established and severe. This finding was enabled by our use of longitudinal imaging, which allowed us to link unstable inflation, future propagation of lung injury, and response to body position. Furthermore, our model recapitulates the early evolution of lung injury, when hypoxemia is still mild and radiological abnormalities are spatially limited. Our short-term studies in pigs showed that, similar to the rats, prone position decreased unstable inflation in the dorsal lung, supporting long term experiments to test this approach in large animals. Similar to our previous studies [50,59], we used a model of secondary VALI superimposed on mild primary injury, as indicated by the relatively mild oxygenation impairment at one hour after acid aspiration in both rat cohorts (Table 4.1). In addition to helping understand how positional therapy improves outcomes, this study's findings suggest a potential new use for prone positioning: it could be used in patients with early lung injury to prevent the development of severe ARDS.

In a clinical trial which recruited only patients with severe hypoxemia, Guerin et al. reported better outcomes with prone *vs*. supine position[12]; in contrast, outcomes were mixed in earlier clinical trials that included patients with less severe ARDS[13]. However, this does not mean that prone position is ineffective in carefully selected subjects with milder hypoxemia, as the discrepancy may be related to heterogeneity of patient characteristics within the study populations[45]. In fact, a one-time measurement of oxygenation impairment is a worse prognostic indicator than either treatment responsiveness[75] or imaging-derived metrics[47,59]. While we do not yet propose clinical implementation of this evidence, the current study suggests that the effectiveness of prone

position may be related to the characteristics described in the dependent lung. In addition to CT scanning, other methodologies (*e.g*. lung ultrasound [76], and electrical impedance tomography [77]) may allow for the efficient measurement of unstable dorsal inflation in order to assess the early risk of injury progression.

CHAPTER 5: POSITIONAL THERAPY AND REGIONAL PULMONARY VENTILATION — HIGH RESOLUTION ALIGNMENT OF PRONE AND SUPINE COMPUTED TOMOGRAPHY IMAGES IN A LARGE ANIMAL MODEL

This chapter has been adapted from the published article, Xin Y, Cereda M, Hamedani H, Martin KT, Tustison NJ, Pourfathi M, Kadlecek S, Siddiqui S, Amzajerdian F, Connell M, Abate N, Kajanaku A, Duncan I, Gee JC, Rizi RR. Positional Therapy and Regional Pulmonary Ventilation: High-resolution Alignment of Prone and Supine Computed Tomography Images in a Large Animal Model. Anesthesiology 2020;133:1093–105. https://doi.org/10.1097/ALN.0000000000003509.

5.1. Introduction

Ventilation in the prone position improves blood gases[54] and decreases mortality in patients with acute respiratory distress syndrome (ARDS)[12]. Imaging studies suggest that redistribution of lung inflation along the gravitational axis may explain such beneficial effects. In fact, pulmonary aeration[14], pleural pressures[15], and regional strain[16,17] are more homogeneous when subjects are prone rather than supine, due to the apparent attenuation of the gravity-related forces that compress and deform the lungs[18]. Studies evaluated the effects of body position on lung aeration in separate prone and supine computed tomography (CT) scans, e.g. by comparing ventro-dorsal gradients of tissue density[14]. However, this approach has limitations. First, it is restricted to measuring the effects of gravity and does not identify positional changes in non-gravitational distributions[78]. Second, it is unable to directly measure tissue deformation, or its effect on regional gas content. Third, it cannot measure the effects of position on small units of tissue, as these are not tracked across images. Mapping small-scale changes of lung tissue density and

deformation could better characterize patterns of regional inflation associated with the prone position[79]. Fortunately, recent advances in image processing may allow such in-depth assessment of the structural effects of position. For example, cluster analysis allows us to partition large datasets in groups with similar attributes, and can be used for the unrestricted assessment of regional distributions of imaging variables[80]. Image registration provides structural correspondence between paired images[63,81] and allows us to map changes in aeration[49] and lung tissue deformation at high resolution[82,83]. However, this methodology has not yet been used to study positional therapy, since aligning paired prone and supine images is complicated by marked shifts of lung and chest wall geometry between respective positions.

In a previous study, prone positioning contained the progression of experimental lung injury through its beneficial effects on inflation of the dorsal lung[84]. However, previous animal studies comparing prone vs. supine positions showed craniocaudal changes in ventilation and perfusion in the vicinity of the diaphragm[78], which were not explained by gravity. These regional gradients are likely explained by non-gravitational effects of position on inflation and tissue compression, which have not been directly visualized. In the current study, we reanalyzed our prior pig data[84] to topographically characterize the effects of body position on lung tissue. We hypothesized that improvements in lung aeration and tissue deformation occur in gravitational and non-gravitational distributions. For this purpose, we aligned paired prone and supine lung images obtained at two levels of positive end-expiratory pressure (PEEP) before and after lung injury, to produce detailed maps of the effects of prone positioning on each lung tissue unit visible on CT. We then

investigated the spatial distribution of position-related changes in density and deformation throughout the lungs using cluster analysis.

5.2. Methods

Animal Preparation: Five Yorkshire pigs (32.4±2.7 kg) were anesthetized with intramuscular injections of ketamine and xylazine. Pigs were orally intubated and anesthesia was maintained by continuous intravenous infusion of ketamine and midazolam through a peripheral catheter. Supplemental doses were given to assure immobility during CT scanning. Peripheral oxygen saturation, heart rate, and body temperature were monitored continuously. The femoral artery was catheterized for blood pressure monitoring and arterial blood gas measurement.

Mechanical Ventilation and Lung Injury: Animals were ventilated with a custom-built mechanical ventilator. Tidal volume (V_T) 8 ml/kg, respiratory rate 15 breaths per minute, and inspired fraction of oxygen 0.6 were constant throughout the experiment. Pigs then received 2 ml/kg hydrochloric acid (HCl, pH 1.25) injected in the endotracheal tube over two equally divided doses with the animals alternately in the right and left lateral position. Pigs were then stabilized supine for 60 minutes with PEEP 10 cmH_2O. Imaging was performed before injury (healthy baseline) as well as after injury and stabilization. Blood gases were obtained after each image acquisition. Airway pressure was monitored using a fiberoptic sensor placed proximally to the endotracheal tube. Tidal volume was recorded from the ventilator display.

CT Imaging: CT scans were acquired with a Siemens SOMATOM Force scanner. The settings were: 120 kVp, 200 mAs, pitch 0.95, slice thickness 0.75 mm, collimation 57.6x0.6

mm, estimated dosage 3–5 mSv. All images were reconstructed to a resolution of 1x1x1 mm. End-inspiratory (EI) images were obtained during 5-second-long inspiratory pauses, applied during ventilation in both supine and prone positions with PEEP 5 and 10 cmH_2O. Each combination of PEEP and position was applied in random order and maintained for 10 minutes prior to imaging, which was shown in pilot studies to assure sufficient stabilization of aeration redistribution. In the prone position, the pigs laid unsupported on their abdomen with their forelegs flexed and their hindlegs extended at the hips. Animals did not receive neuromuscular blocking agents, but sedation was adjusted to achieve immobility, which was confirmed on CT scans by the absence of motion artifacts near the diaphragm.

Image Processing: Our CT analysis measured changes in CT density (i.e. aeration) and dimensions (i.e., spatial deformation) in individual small units (voxels) of tissue. For this purpose, images were registered, i.e., reshaped (warped) and aligned to each other to match the position of each voxel on shared spatial coordinates. This registration corrected for the effects of body position on lung and chest wall geometry. The outlines of the lungs were segmented (separated) from non-pulmonary tissue.

Image Registration and Segmentation: We registered corresponding supine and prone images using Advanced Normalization Tools (ANTs)[28,81]. During Step 1 of the registration, the outline (mask) of the lungs was segmented from non-pulmonary tissue using previously published methods[34]. In Step 2 of the registration, the prone lung outline was aligned to the supine outline, resulting in a "warped-prone" outline with identical outer geometry to the supine lungs. During Step 3 of the registration, all the pulmonary structures contained

within the outlines of the prone and supine CT scans were aligned, yielding a warped image of the prone lungs for each study condition[63]. The quality of the registration was assessed in three ways. First, overlap between the warped-prone and supine lung outlines was quantified using the Dice similarity coefficient. The Dice coefficient was 0.988±0.002 before injury and 0.983±0.006 after injury, suggesting optimal overlap of the lung outlines between warped-prone and supine images. Second, trained operators measured minimal differences in the spatial coordinates of anatomical landmarks between warped-prone and supine images, suggesting conserved spatial orientation of parenchymal structures. Third, we compared regional density distributions between original and warped prone images.

Analysis of lung inflation: In Step 4, we measured small-scale aeration changes by calculating the differences in X-ray attenuation, measured in Hounsfield Units (ΔHU), between tissue voxels of warped-prone and supine images. Each voxel's ΔHU value quantifies the increase or decrease of gas content in that same tissue unit. We quantified body position-related changes in the dimensions of each tissue voxel as its corresponding Jacobian[85]. A Jacobian is a unitless metric of tissue deformation calculated during image registration. When comparing corresponding warped-prone and supine images, a voxel with a negative determinant of the log Jacobian represents contraction, whereas a positive value indicates expansion incurred by the same lung tissue unit. Detailed analysis of lung recruitment was performed by identifying and mapping the voxels that shifted from the high density, non-aerated range (-100 to + 100 HU), to lower density ranges[30] when comparing the warped-prone to the supine images. Derecruitment was measured as voxels that increased density to higher than -101 HU when turning prone. Whole-lung contents of

gas and tissue were estimated by density measurements on the non-registered images[86]. Cluster analysis: K-means clustering was performed on the voxel distribution of ΔHU (x-axis) and of Jacobian (y-axis) to characterize three different groups (reinflation, limited-change and deflation). The number of clusters (k=3) was chosen during preliminary analysis because it maintained physiologically plausible inflation responses and stable distributions among animals. Both HU and Jacobian were normalized by standard score $[(x-\mu)/\sigma]$ to prevent bias due to the value dispersion between x and y axis. For each cluster, the percentage of total lung mass and volume it occupied, and its mean values of HU, Jacobian, and CT intensity were calculated in each condition. Gravitational and non-gravitational patterns of cluster distribution were separately investigated by partitioning the lung images into ten horizontal and ten vertical bins of equal mass.

Statistics Analysis: No power analysis was performed due to the retrospective design of the study. Descriptive statistics were performed on the clusters identified by K-means, characterizing their size as a percent fraction of total lung volume and mass, and their values of mean CT intensity, HU, and Jacobian. All continuous data were reported as mean ± standard deviation. Repeated measures analysis of variance (ANOVA) was performed to compare the cluster distributions across spatial compartments. Two-tailed paired T-tests were performed for relevant cluster distribution comparisons, and to compare physiologic values between data obtained at healthy baseline vs. injury, prone vs. supine, and lower vs. higher PEEP. An experiment-wide $p < 0.05$ was selected as the threshold for statistical significance. Data was reformatted and prepared in Jupyter Notebook using Python 3.6.

Statistical analysis was performed using RStudio 1.2.5001 (R Foundation for Statistical Computing; Vienna, Austria).

5.3. Results

The imaging results are a re-analysis of a previously published CT dataset from a pig model of mild lung injury. All animals survived and were included in the analysis. HCl injection caused mild lung injury, with a decrease in PaO_2 from 251.5±50.4 to 161.1±116.9 mmHg (P=0.047), and with a decrease in respiratory system compliance from 20.1±3.1 to 14.6±4.2 ml/cmH_2O (P=0.046) at PEEP 5 cmH_2O in the supine position, showing blood gases and respiratory mechanics data). After injury, the prone position increased PaO_2 at both PEEP levels, but it did not affect compliance. Higher PEEP did not modify gas exchange or compliance.

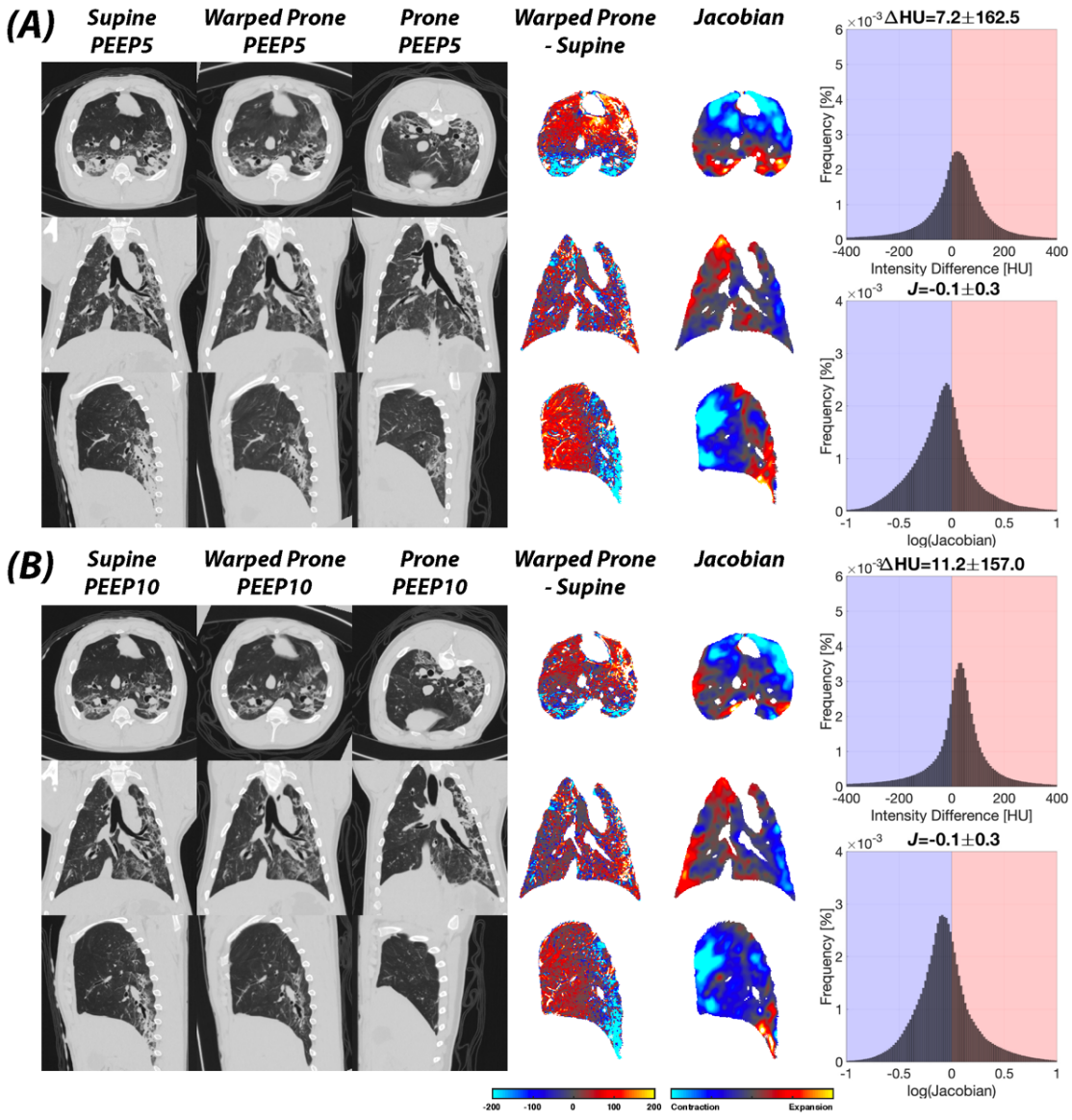

Figure 5.1 Images were repeated in all tested conditions after lung injury induction by acid aspiration and are shown in A) at PEEP 5 cmH_2O and in B) at PEEP 10 cmH_2O. The left panels show the target supine images, warped-prone image (shown inverted), and original (non-warped) prone image. The middle panel shows the ΔHU and Jacobian maps side-by-side, with the corresponding cumulative frequency distribution in the right panels.

Post-injury images at PEEP 5 and 10 cmH_2O (Figure 5.1 A,B, left panels) show that, after registration, supine and warped-prone images differed only in the distribution of pulmonary

densities, which were more prominent in the supine position. Similar to healthy baseline, the regional ΔHU values at both PEEP levels were generally negative (improved aeration) in the dorsal lung and positive (decreased aeration) in the ventral regions (Figure 5.1 A,B, middle panels). The Jacobian maps also displayed similar behavior (ventral contraction, dorsal expansion) to that in healthy lungs.

Cumulative frequency distributions (including all animals) of ΔHU and Jacobian values were more heterogeneous after injury (Figure 5.1 A, B, right panels). Mean ΔHU values were near zero in all the tested conditions, suggesting that the prone position had minimal net effect on whole-lung gas content. This was confirmed by the stability of mean lung density and whole lung gas volumes between prone and supine positions.

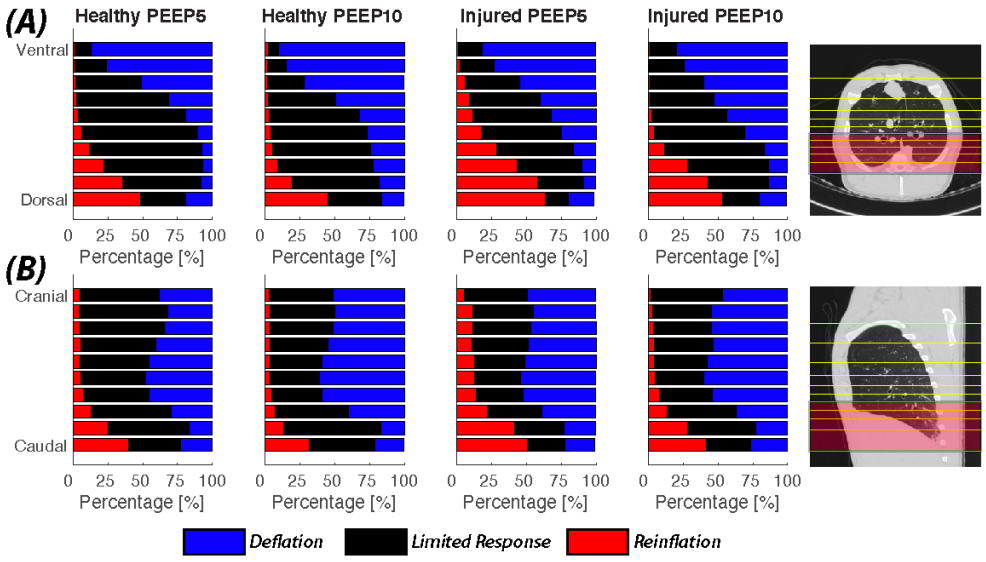

Figure 5.2 Segment analysis among all end expiratory (EI) conditions partitioned the lung into 10 segments of equal mass along the A. Dorsal-Ventral axis and B. the Caudal-Cephalad axis. The cluster frequencies of reinflation (red), limited response (black), and deflation (blue) are displayed at the level of each segment. The far-right column shows the spatial orientation of the 10 equal mass segments which were used in the compartment analysis of cluster distribution. In

A. the top 5 segments correspond to the ventral compartment and the bottom 5 segments are the dorsal compartment. In B. segments that contain a pixel adjacent to the diaphragm are considered to be in the diaphragmatic compartment. The dorsal and caudal bins were shaded with red color.

Cluster Analysis: Cluster analysis assigned lung tissue voxels to clusters with distinct characteristics. The following cluster characterization represents general trends, derived from analysis of all conditions with descriptive statistics of CT-derived characteristics of each cluster. Regional quantification of cluster distribution in ten vertical and ten horizontal bins of equal mass showed both ventro-dorsal and craniocaudal gradients (Figure 5.2). The ten horizontal bins (Figure 5.2.A) were partitioned evenly into dorsal and ventral compartments, while the vertical bins (Figure 5.2.B) that interfaced the diaphragm were grouped into a caudal vs. a cranial compartment. Cluster distribution significantly differed between both ventro-dorsal ($F(1,4)=103.9$, $P<0.001$), and cranio-caudal compartments ($F(1,4)=117.5$, $P<0.001$). 86.4±8.5% of the reinflation cluster was located within the dorsal compartment vs. 13.6±8.5% in the ventral compartment ($P<0.001$). 63.4±11.2% of the reinflation cluster was contained in the caudal, peridiaphragmatic bins vs. 36.6±11.2% ($P<0.001$) in the remaining bins.

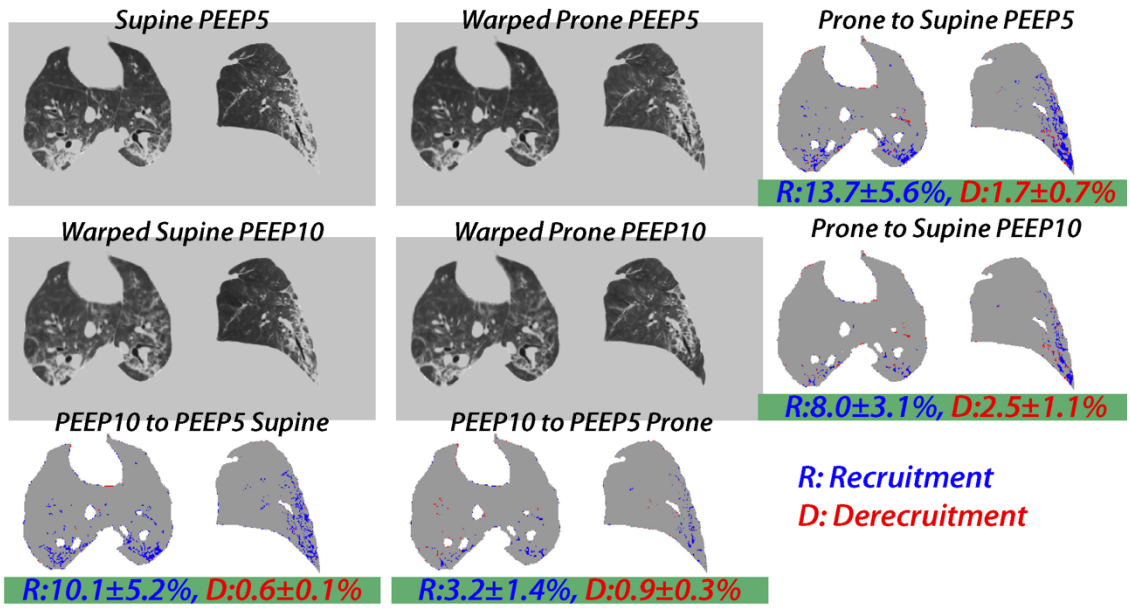

Figure 5.3 Paired computed tomography scans obtained in the supine and prone positions are shown with the corresponding recruitment maps. Registration was performed between supine and prone images, yielding maps of position-related (from supine to prone) recruitment (R) and derecruitment (D) at PEEP 5 cmH_2O (top row) and PEEP 10 cmH_2O (second row). Recruited voxels are shown in blue; derecruitment was small and shown in red. Numeric values are shown for each map. In addition, images at PEEP 5 and 10 cmH_2O were registered to each other, showing the PEEP-related recruitment in the supine and prone positions (bottom row).

Lung Recruitment: Figure 5.3 displays representative post-injury maps of recruitment and derecruitment due to prone position at end-inspiration at both PEEP 5 cmH_2O and PEEP 10 cmH_2O, with group mean ± SD values shown below each map. Prone positioning recruited 64.5±36.7g of tissue (11.4±6.8% of total lung mass) at low PEEP and 49.9±12.9g (8.9±2.8% of total mass) at higher PEEP. 59.0±13.0% of recruited voxels were in the caudal region. Derecruitment was relatively small in both conditions. We also registered PEEP 5 and 10 cmH_2O images to each other for each position (left two columns) in order

to visualize tissue with restored aeration at higher PEEP. The images show that this and position-related recruitment were quantitatively similar. Both recruitment and derecruitment were low in healthy lungs.

5.4. Discussion

We directly visualized the effects of positioning on each unit of lung tissue in paired prone-supine CT scans of ventilated pigs. We then identified which regions of the lung responded to the prone position with reinflation, deflation, or limited change. These patterns followed both gravitational and non-gravitational distributions: reinflation was mostly concentrated in the caudal lung region near the dorsal portion of the diaphragm (Figures 5.2). Recruitment of non-aerated tissue contributed to reinflation in this same region after injury (Figure 5.3).

Using image registration, we were able to match lung structures in paired images to provide a detailed quantification of position-related changes in regional lung volume and gas content (Figure 5.1). Following this step, cluster analysis grouped tissue units according to changes in density (aeration) and dimensions (expansion or contraction). We then mapped the spatial distribution of the three clusters, which had distinct responses to prone positioning: ventral deflation (increased density and contraction), limited tissue response in the mid-lung, and dorsal reinflation (decreased density and tissue expansion). We used K-means clustering[87], with its simplicity and low computational complexity, to generate non-subjective regions of interest that shared similar patterns of the two markers we presented in this work (density change and tissue deformation). This method is suitable for classifying an image into different regions when the number of clusters is known for

particular human anatomy and/or physiology[88,89]. We postulated a three-cluster model, as it would reflect expected simple airspace responses. We are confident in this model, as it resulted in stable classifications between animals and conditions. Furthermore, the opposite density changes measured in the reinflation and deflation clusters were physiologically plausible.

Our methods allow us to quantify the effects of compressive phenomena on the distribution of aeration in prone vs. supine position. The observed ventral contraction and dorsal expansion of lung tissue corroborates studies proposing that attenuation of the gravitational gradient of lung density in prone ARDS patients[14] is due to redistribution of the forces that deform the lung[18,90,91], causing more uniform pleural and transpulmonary pressures than in the supine position[15,92]. Additionally, we measured predominant reinflation and recruitment (after injury) in the dorso-caudal lungs, indicating localized positional responses near the diaphragm. The concurrent craniocaudal and ventro-dorsal aeration patterns confirm the coexistence of gravitational and non-gravitational forces. This finding is in accordance with the results of a detailed ex-vivo analysis of lung tissue, which showed that gravity does not dominate the topographic effects of position on lung function[78]. In fact, position-related changes to perfusion and ventilation were prominent in the dorso-caudal lung region of ventilated pigs[78], which could be explained by focal compression and deflation in the same regions when animals are in the supine position. Such regional patterns result from the reconfiguration of the diaphragm profile that occurs with position due to changes in abdominal pressure[15]. These effects of positioning on the

diaphragm are known[93,94], but here we proved a first clear, direct visualization of their implications on regional lung inflation.

Prone position had negligible effects on the average density and gas volume of the whole lungs, results which are in discordance with studies where prone positioning improved lung capacity[95]. However, other studies reported stability of lung volumes when comparing prone to supine positions in animals[96] as well as in humans[58]. Similar to human studies[97,98], we did not observe improvements in respiratory system compliance in the prone position. This absence of effect was likely related to compression of the ventral chest wall reducing chest wall compliance which offset improvements in lung compliance[99,100]. We did not support shoulders and hips in the prone position, which restrains lung expansion and limits ventral inflation[12,58], and likely caused density to increase in a large region of ventral lung.

In the setting of unchanged gas content, gas exchange improvements in the prone position were likely related to focally improved recruitment and ventilation-perfusion matching in the dorso-caudal region of the lung. Studies by others have quantified lung recruitment by prone position[58,71], but registering paired images allowed us to map the reopening of collapsed tissue with voxel-level detail. As shown in Figure 5.3, tissue voxels recruited by the prone position were dorsally distributed and were predominantly located within the dorso-caudal region occupied by the reinflation cluster. Dorsal recruitment was not matched by an equivalent amount of ventral derecruitment in this model. The net balance in favor of recruitment was compatible with the mild injury and dorsal distribution of the lesions, with less tendency for lung collapse in the ventral lung regions. Furthermore, density was more homogeneous between clusters in the prone compared to supine position.

Similar to previous studies[72], such even aeration indicated reduced tendency for ventilation loss in the prone position. Oxygenation and recruitment improved in the prone position at both levels of PEEP; however, improvement in aeration due to higher PEEP (Figure 5.3) was not associated with improved oxygenation. This discrepancy was probably related to more favorable distributions of perfusion and of ventilation observed in the prone position vs. higher PEEP[101]. However, a larger gradient between tested PEEP level could have revealed whether spatial patterns of reinflation are superimposable when comparing higher PEEP vs. prone positioning.

Implications: Our study is unique in that we were able to directly visualize improvements in small-scale aeration and match them with tissue expansion and local recruitment due to prone position. Although we did not directly test their biological implications, these patterns are important because the effects of positional therapy on patient mortality are not explained by better gas exchange[55]. Therefore, imaging characteristics may be implicated in predicting injury progression and response to therapy. The current study shows that the beneficial effects of prone position on lung recruitment and aeration are concentrated in the same dorso-caudal region. It is therefore likely that the presence of opacifications in the dorsal lung and their responses to prone position (recruitment, reinflation) are key indicators of the therapeutic and protective effects of this therapy. Non-invasive imaging tools such as lung ultrasound[102] can assess localized responses in the dorso-caudal lung and possibly predict outcome and personalize care in individual patients.

CHAPTER 6: DIMINISHING EFFICACY OF PRONE POSITIONING WITH LATE APPLICATION IN EVOLVING LUNG INJURY

This chapter has been adapted from the published article, Xin Y, Martin K, Morais CCA, Delvecchio P, Gerard SE, Hamedani H, Herrmann J, Abate N, Lenart A, Humayun S, Sidhu U, Petrov M, Reutlinger K, Mandelbaum T, Duncan I, Tustison N, Kadlecek S, Chatterjee S, Gee JC, Rizi RR, Berra L, Cereda M. Diminishing Efficacy of Prone Positioning With Late Application in Evolving Lung Injury. *Crit Care Med* 2021. https://doi.org/10.1097/CCM.0000000000005071.

6.1. Introduction

While the morphologic and functional characteristics of lungs with acute respiratory distress syndrome (ARDS) change over time[103,104], this evolution is poorly characterized. Pulmonary stress during mechanical ventilation accelerates ARDS progression[7] and may diminish the efficacy of therapeutic strategies, narrowing the opportunity for successful treatment. Better understanding the evolution of ARDS could therefore help refine both indications and timing of treatment.

Prone ventilation improves gas exchange compared with supine positioning[72] and decreases mortality in severe ARDS[12]. Improvements in oxygenation after prone positioning did not predict survival [55], but lower regional tissue stress and more homogeneous gas distribution might explain the outcome effects of this treatment[14,16]. Supporting this hypothesis, serial computed tomography (CT) scans showed that prone ventilation contained the early propagation of experimental lung injury by stabilizing posterior inflation[84]. However, only 16 to 33% of patients with severe ARDS receive such treatment[3,105]. Clinicians may view prone positioning as a rescue maneuver[105] and attempt other strategies first, such as higher positive end-expiratory pressure (PEEP) or inhaled

vasodilators to increase arterial oxygenation. If injury progression diminishes the lung's ability to improve regional mechanics, delayed initiation could decrease the positive clinical impact of positional therapy. ARDS lungs become resistant to recruitment maneuvers after prolonged ventilation [106], which may explain why the effects of prone positioning on oxygenation decrease over time [54]. However, no experimental studies have prospectively assessed the evolving response of regional lung aeration to positional therapy.

Using paired prone-supine CT images in a large animal model of early lung injury, we found that reaeration and recruitment by the prone position were chiefly localized in posterior lung regions near the diaphragm [107]. In the current study, we used a similar imaging approach in ventilated pigs to test the hypothesis that lung injury progression diminishes prone positioning's ability to reaerate the lungs. In addition, we explored the variability in how regional lung mechanics respond to positioning in a small group of patients with late vs. early ARDS.

6.2. Methods

Animal Preparation and Protocol: Ten Yorkshire pigs (30.7 ± 1.1 kg) were anesthetized, intubated, and mechanically ventilated. 3.5 ml/kg of hydrochloric acid (HCl, pH 1.0) was instilled via bronchoscopy into the lobar bronchi. After a two-hour stabilization period, CT scans were obtained (Day 1). All animals were then ventilated supine for 24 hours on volume-controlled ventilation with non-protective settings: PEEP 3 cmH_2O and tidal volume (V_T) 12 ml/kg. Inspired fraction of oxygen and respiratory rate were set at 0.5 and 25 bpm, respectively, and then adjusted to arterial oxygen saturation (>90%) and $PaCO_2$

(35–45 mmHg). After 24 hours, CT was repeated (Day 2). Hemodynamic and respiratory variables were recorded. Animals were euthanized after Day 2 imaging, lung tissue samples were obtained.

Image Acquisition and Analysis: In the CT scanner, all animals were sequentially placed in both supine and prone positions in random order. After each position change, the animals received a recruitment maneuver. They were then ventilated with each of two settings that were randomly applied for 15 minutes each and followed by CT scans and physiologic measurements: low PEEP (3 cmH_2O) non-protective ventilation (V_T 12 ml/kg, rate 25 bpm), and high PEEP (15 cmH_2O) ventilation chosen to maximize lung recruitment. At high PEEP, V_T 6 ml/kg and rate 40 bpm were dialed to avoid barotrauma. Lungs were scanned during 5-second end-expiratory pauses, and images were reconstructed to a resolution of 1x1x1 mm.

To quantitatively analyze aeration changes, we first segmented lung images via validated deep-learning methodology[108] and calculated lung weights[47] and gas volumes[109]. We then registered (warped) segmented CT scans obtained in the prone position to the supine images using deformable registration to align lung borders and internal features between images, thus placing corresponding voxels on the same reference system[28]. This allowed us to measure the effects of positioning and PEEP on the density (aeration) of each voxel. Voxels were then classified as 'recruitment' or 'derecruitment', respectively, if their density decreased or increased across a threshold of -100 Hounsfield units (HU) with position or PEEP change[107].

Patients: Four patients with ARDS were imaged with electrical impedance tomography (EIT) in both prone and supine positions while volume-control ventilated with V_T 5–6 ml/kg and PEEP 15 cmH_2O. At the time of imaging, two of the patients had been ventilated for <7 days ('early ARDS') and two for >7 days ('late ARDS') [110]. Images were partitioned into 32 anterior-posterior bins [111]. For each bin, tidal ventilation and regional compliance were calculated by impedance changes.

Statistical Analysis: Statistical analysis was performed using RStudio 1.2.5001 (R Foundation for Statistical Computing; Vienna, Austria). Two-tailed paired T-tests with Bonferroni correction were performed for comparisons between time points. A mixed-effect regression model (lme4, R package) [112,113] was used to study the effects of PEEP, positioning, and their combination (fixed terms) on physiologic and imaging variables. 'Individual subject' was retained as random effect. An experiment-wide $P<0.05$ was selected as the threshold for statistical significance.

	Healthy	HCl	12h	24h
pH	7.5±0.1	7.4±0.1	7.5±0.0	7.4±0.1
Lactic Acid (mmol/L)	0.7±0.4	1.0±0.3 †	0.7±0.2 ‡	0.7±0.4
Creatinine (mg/dL)	1.8±0.4	1.8±0.2	2.0±0.3 ‡	2.0±0.5
Blood Glucose (mg/dL)	83.0±17.1	76.0±21.2	82.4±19.6	78.5±21.5
FiO_2	0.5±0.0	0.6±0.2	0.5±0.1	0.7±0.2
SpO_2 (%)	99.5±0.7	98.4±1.1 †	97.4±1.6	96.3±2.3
Respiratory Rate	22.2±2.6	22.5±2.6	22.4±3.7	22.8±5.1
Peak Inspiratory Pressure (cmH_2O)	17.6±2.4	32.4±3.3 †	34.9±6.4	41.4±6.4 §
Plateau Pressure (cmH_2O)	12.9±2.5	25.3±4.3 †	26.6±5.6	32.2±3.9 §
Mean Airway Pressure (cmH_2O)	6.3±0.7	9.3±1.1 †	9.4±1.3	12.1±2.1 §
Auto PEEP (cmH_2O)	0.1±0.3	0.5±0.7	0.6±0.7	0.3±0.5
Airway Resistance	11.1±1.2	21.8±5.5 †	18.0±6.5	21.0±9.4
Total Fluids (ml)				3162.7±1284.6
Total Urine Output (ml)				2677.6±883.6
Mean Blood Pressure (mmHg)	87.9±14.6	75.6±13.0	72.0±13.3	67.5±10.4
$ETCO_2$ (mmHg)	34.3±1.7	36.0±3.6	35.0±2.9	35.9±5.0
Heart Rate	73.5±6.1	83.9±4.6 †	83.9±16.5	92.8±20.0

Table 6.1 Physiological and laboratory values before and after lung injury and during 24 hours of non-protective ventilation. †: P<0.05 healthy vs. HCl, ‡: P<0.05 HCl vs. 12h, §: 12h vs. 24h.

6.3. Results

Lung Injury Progression: Acid aspiration worsened gas exchange and respiratory compliance after two hours, followed by further deterioration over the next 24 hours (**Table 6.1**). Analysis of tissue samples confirmed injury, which was more severe in the middle and lower lobes than in the upper. Day 1 CT images showed consolidations and ground glass opacities, which became more prominent on Day 2 (**Figure 6.1**). Lung weight increased from 764.6±74.7 to 859.9±92.0 grams of tissue (P<0.001) between Days 1 and 2.

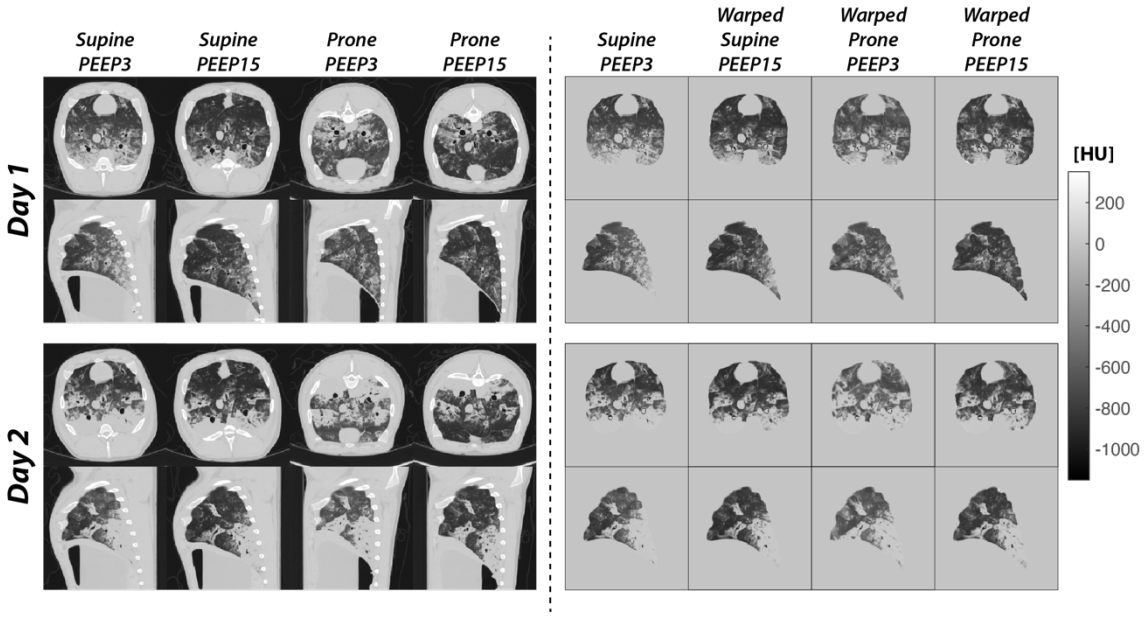

Figure 6.1 Representative axial and coronal images obtained in early acid aspiration injury (Day 1) and after 24 hours of ventilation with non-protective settings (Day 2). The left panels show the unprocessed images, which were obtained during expiratory pauses after ventilation in both supine and prone positions at two levels of PEEP. Day 2 images show the radiological progression of lung injury, with expansion of high-attenuation areas. The right panels show the same images after segmentation and registration (warping). All images were registered to the supine-low PEEP scans obtained on the same day, which were used as a reference to create high-resolution maps of the changes in aeration resulting from the tested treatments. In this figure, the warped prone images are inverted to facilitate anatomic comparisons.

Effects of Positioning and PEEP: Respiratory Parameters: On Day 1, prone vs. supine positioning increased PaO_2/FiO_2 ($P<0.001$, Cohen's $d = 1.87$) and compliance ($P<0.001$, Cohen's $d = 1.74$), while high vs. low PEEP decreased both variables. On Day 2, prone positioning slightly worsened PaO_2/FiO_2 ($P=0.003$, Cohen's $d = -1.22$) while still increasing compliance ($P=0.001$, Cohen's $d = 1.46$); high PEEP had no significant effect on PaO_2/FiO_2, but worsened compliance similarly to Day 1 ($P<0.001$, Cohen's $d = -3.19$).

$PaCO_2$ was unaffected by positioning on Day 1, but increased in the prone position on Day 2 (P=0.017, Cohen's d = 0.96). $PaCO_2$ increased at higher PEEP on both days in both positions, mostly due to the lower V_T.

Regional Aeration: After segmentation and registration (Figure 6.1), the effects of PEEP and positioning on regional lung aeration were calculated by subtracting density values between each voxel of the warped image and the spatially corresponding voxel of the low-PEEP supine scan. The resulting subtraction maps (Figure 6.2, left panels) show that, on Day 1, proning caused density to decrease (improved aeration) in the posterior-caudal lung (blue) and to increase (worse aeration) in the anterior regions (red). Raising PEEP in the supine animal improved aeration predominantly in the posterior lung. Joint application of high PEEP and prone positioning further enhanced the posterior improvement of aeration. On Day 2, the prone position and high PEEP (alone and in combination) were unable to meaningfully improve posterior and caudal aeration, while their effects on the anterior lung were similar to Day 1.

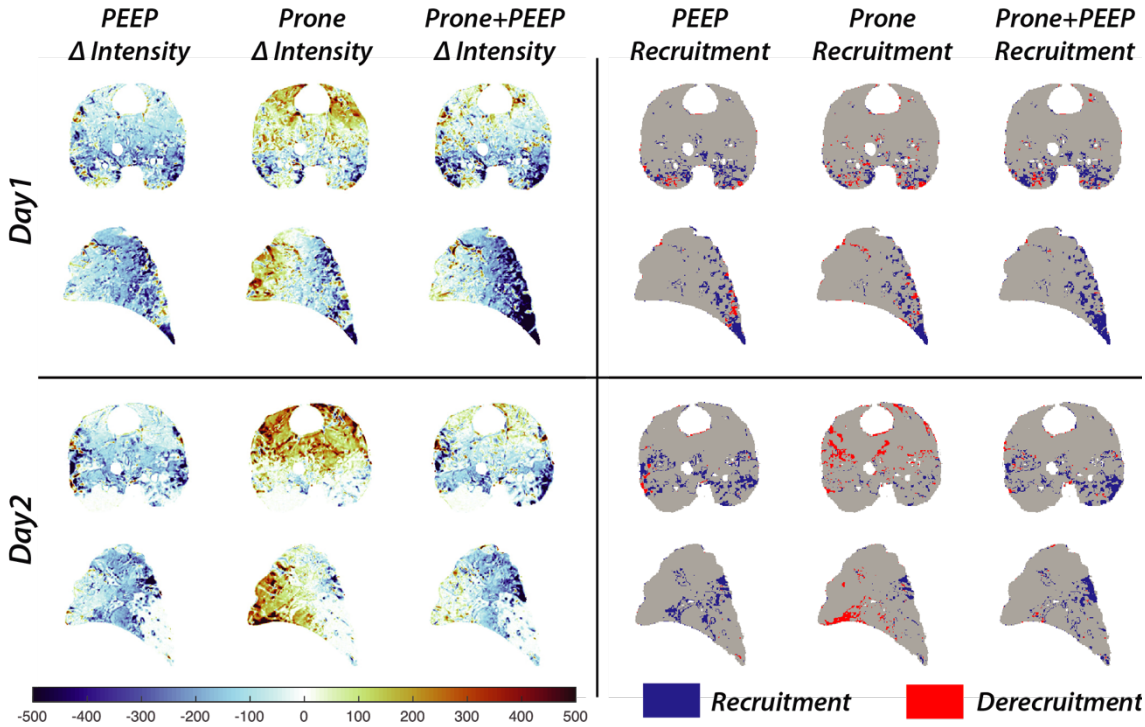

Figure 6.2 Subtraction maps display voxel-by-voxel density changes (left panels) and lung recruitment-derecruitment (right panels) on Day 1 (upper panels) and Day 2 (lower panels) of the experiment. The density changes were calculated by subtracting the CT densities of the warped images from those of the supine-low PEEP images, which were used as a reference to calculate the effects on the gas content of each voxel of high PEEP alone, prone position alone, and their joint application. Recruitment and derecruitment were mapped by identifying voxels where the CT density changes due to PEEP or positioning crossed a threshold (-100 Hounsfield Units) indicating near complete loss of aeration. Recruited voxels are shown in blue; derecruitment is shown in red.

Lung Recruitment: Voxels of tissue undergoing recruitment or derecruitment were mapped (Figure 6.2, right panels) and quantified. Most tissue recruited by the prone position was located in the posterior lung regions on Day 1, but the total amount of recruited tissue diminished from 18.9±5.2% to 7.3±1.5 % of total lung mass ($P<0.05$) on Day 2. Tissue

recruited by high PEEP was also distributed in the posterior territories on Day 1, but shifted to more anterior regions and decreased from 22.5±5.7% to 15.8±2.9 % of lung mass (P<0.05) on Day 2. Combining prone position and high PEEP enhanced recruitment vs. high PEEP alone on Day 1 (28.3±6.1% vs 22.5±5.7%, P<0.001, Cohen's *d* = 2.58), while this additional effect was smaller on Day 2 (17.7±4.2% vs 15.8±2.9%, P=0.072, Cohen's *d* = 0.90). On both days, the prone position was associated with a quota of anterior derecruitment (5.9±3.0% on Day 1, 6.5±2.8% on Day 2) which was attenuated at high PEEP.

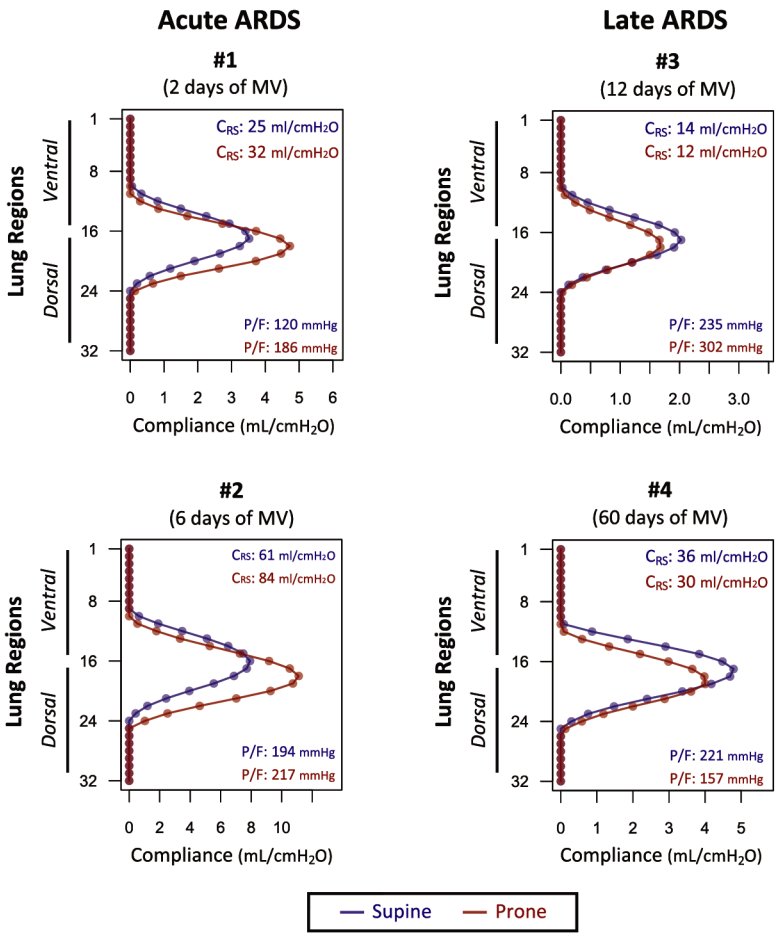

Figure 6.3 Changes in regional compliance measured by electrical impedance tomography (EIT) in 32 horizontal bins (region 1: most anterior, region 32: most posterior) in patients with early and late ARDS imaged in supine (blue) and prone (in red) positions. Global respiratory system compliance (CRS) and PaO_2/FiO_2 ratio (P/F) were added to each graph for each position. Please note that regional ventilation and compliance are measurable mostly in the central bins (e.g. 8–24), as the more peripheral bin values reflect extrapulmonary tissue impedance.

ARDS Patients: Patients were 35 to 69 years old and were ventilated for 6 to 60 days (see text in Supplemental Digital Content 1 for additional details). In patients with "early ARDS" (patients 1 and 2 in Figure 6.3), prone position increased both global respiratory system compliance and the EIT-measured compliance of the posterior bins, suggesting lung recruitment in the same areas. In "late ARDS" patients (patients 3 and 4 in Figure 6.3), global compliance was reduced in prone compared to supine position. EIT revealed that regional compliance did not improve in the posterior bins but worsened in the anterior regions.

6.4. Discussion

Overall, the results of the animal studies suggest that injury progression in ventilated lungs may lessen prone positioning's ability to improve aeration and recruit posterior lung regions. Furthermore, EIT measurements hint that prone positioning may be unable to improve posterior lung mechanics after prolonged ventilation in clinical ARDS.

Injury Progression and Regional Inflation: Our large animal model mirrored the secondary progression of a primary lung insult. Previous small animal data showed that the evolution of lung injury led to progressive loss of recruitability by PEEP[114]. Our study shows that the

lungs' ability to respond to prone positioning was similarly altered over time. To quantify these evolving responses, we performed a detailed analysis of the effects of both prone positioning and PEEP on regional lung inflation. We used our registration method to map lung density shifts with voxel-level resolution [107]. In early injury, switching position from supine to prone caused opposing changes in lung aeration in ventral vs. dorsal lung territories: a posterior-caudal region of the lungs was reinflated, while the anterior territory was deflated (Figure 6.3, left panels), as in previous observations by our group [107] and others [96]. These changes were likely due to shifts of the gravitational and non-gravitational forces that deform the lungs [18]. However, after 24 hours, the posterior lung region became resistant to these forces. Furthermore, anterior lung deflation was also visible in the prone images on the second day, with the net result of a smaller lung volume than in the supine position.

Previous studies reported that recruitment and derecruitment coexisted when changing body position [101]. Using high-resolution analysis, we showed that the net balance between these opposing events shifted during injury progression. In early injury, posterior recruitment was prominent, while derecruitment was smaller and mostly anterior. This favorable balance was likely due to smaller cross section of anterior vs. posterior lung [18]. On the second day, derecruitment by prone positioning nearly offset recruitment, suggesting that geometric factors do not guarantee the net beneficial effect of positioning when the posterior lung regions are consolidated. This evolution was paralleled by physiological changes. Recruitment in the posterior-caudal region, which was likely well perfused [78], explains the effect of positioning on oxygenation on the first day, while neither

recruitment nor PaO_2 improved in late injury. In absence of perfusion data, we cannot definitively determine whether the higher $PaCO_2$ observed in the prone vs. supine position on Day 2 was primarily related to regional hypoventilation or blood flow redistribution. This negative response could be a marker of deteriorating lung conditions. In contrast, improved $PaCO_2$ after prone positioning was associated with higher lung recruitability[115] and survival[116] in ARDS patients. Recruitment can also explain increased compliance with prone positioning on Day 1, although this mechanism does not completely account for the higher compliance also observed on Day 2, when recruitment by prone positioning was minimal. It is possible that restrained anterior inflation improved chest wall mechanics enough to offset the lack of net recruitment in the prone position[71].

Image registration enabled us to observe that, when applied separately in late injury, PEEP and prone positioning recruited non-overlapping regions of lung (Figures 6.2): tissue recruited at high PEEP was more anterior in late vs. early injury since the posterior lung had become harder to reinflate. Despite recruitment, high PEEP worsened compliance on both days of the study, which was probably due to maximized inflation in the anterior region. This state was likely associated with anterior lung hypoperfusion [117], contributing to lower oxygenation at higher PEEP.

Biologic Mechanisms: Fibroproliferative responses occur early in both human[118] and experimental[119] lung injury, and are likely involved in the loss of positional response in our patients[110]. However, fibrosis is unlikely to have measurable physiologic and radiologic consequences in the timeframe of our animal studies. Edema could explain the loss of posterior recruitability observed in our study, as suggested by the increased tissue weight,

but it is also likely that supine ventilation provoked progressive induration of lung tissue, as described in an acid aspiration model[114]. This evolution is probably mediated by protein accumulation in the airspaces and resulting surfactant deterioration[114], which increases the tendency to unrecoverable derecruitment[120].

Clinical Implications: Cornejo *et al.* showed smaller effects of positioning in ARDS patients with poorly recruitable lungs[58]. Although other factors such as origin of injury[47] are likely involved, our experimental results suggest that the stage of disease could contribute to variability of treatment responses.

The most successful clinical trial on prone positioning[12] showed a strong outcome benefit when treatment was applied within 72 hours of onset. Nevertheless, initiation of positional therapy is often delayed or replaced by other treatments with less established clinical efficacy[121]. Among other factors, incomplete knowledge of the injury-containing effects of positional therapy hinders its implementation[122]. Our experimental results provide a physiological rationale to avoid delaying treatment, corroborating reports of decreased lung recruitability in late vs. early ARDS[106]. Furthermore, we suggest posterior lung recruitability as a possible early marker of the potential clinical success of prone positioning. Animal studies by our group [84] and others show that improved inflation in the posterior lung may help contain early injury progression [33]. Future human studies could confirm the temporal evolution of such positional responses and reveal correlations with outcomes.

While our exploratory EIT measurements were performed in a small number of patients with scattered timing from ARDS onset, they nevertheless illustrate how this instrument,

although limited by low spatial resolution, can visualize the variable effects of prone positioning in human ARDS. Regional responses may be particularly relevant in obese patients, who suffer from posterior lung collapse and benefit disproportionately from positional therapy[123], or in COVID-19 patients, in whom prone positioning is used extensively[124] but in whom lung recruitability might be low [125]. Patients with reactivation of lung injury during protracted ventilation can also benefit from topographic assessment of positional inflation changes.

CHAPTER 7: TYROSINE KINASE INHIBITOR IMATINIB ALLEVIATES THE PROGRESSION OF VENTILATOR INDUCED LUNG INJURY

7.1. Introduction

Acute respiratory distress syndrome (ARDS) is a hypoxemic condition resulting from inflammatory lung injury triggered by pulmonary (e.g., pneumonia, gastric aspiration) or extrapulmonary (e.g., sepsis) insult[3,35]. Disruption of the capillary endothelial barrier initiated by local or systemic inflammation causes high-permeability edema in ARDS, resulting in airspace collapse and hypoxemia[126]. Elevated blood flow and transmural vascular pressures further compound endothelial barrier dysfunction through mechanisms of capillary stress-failure[127]. Mechanical ventilation, though required to avoid immediate death, imposes inspiratory stress on lung tissue, which is then focally amplified by loss of ventilated airspaces[128] and inhomogeneous lung aeration[120], resulting in ventilator-induced lung injury (VILI). The only strategies that improve survival, likely by limiting VILI, are protective ventilation with lower tidal volume (V_T) and sufficient positive end-expiratory pressure (PEEP)[7] and prone positioning[12].

Treatments to decrease edema could improve both hypoxemia and ARDS survival. Imatinib is a tyrosine kinase inhibitor used for chronic myeloid leukemia[129] which also protects and strengthens the endothelial cell barrier, decreasing edema in inflamed tissue[130]. It has been shown to reduce systemic capillary leak in a clinical case study[25] and improve lung injury in septic models of ARDS[23,24,131]. What is more, these studies showed that, in addition to ameliorating edema, imatinib may also improve lung inflammation[132]. However, it remains unclear whether imatinib has the ability to improve survival or

attenuate injury progression when the pulmonary epithelium is directly damaged (e.g., in aspiration pneumonitis) and the endothelium is secondarily involved[133]. Imatinib's efficacy when lung injury is compounded by mechanical ventilation is also unclear, since this drug did not consistently prevent VILI in animals[23,134]. Finally, the physiological and biological effects of imatinib require further characterization.

Most previous attempts to identify effective drug treatments for human ARDS have failed[135], but new research paradigms may be more successful[136]. In addition to better ARDS characterization, such research can benefit from intermediate-throughput pre-clinical studies that inform subsequent translational steps via improved quantification of physiologic and biologic treatment responses[137]. Sequential computed tomography (CT) enables repeat non-invasive measurements of lung injury progression, as the entire lung mass and gas volume can be quantified to measure edema and aeration loss in multiple images[30]. In our previous studies, serial CT showed that prone vs. supine ventilation slowed the radiological and physiological progression of early lung injury in a rat model where the primary insult (acid aspiration) was followed by non-protective mechanical ventilation[84]. In the current study, we used CT in this same realistic model of progressive lung injury to test the hypothesis that imatinib attenuates the evolution of pulmonary edema and its physiological consequences during mechanical ventilation, while improving survival as well as biological markers of injury severity. Some of these results have been presented in abstract form[138].

7.2. Methods

Experimental outline: All animal studies were approved by the Animal Care and Use Committee of the University of Pennsylvania (Philadelphia, PA). Figure 7.1 presents an outline of the experiments performed. 34 male Sprague-Dawley rats (341.4±33.1 g) were anesthetized, instrumented, and randomized to receive an intraperitoneal dose of either imatinib or placebo, immediately followed by lung injury and supine mechanical ventilation for up to 4 hours or animal death. CT images were obtained at healthy baseline and then hourly until the end of the experiment.

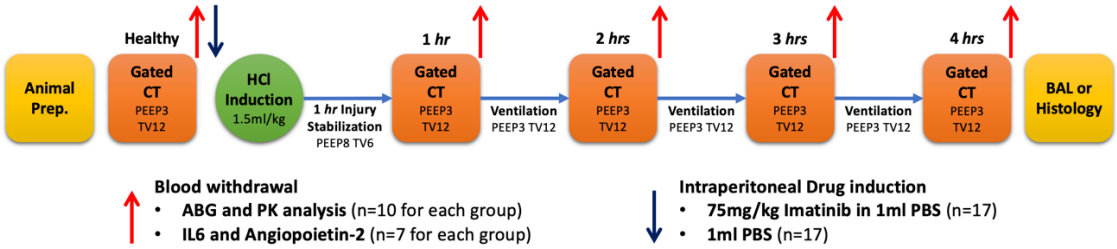

Figure 7.1 Experimental timeline in rats ventilated with non-protective ventilation after HCl instillation. After animal preparation (prep), CT was performed pre-injury. Right before HCl induction, 75mg/kg imatinib was injected into the peritoneum. HCl was injected into the trachea, followed by 1 h of stabilization with protective ventilation. Hourly CT scans were acquired during non-protective ventilation for up to 4 h after HCl, or until death. Blood was withdrawn hourly for arterial blood gas (ABG) measurements and pharmacokinetic (PK) analysis or biomarkers (IL-6 and angiopoyetin-2). Bronchoalveolar lavage (BAL) or lung tissue collection was performed at the end of each experiment.

Animal preparation: General anesthesia was induced with intraperitoneal ketamine (75-100 mg/kg) and xylazine (10 mg/kg) and maintained with boluses of ketamine every hour thereafter. Paralysis was obtained using pancuronium bromide (1mg/kg, IV) every hour.

The carotid artery was catheterized (24 gauge), the trachea was intubated with a 14-gauge catheter, and the glottis was sealed with adhesive putty to prevent gas leakage. All animals received subcutaneous (30 ml/kg) hydration with normal saline at the beginning of the experiment. Animal body temperature was maintained at 37°C using a water-based heated blanket.

Mechanical ventilation and lung injury: After instrumentation, rats were ventilated using a Servo-I ventilator set at tidal volume (V_T) 12 ml/kg, positive end expiratory pressure (PEEP) 3 cmH_2O, FiO_2 1.0, inspiratory-expiratory ratio 1:2, and frequency 50 breaths/min. Following a recruitment maneuver and baseline CT scan, lung injury was induced by sequential injection of 1.5 ml/kg hydrochloric acid (HCl, pH 1.25) through the endotracheal tube in two aliquots, in the right and left lateral positions, respectively, at a 45° head elevation. Rats were ventilated with V_T 6 ml/kg and PEEP 8 cmH_2O (protective ventilation) for the first hour after HCl to stabilize animal conditions, then with V_T 12 ml/kg and PEEP 3 cmH_2O (non-protective ventilation) for the rest of the experiment.

Imatinib dosing: Animals were randomized to receive either 75 mg/kg imatinib dissolved in 1ml PBS (n=17) or 1ml PBS (n= 17). The solution was injected in the peritoneum immediately before HCl instillation.

CT imaging: High-resolution computed tomography (CT) was performed at healthy baseline, 1 hour after HCl instillation, and every hour thereafter, using a commercial microCT scanner (eXplore CT120 system, Trifoil Imaging, Inc., Chatsworth, CA) and with identical ventilator settings (V_T 12 ml/kg, PEEP 3 cmH_2O). The scanner settings were: 80 kVp, 32 mA, 16 mS exposure time, 220 projections (half-scan), and reconstruction to 200

μm isotropic resolution. Imaging was ventilator-gated and performed during 70 ms breath-holds at end-inspiration. The total scan time was about 10 minutes. In the CT images obtained, the entire lung was semi-automatically segmented using previously developed algorithms[34]. Lung gas volume, mass, and mean intensity were then calculated[34]. Density distributions for each image were separated into four aeration compartments: hyper-aerated (-1000<HU<-900), normally aerated (-900<HU<-500), poorly aerated (-500<HU<-100), and non-aerated (-100<HU<100)[30] . All analysis was performed using MATLAB (Mathworks, Natick, MA) codes developed in the authors' laboratory[50,59].

Physiological monitoring and serum biomarker analysis: Airway pressure was continuously recorded in all animals, inspiratory plateau airway pressure (P_{plat}) was recorded during inspiratory holds, driving pressure was calculated as P_{plat} -PEEP, and respiratory system compliance was calculated as $V_T/[P_{plat}$ -PEEP]. Blood pressure was also monitored continuously. 0.3 ml arterial blood was collected from 10 rats in each group 30 min after HCl (for drug level only) and at the time of each CT scan. 0.1 ml blood was used for gas analysis, and the rest was used for drug level measurement. In the remaining 7 rats from each group, 0.3 ml blood was obtained hourly and processed to measure interleukin-6 (IL-6) and angiopoitin-2 using Quantikine ELISA kit (R&D Systems, MN).

Bronchoalveolar lavage (BAL) analysis: Rats underwent BAL (n=7 for each group) using 24 ml of 1x PBS in three separate aliquots of 8 ml each after euthanasia at the end of the experiment. Each aliquot was centrifuged (1000 G, 15 min), and supernatant was collected and frozen at -80°C. BAL protein was quantified using Bradford protein assay. BAL angiopoitin-2 (R&D Systems), TNFα (R&D Systems), and myeloperoxidase (MPO)

(Hycult Biotech) were quantified using separate rat ELISA kits. The concentration was normalized to the total amount of supernatant collected from the animals.

Histology: Lungs from 2 rats in each group that did not receive BAL were fixed with 4ml formalin, processed with paraffin, and sectioned (6 μm) into three axial slides comprehending the cranial, middle, and caudal lung, respectively. Slides were stained with hematoxylin and eosin and scored using a previously described lung injury score[139] that assigns scores for neutrophilic infiltration, airspace edema, and alveolar structure. Slides were scored blindly and decoded at the end of scoring.

Pharmacokinetics analysis: Blood samples were processed by centrifugation at 1000 G for 15 min, then supernatant was collected and stored at -80°C. The protein in serum supernatant was denatured with 26.5% acetonitrile and 73.5% 0.1M ammonium formate buffer (pH 4.5); it was then filtered with a 0.22 μM filter. Next, imatinib serum concentration was quantified by reversed-phase C18 (Agilent ZORBAX) high performance liquid chromatography (HPLC) with UV detector. Pharmacokinetic analysis was performed using noncompartmental analysis of serum blood concentrations (MATLAB). Maximum concentration (C_{max}) and time at which maximum concentration was reached (T_{max}) were averaged in each group.

Statistical analysis: Data are expressed as mean ± STD. Survival was chosen as the primary outcome of the study, and the necessary study sample size was determined using power analysis based on our previous experiments with our ventilated HCl model of injury[50,59]. Kaplan-Meier analysis was used to estimate the survival curve, and the log rank test provided the statistical comparison between groups[140]. Each longitudinal physiological and

CT parameter was fitted to a linear function starting 1 hour post-injury until death in order to quantify the effect of injurious ventilation after injury. The slope of each parameter was used to compare the trend of evolution between groups. A T-test was also used to compare groups. $P<0.05$ was considered significant for all comparisons. All calculations were performed in MATLAB.

7.3. Results

Representative CT images 1 hour after HCl (**Figure 7.2A**) showed high-density opacifications due to HCl in all rats, but these were milder in the animal that received imatinib (top series of images) than in the two untreated animals (lower images). The radiological progression of lung injury was relatively contained in the imatinib-treated animals in subsequent scans, but continued unabated in both control rats (bottom images) and was fastest in the animal that died before the end of the experiment. The survival rate was significantly higher in the imatinib group compared to controls ($P=0.018$). Kaplan-Meyer analysis **(Figure 7.2B)** shows that more than 50% of control animals died within 3 h of HCl injection, and only 2 of 17 untreated rats survived until the end of the experiment. In the imatinib-treated group, only 2 out of 17 rats died within 3 h of HCl, and 8 out of 17 survived until the end of the experiment.

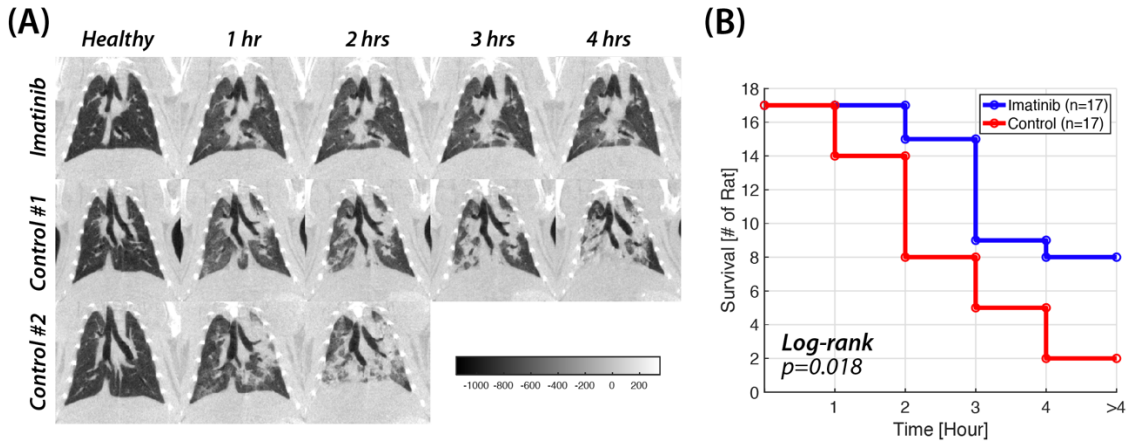

Figure 7.2 (A) Radiological injury propagation in three representative rats. CT images were obtained at healthy baseline, 1 hour after acid aspiration, and then hourly. The imatinib-treated rat showed limited injury progression on CT and survived until the end of the experiment, while the untreated rats experienced more rapid injury propagation over 4 h (control rat #1) or died after 2 h of ventilation (control rat #2). (B) The number of survival rats over the course of 3 h of non-protective ventilation. A significant decrease in mortality was observed in the imatinib cohort compared to untreated rats, with more than half of treated rats surviving until the end of the experiment. Only 2 out of 17 untreated rats survived the full 3 h, while 3 rats died within 1 h of starting ventilation.

Figure 7.3 displays the longitudinal evolution of respiratory mechanics, blood gases, and CT-derived variables. 1 hour after HCl injection, both respiratory system compliance (**Figure 7.3A**) and PaO_2/FiO_2 (**Figure 7.3B**) were lower in the control group compared to the imatinib-treated rats, while $PaCO_2$ was higher (**Figure 7.3C**). During the subsequent hour of ventilation, compliance and PaO_2/FiO_2 further decreased in controls vs. treated animals. None of the 10 control animals for which blood gases were measured survived beyond 2 hours after HCl, so no comparisons could be made beyond this point. Compared to controls, CT-derived lung mass (**Figure 7.3D**) was lower in the imatinib-treated group

1 h after HCl, while the percent fraction of non-aerated lung tissue was lower after both 1 and 2 hours (**Figure 7.3E**). Starting 1 hour after HCl, the trend of deterioration was significantly steeper in controls vs. treated rats for compliance ($P<0.02$) PaO_2/FiO_2 ($P<0.03$), $PaCO_2$ ($P<0.05$), lung gas volume ($P<0.05$), and non-aerated tissue (**Figure 7.3F**, $P<0.05$).

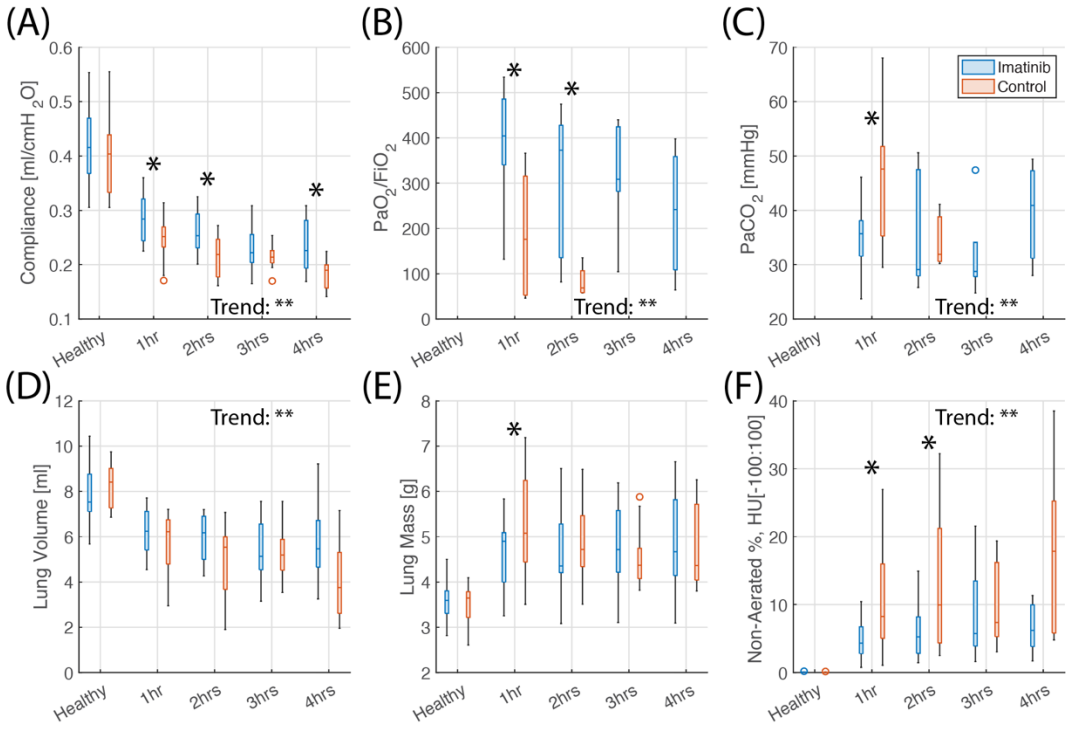

Figure 7.3 Summary statistics (median, interquartile range, and extremes of the distribution) for (A) respiratory compliance, (B) PaO_2/FiO_2, (C) $PaCO_2$, (D) lung gas volume, (E) lung mass, and (F) non-aerated lung (HU=[-100 100]) in imatinib and untreated rats over the entire experiment. *, $P<0.05$ between two groups. Trend **, $P<0.05$ between the evolution of two groups post-HCl injury.

We also found that the measured gain in lung tissue mass from healthy baseline **(Figure 7.4A)**, the driving pressure **(Figure 7.4B)**, and the percent amount of non-aerated tissue **(Figure 7.4C)** 1 hour after HCl injection correlated negatively with survival time, while there was a positive correlation between PO_2 at and survival duration at the same time point **(Figure 7.4D)**.

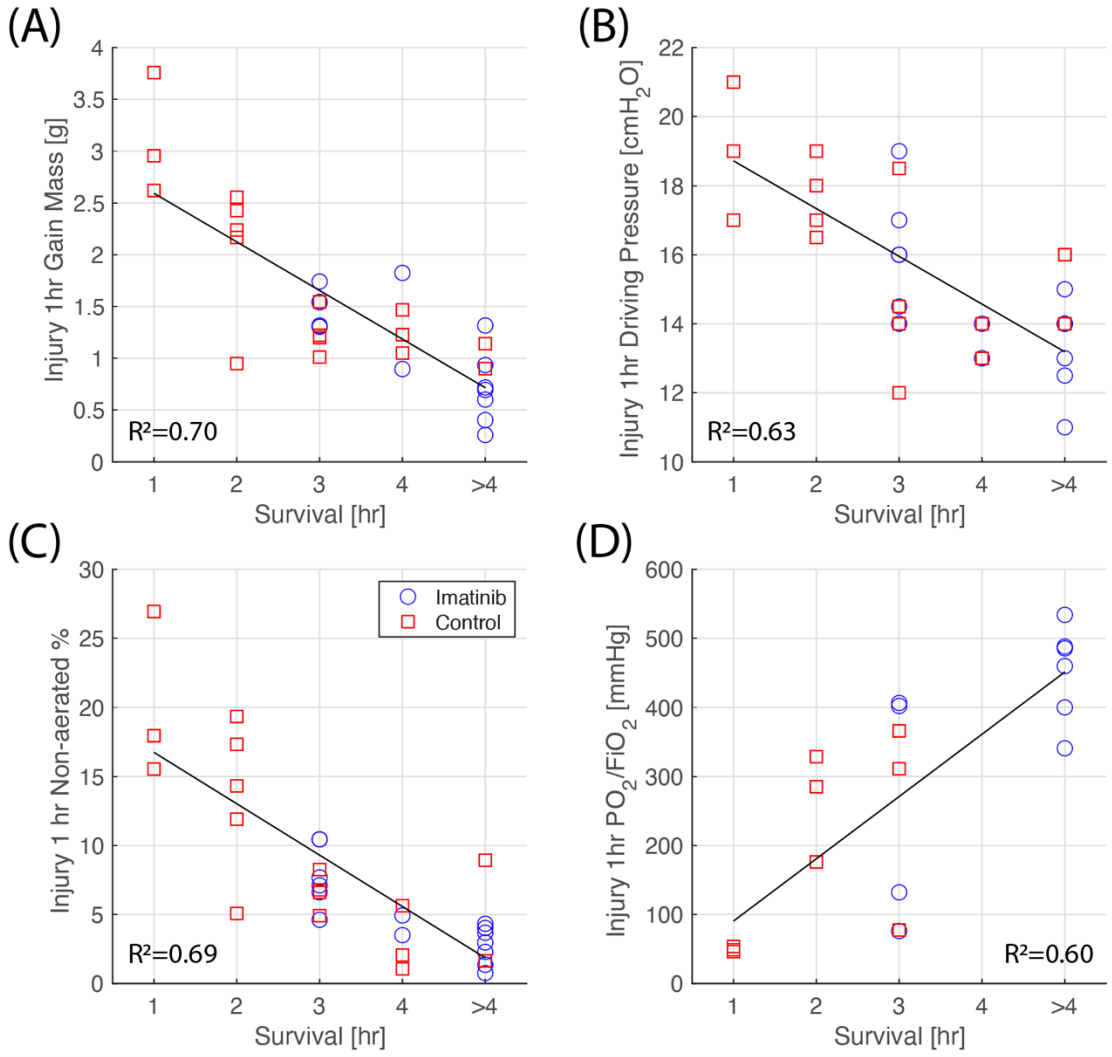

Figure 7.4 Correlations of survival time with: A) lung mass increase from healthy baseline, B) driving pressure, C) percentage of non-aerated parenchyma, and D) PaO_2/FiO_2. All variables were measured 1 hour after HCl. Imatinib group: blue circles; control group: red squares.

	BAL Ang2 (pg/mL)			BAL TNFa (pg/mL)			MPO (ng/mL)			Total protein (ug/mL)		
Imatinib (n=7)	1065.2	±	867.2	54.1	±	37.8	1122.3	±	535.0	4340.2	±	596.9
Control (n=6)	1503.3	±	825.7	278.8	±	387.9	1144.0	±	764.1	5464.9	±	531.1
P-value	NS			NS			NS			**0.04**		

Table 7.1 Group average and standard deviation of angiopoietin-2, TNF-alpha, MPO, and total protein concentration in BAL samples.

In the BAL samples, total protein concentration was significantly lower in the imatinib group compared to controls (P<0.04) **(Table 7.1)**. The mean BAL values of angiopoietin-2 and TNFα were also lower in the imatinib group, but this difference did not reach statistical significance **(Table 7.1)**. In the rats from both groups for which BAL angiopoietin-2 was measured, a positive correlation was observed between its values and the driving pressure measured at the end of the experiment (R^2=0.52) **(Figure 7.5)**. In hourly serum biomarker measurements, average IL-6 values 1 hour after HCl were doubled in the control vs. imatinib group (P<0.02) **(Table 7.2)**.

Serum IL-6 (pg/mL)															
	Healthy			1hr			2hrs			3hrs			4hrs		
Imatinib	179.9	±	234.4	3629.6	±	829.1	4267.6	±	2396.5	5946.2	±	3264.6	5872.0	±	2554.6
Control	163.3	±	179.7	6619.0	±	3179.2	5550.7	±	4125.5	3627.7	±	1820.1	3897.0	±	2974.1
P-value	NS			**0.02**			NS			NS			NS		
Serum Ang2 (pg/mL)															
	Healthy			1hr			2hrs			3hrs			4hrs		
Imatinib	11749.2	±	2811.6	14728.3	±	4674.8	15146.3	±	3224.6	20580.4	±	5010.3	24748.0	±	5255.9
Control	12145.7	±	2076.8	17747.6	±	4107.1	19574.8	±	5685.0	19200.9	±	3258.0	26465.0	±	1463.7
P-value	NS			NS			NS			NS			NS		

Table 7.2 Group average (n=7 for each group) and standard deviation of IL-6 and angiopoietin-2 in serum samples obtained at healthy baseline, injury baseline, and hourly time points.

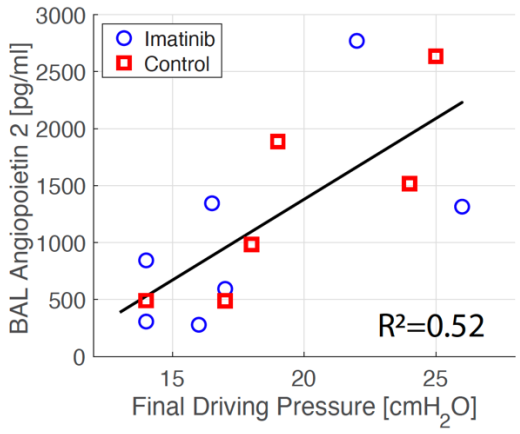

Figure 7.5 Correlation between the last value of driving pressure measured before euthanasia or death and BAL angiopoietin-2 concentration.

Imatinib concentrations were variable in the ten animals that underwent drug level testing. The mean time to peak concentration (T_{max}) was about 70 minutes and the mean peak concentration (C_{max}) was 327.9±77.5 ng/µl. The drug half-life was 150 minutes **(Figure 7.6)**.

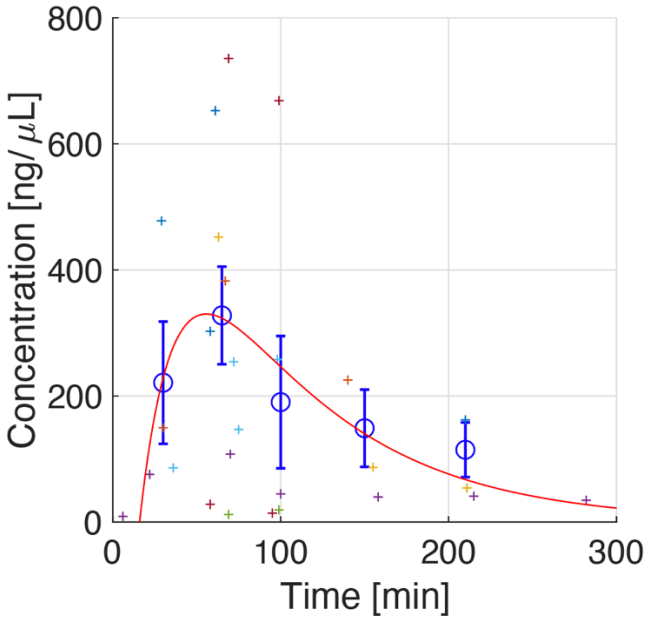

Figure 7.6 Group average and standard error of imatinib plasma concentration over the entire experiment in 10 rats treated with imatinib for which drug concentration were measured.

7.4. Discussion

Our results supported the hypothesis that imatinib improves survival and mitigates lung injury in mechanically ventilated rats, showing that: 1) imatinib reduced mortality while delaying functional and radiological injury progression; 2) imatinib attenuated edema (increase of lung tissue mass on CT) and capillary leak (BAL protein concentration); 3) treated animals had fewer histological and biological markers of inflammatory lung injury.

Because disruption of the capillary barrier is a key characteristic of ARDS[126], treatment to protect or repair endothelial function could improve outcomes. Recent studies have shown that imatinib reduces pulmonary edema, endothelial cell dysfunction, and lung

inflammation in experimental ARDS[23,24,26,131], but this is the first study demonstrating that imatinib improves survival in a model of lung injury.

Imatinib can have negative effects on tissue edema[24], and worsened VILI in a ventilated model[134]. These reported adverse actions of imatinib could hinder the clinical use of this otherwise promising drug, as the majority of ARDS patients are mechanically ventilated and thus exposed to VILI. However, the results of our study offer some reassurance that imatinib administration can be efficacious even when injured lungs are mechanically ventilated.

Imatinib administration attenuated lung injury during both stages of mechanical ventilation included in this study (**Figure 7.3**). During the first hour after HCl, animals were ventilated with protective settings (higher PEEP and lower V_T) to avoid early death due to the immediate effects of the acid, which was observed in preliminary studies. The impact of mechanical ventilation on lung injury progression was therefore likely small during this period[37]. Compared to control animals, imatinib was able to effectively limit pulmonary edema (increase of lung weight) and physiological impairment in the first hour after injury. These early effects likely contributed to reduced mortality in the later stage of the experiment. In fact, the severity of injury at 1 hour post-HCL predicted the duration of survival (**Figure 7.4**). Finally, plasma levels of IL-6 were also lower at this time point in treated vs. control animals, suggesting milder inflammatory response.

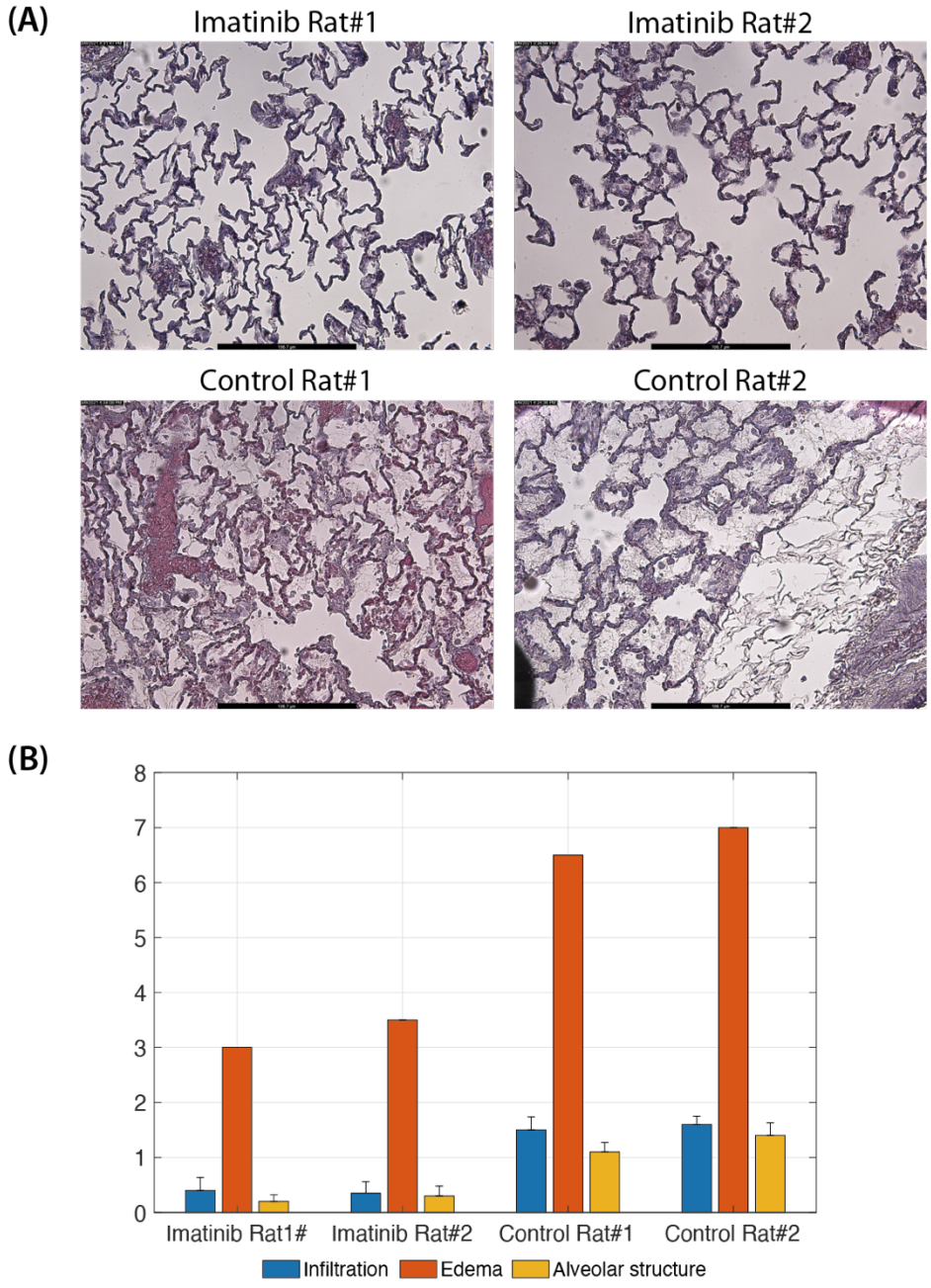

Figure 7.7 Representative Hematoxylin & Eosin stains (20x) from two representative rats in each group. The untreated group displayed edema fluid and cell infiltrates in the alveolar spaces, together with cell infiltrates in the interstitial spaces consistent with severe inflammatory status. Using a semi-quantitative score, the histograms show the extent of infiltration (blue), edema fluid (red), and alveolar structure disruption (yellow) in each rat.

Injury continued to progress after institution of non-protective ventilation (larger volume, lower PEEP): physiological variables, lung volumes, and non-aerated tissue worsened more rapidly in controls than in treated rats (**Figure 7.3**), although lung weight did not differ significantly between groups after the first hour. We note that there was significantly higher non-survival in the control group, which likely biased any differences in lung weight towards the null due to that fact that the rats with the worst pulmonary edema died. These trends suggest that, after mitigating the early effects of acid aspiration, the benefits of imatinib were maintained during subsequent non-protective ventilation. These settings likely accelerated the progression of lung injury, although our animals were ventilated with smaller V_T than the very large volumes (30 ml/kg) necessary to induce VILI in previous imatinib studies[23,134]. However, pre-injured lungs are more susceptible to mechanical stress, as shown in our previous work using a similar experimental set up[50]. In those studies, we showed that inhomogeneous and unstable inflation locally amplified lung stress in regions surrounding the initial lesions, thereby worsening injury. The fraction of lung tissue with unstable inflation was associated with injury progression and mortality[59], while ventilating rats in the prone position reduced unstable inflation and contained injury[84]. Our model here therefore recapitulates the progression of lung injury during mechanical ventilation, and imatinib retained its efficacy in this context.

Imatinib is used to treat leukemia by silencing the Bcr-Abl tyrosine-kinase[129], but also inhibits other categories of Abl, such as c-Abl and ABl related gene (Arg). Early literature suggested that inhibiting c-Abl impairs endothelial barrier function, with an opposite effect of Arg inhibition[141]. However, a more recent study in cultured human endothelial cells

suggested that imatinib affects vascular integrity by silencing Arg but not c-Abl, possibly explaining the contrasting effects of inhibiting c-Abl vs. Arg[26]. Meanwhile, multiple groups have reported the protective effect of imatinib on lung injury in studies focused mostly on septic ARDS models in cultured endothelial cells[24,26], murine LPS models[23,131], and a murine CLP model[24]. However, Letsious et al. reported a negative effect of imatinib in a murine VILI model[134], suggesting that this drug exacerbated injury via excessive cyclic stretch. Yet a separate study by the same group reported a positive effect of imatinib when using a two-hit model of LPS followed by VILI[23]. Notwithstanding the different injury models and ventilator settings, our results align with those of this second study and suggest that the effects of imatinib on lung injury could follow different mechanisms in pre-injured lungs vs. previously healthy lungs exposed to VILI. The topographic pattern of injury propagation on CT scans, observed in this study (Figure 7.2A) as well as in our previous work[50], also hints at different mechanisms of injury progression when lung stretch is imposed in the presence or absence of direct lung injury.

In this study, imatinib decreased capillary leak in treated rats, in line with the known mechanisms of endothelial protection. Our results also suggest that imatinib may exert an anti-inflammatory effect, as shown in previous studies using sepsis models—where whole lungs and cultured endothelial cells responded to imatinib with reduced expression of both interleukins and vascular cellular adhesion molecules[134], in addition to intercellular gap formation[24]. Direct epithelial damage following acid aspiration triggers alveolar cell death and surfactant depletion/inactivation causing alveolar collapse[133]. Injury mechanisms may be relatively insensitive to imatinib in such a model; however, acid aspiration also results

in endothelial damage, capillary leak, and expression of adhesion molecules[142], all of which are mechanisms targeted by imatinib. In addition, the lower concentration of BAL angiopoietin in treated animals in our study suggests the presence of endothelial damage in acid aspiration and its mitigation by imatinib. Finally, the correlation of BAL angiopoietin with driving pressure (**Figure 7.5**), an estimate of tidal lung stretch, suggests that mechanical stress may play a role in worsening endothelial dysfunction which could be mediated by mechanisms of capillary stress-failure contributing to edema[127].

Pharmacokinetic analysis performed in human leukemia studies showed that 1 ng/µl blood concentration of imatinib successfully inhibited BCR-Abl kinase. However, studies in experimental ARDS adopted a 75mg/kg intraperitoneal injection dose in mice. We adopted this same dosage in our rats and measured blood levels, which suggested that the mean peak concentration of imatinib was 327.9±77.5 ng/µl, a much higher value than what was reported in the clinical study. The half-life (150 minutes) of imatinib in rats was also much shorter than in humans (~18 hours). In addition to the exceedingly high drug levels, intraperitoneal dosing is not a realistic route of delivery in humans. Imatinib is currently formulated for oral delivery, which has a slower rise time for blood drug concentration. An intravenous imatinib formulation will therefore need to be developed for human use. Recent studies have also targeted more specific binding sites in the pulmonary endothelium, which will largely reduce the potential drug toxicity while achieving higher precision and efficacy[143].

In addition to the obvious one of being a small animal experiment, our study has several limitations. First, because imatinib was administered immediately prior to HCl instillation

in the trachea, we cannot establish whether imatinib has a therapeutic effect on established lung injury as opposed to a preemptive one. It is encouraging, however, that, imatinib reduced edema and inflammatory biomarkers when delivered after the initial injury was established in a study using lipopolysaccharide and VILI as a two-hit model of lung injury[23]. Furthermore, imatinib reached its peak concentration in our rats 70 minutes after intraperitoneal administration, suggesting that its action was extended over time and probably not at its maximum in the early stages of injury. Second, due to the design of our study, we cannot establish whether imatinib would be efficacious compared to untreated controls during extended lung protective ventilation. However, we found significant differences between groups after one hour of protective ventilation, and it is unlikely that this difference would have been attenuated if the duration of protective ventilation had been further extended.

This study adds to our existing knowledge of the effects of imatinib by demonstrating its positive effect on survival in a clinically pertinent model of lung injury ventilated with settings that, although non-protective, are not unrealistically distant from clinical practice. Furthermore, the effects of imatinib on radiological and physiological abnormalities were qualitatively comparable to those of prone positioning observed in our previous study using a similar model and experimental set up[84]. If confirmed in laboratory and clinical studies, these results are encouraging, since prone ventilation has been proven to have a major mortality benefit in ARDS[12]. While more investigation is needed to further elucidate its mechanisms of action, clinical testing of imatinib in ARDS is not implausible given both the current knowledge on its effects and its safety record in leukemia treatment. In fact,

multiple clinical trials are currently testing imatinib's use for treating both ARDS[144] and COVID pneumonia[145–147]. Finally, this study demonstrates how the combined utilization of quantitative imaging, physiologic measurements, and biomarkers in a small animal model can provide a useful platform for pre-clinical testing of candidate therapeutic molecules and treatment strategies for ARDS and other critical conditions.

CHAPTER 8: CONCLUSION AND FUTURE WORK

8.1. Conclusion

We provided visual evidence of VILI's spatial propagation: in the presence of pre-existing injury, propagation begins in regions of primary injury and spreads concentrically. In addition, we developed a method that topographically links unstable inflation, regional lung injury trajectory and outcome using paired EI–EE CT images. We then adapted our registration pipeline to directly measure and map the effects of prone position on lung density and small-scale inflation, and found that improvements in both metrics were concentrated in the dorso-caudal region of the lung. Our studies in an animal model of early vs. late injury supported the hypothesis that evolving lung injury is characterized by a time-dependent loss of aeration response to prone positioning in the posterior lung—a deterioration that likely contributes to variability in responses to positional therapy and may undermine the clinical outcome benefits of this treatment. Finally, we showed that Imatinib is capable of mitigating lung injury, reducing mortality, and attenuating pulmonary edema and capillary leak in mechanically ventilated rats. These findings have the potential to enrich clinical trials and facilitate personalized care.

8.2. Future Works

8.2.1. Imaging Pulmonary Perfusion Using Dual Energy CT (DECT)

To date, only a handful of studies have successfully visualized the pulmonary circulation in ARDS patients. Our future goal is to integrate maps of inflation mechanics and pulmonary perfusion using Dual energy CT (DECT) in order to phenotype ARDS and

guide treatment strategies. Imaging pulmonary circulation requires accurate, non-invasive instruments. DECT visualizes perfusion by mapping pulmonary blood flow (PBF) and perfused blood volume (PBV) after contrast injection[148,149]. PBV is more suitable for clinical investigation[150] compared to PBF, as it yields whole-lung (vs. slice) images with lower radiation doses. In an effort to develop CT-based markers of lung injury severity[59,84], we generated preliminary data combining high-resolution PBV and PBF maps with inflation scans to comprehensively assess regional perfusion and lung stretch. We hypothesized that locally elevated perfusion contributes to both endothelial damage and more severe edema in injured lungs with uneven perfusion. If this is the case, treatments to improve the homogeneity of pulmonary perfusion and protect the endothelial barrier could attenuate the progression of lung injury.

8.2.2. Testing the Efficacy of Imatinib on Ischemia Reperfusion Injury (IRI)

Ischemia reperfusion injury (IRI) is an inevitable process that can lead to major clinical complications during lung transplantation[151]. For example, severe IRI leads to primary graft dysfunction (PGD), which is itself associated with elevated risk of bronchiolitis obliterans syndrome (BOS)[152,153]—both of which contribute significantly to poor post-transplant survival. IRI typically develops as a result of elevated oxidative stress and endothelial damage during ischemia and reperfusion. As a tyrosine kinase c-Abl inhibitor, Imatinib protects endothelial barriers, and studies have demonstrated the protective effects of Imatinib on inflammation and IRI in both rodent[154] and rabbit[155] lungs. We plan to test Imatinib's efficacy during ex-vivo lung perfusion (EVLP) in a clinically relevant model of VILI, and anticipate that it will significantly lessen IRI by reducing vascular leakage. The

EVLP lungs will eventually be transplanted, and long-term survival of recipient animals will be monitored and evaluated, in addition to other outcome measures.

REFERENCES

1 Matthay MA, Ware LB, Zimmerman GA. The acute respiratory distress syndrome. *J Clin Invest* 2012;**122**:2731–40. https://doi.org/10.1172/JCI60331;

2 Rubenfeld GD, Caldwell E, Peabody E, Weaver J, Martin DP, Neff M, Stern EJ, Hudson LD. Incidence and Outcomes of Acute Lung Injury. *N Engl J Med* 2005;**353**:1685–93. https://doi.org/10.1056/NEJMoa050333.

3 Bellani G, Laffey JG, Pham T, Fan E, Brochard L, Esteban A, Gattinoni L, van Haren F, Larsson A, McAuley DF, Ranieri M, Rubenfeld G, Thompson BT, Wrigge H, Slutsky AS, Pesenti A, Investigators LS, Group ET. Epidemiology, Patterns of Care, and Mortality for Patients With Acute Respiratory Distress Syndrome in Intensive Care Units in 50 Countries. *JAMA* 2016;**315**:788–800. https://doi.org/10.1001/jama.2016.0291.

4 Grasselli G, Greco M, Zanella A, Albano G, Antonelli M, Bellani G, Bonanomi E, Cabrini L, Carlesso E, Castelli G, Cattaneo S, Cereda D, Colombo S, Coluccello A, Crescini G, Forastieri Molinari A, Foti G, Fumagalli R, Iotti GA, Langer T, Latronico N, Lorini FL, Mojoli F, Natalini G, Pessina CM, Ranieri VM, Rech R, Scudeller L, Rosano A, Storti E, *et al.* Risk Factors Associated With Mortality Among Patients With COVID-19 in Intensive Care Units in Lombardy, Italy. *JAMA Intern Med* 2020;**180**:1345–55. https://doi.org/10.1001/jamainternmed.2020.3539.

5 Ashbaugh DavidG, Boyd Bigelow D, Petty ThomasL, Levine BernardE. ACUTE RESPIRATORY DISTRESS IN ADULTS. *The Lancet* 1967;**290**:319–23. https://doi.org/10.1016/S0140-6736(67)90168-7.

6 Pham T, Rubenfeld GD. Fifty years - The Epidemiology of Acute Respiratory Distress Syndrome. A 50th Birthday Review. *Am J Respir Crit Care Med* 2017;**195**:860–70. https://doi.org/10.1164/rccm.201609-1773CP.

7 Acute Respiratory Distress Syndrome Network, Brower RG, Matthay MA, Morris A, Schoenfeld D, Thompson BT, Wheeler A. Ventilation with lower tidal volumes as compared with traditional tidal volumes for acute lung injury and the acute respiratory distress syndrome. *N Engl J Med* 2000;**342**:1301–8. https://doi.org/10.1056/NEJM200005043421801.

8 Rubenfeld GD, Herridge MS. Epidemiology and outcomes of acute lung injury. *Chest* 2007;**131**:554–62. https://doi.org/10.1378/chest.06-1976.

9 Prescott HC, Calfee CS, Thompson BT, Angus DC, Liu VX. Toward Smarter Lumping and Smarter Splitting: Rethinking Strategies for Sepsis and Acute Respiratory Distress Syndrome Clinical Trial Design. *Am J Respir Crit Care Med* 2016;**194**:147–55. https://doi.org/10.1164/rccm.201512-2544CP.

10 Slutsky AS, Ranieri VM. Ventilator-Induced Lung Injury. *N Engl J Med* 2013;**369**:2126–36. https://doi.org/10.1056/NEJMra1208707.

11 Beitler JR, Malhotra A, Thompson BT. Ventilator-induced Lung Injury. *Clin Chest Med* 2016. https://doi.org/10.1016/j.ccm.2016.07.004.

12 Guérin C, Reignier J, Richard J-C, Beuret P, Gacouin A, Boulain T, Mercier E, Badet M, Mercat A, Baudin O, Clavel M, Chatellier D, Jaber S, Rosselli S, Mancebo J, Sirodot M, Hilbert G, Bengler C, Richecoeur J, Gainnier M, Bayle F, Bourdin G, Leray V, Girard R, Baboi L, Ayzac L. Prone Positioning in Severe Acute Respiratory Distress Syndrome. *N Engl J Med* 2013;**368**:2159–68. https://doi.org/10.1056/NEJMoa1214103.

13 Sud S, Friedrich JO, Taccone P, Polli F, Adhikari NKJ, Latini R, Pesenti A, Guérin C, Mancebo J, Curley MAQ, Fernandez R, Chan M-C, Beuret P, Voggenreiter G, Sud M, Tognoni G, Gattinoni L. Prone ventilation reduces mortality in patients with acute respiratory

failure and severe hypoxemia: systematic review and meta-analysis. *Intensive Care Med* 2010;**36**:585–99. https://doi.org/10.1007/s00134-009-1748-1.
14 Gattinoni L, Pelosi P, Vitale G, Pesenti A, D'Andrea L, Mascheroni D. Body position changes redistribute lung computed-tomographic density in patients with acute respiratory failure. *Anesthesiology* 1991;**74**:15–23.
15 MUTOH T, Guest J, Lamm JE, Albert RK. Prone Position Alters the Effect of Volume Overload on Regional Pleural Pressures and Improves Hypoxemia in Pigs In ViV01, 2. *Am Rev Respir Dis* 1992;**146**:300–6.
16 Motta-Ribeiro GC, Hashimoto S, Winkler T, Baron RM, Grogg K, Paula LFSC, Santos A, Zeng C, Hibbert K, Harris RS, Bajwa E, Vidal Melo MF. Deterioration of Regional Lung Strain and Inflammation during Early Lung Injury. *Am J Respir Crit Care Med* 2018;**198**:891–902. https://doi.org/10.1164/rccm.201710-2038OC.
17 Perchiazzi G, Rylander C, Vena A, Derosa S, Polieri D, Fiore T, Giuliani R, Hedenstierna G. Lung regional stress and strain as a function of posture and ventilatory mode. *J Appl Physiol* 2011;**110**:1374–83. https://doi.org/10.1152/japplphysiol.00439.2010.
18 Hubmayr RD, Walters BJ, Chevalier PA, Rodarte JR, Olson LE. Topographical distribution of regional lung volume in anesthetized dogs. *J Appl Physiol* 1983;**54**:1048–56. https://doi.org/10.1152/jappl.1983.54.4.1048.
19 Guo L, Wei D, Zhang X, Wu Y, Li Q, Zhou M, Qu J. Clinical Features Predicting Mortality Risk in Patients With Viral Pneumonia: The MuLBSTA Score. *Front Microbiol* 2019;**10**:2752–2752. https://doi.org/10.3389/fmicb.2019.02752.
20 Artigas A, Camprubí-Rimblas M, Tantinyà N, Bringué J, Guillamat-Prats R, Matthay MA. Inhalation therapies in acute respiratory distress syndrome. *Ann Transl Med* 2017;**5**:. https://doi.org/10.21037/atm.2017.07.21.
21 Peter JV, John P, Graham PL, Moran JL, George IA, Bersten A. Corticosteroids in the prevention and treatment of acute respiratory distress syndrome (ARDS) in adults: meta-analysis. *BMJ* 2008;**336**:1006–9. https://doi.org/10.1136/bmj.39537.939039.BE.
22 McAuley DF, Laffey JG, O'Kane CM, Perkins GD, Mullan B, Trinder TJ, Johnston P, Hopkins PA, Johnston AJ, McDowell C, McNally C, Investigators H-, Irish Critical Care Trials G. Simvastatin in the acute respiratory distress syndrome. *N Engl J Med* 2014;**371**:1695–703. https://doi.org/10.1056/NEJMoa1403285.
23 Rizzo AN, Sammani S, Esquinca AE, Jacobson JR, Garcia JGN, Letsiou E, Dudek SM. Imatinib attenuates inflammation and vascular leak in a clinically relevant two-hit model of acute lung injury. *Am J Physiol-Lung Cell Mol Physiol* 2015;**309**:L1294–304. https://doi.org/10.1152/ajplung.00031.2015.
24 Aman J, Bezu J van, Damanafshan A, Huveneers S, Eringa EC, Vogel SM, Groeneveld ABJ, Noordegraaf AV, Hinsbergh VWM van, Amerongen GP van N. Effective Treatment of Edema and Endothelial Barrier Dysfunction With Imatinib. *Circulation* 2012.
25 Aman J, Peters MJL, Weenink C, van Nieuw Amerongen GP, Vonk Noordegraaf A. Reversal of Vascular Leak with Imatinib. *Am J Respir Crit Care Med* 2013;**188**:1171–3. https://doi.org/10.1164/rccm.201301-0136LE.
26 Rizzo AN, Belvitch P, Demeritte R, Garcia JGN, Letsiou E, Dudek SM. Arg mediates LPS-induced disruption of the pulmonary endothelial barrier. *Vascul Pharmacol* 2020;**128–129**:106677. https://doi.org/10.1016/j.vph.2020.106677.
27 Simon BA KD. Bankier AA, Parraga G: What can computed tomography and magnetic resonance imaging tell us about ventilation? *J Appl Physiol* 1985:113–647.
28 Tustison NJ, Avants BB. Explicit B-spline regularization in diffeomorphic image registration. *Front Neuroinformatics* 2013;**7**:. https://doi.org/10.3389/fninf.2013.00039.

29 Frank JA, Parsons PE, Matthay MA. Pathogenetic significance of biological markers of ventilator-associated lung injury in experimental and clinical studies. *Chest* 2006;**130**:1906–14. https://doi.org/10.1378/chest.130.6.1906.
30 Gattinoni L, Pesenti A, Avalli L, Rossi F, Bombino M. Pressure-volume curve of total respiratory system in acute respiratory failure. Computed tomographic scan study. *Am Rev Respir Dis* 1987;**136**:730–6. https://doi.org/10.1164/ajrccm/136.3.730.
31 Bellani G, Guerra L, Musch G, Zanella A, Patroniti N, Mauri T, Messa C, Pesenti A. Lung Regional Metabolic Activity and Gas Volume Changes Induced by Tidal Ventilation in Patients with Acute Lung Injury. *Am J Respir Crit Care Med* 2011;**183**:1193–9. https://doi.org/10.1164/rccm.201008-1318OC.
32 Tsuchida S, Engelberts D, Peltekova V, Hopkins N, Frndova H, Babyn P, McKerlie C, Post M, McLoughlin P, Kavanagh BP. Atelectasis causes alveolar injury in nonatelectatic lung regions. *Am J Respir Crit Care Med* 2006;**174**:279–89. https://doi.org/10.1164/rccm.200506-1006OC.
33 Broccard A, Shapiro RS, Schmitz LL, Adams AB, Nahum A, Marini JJ. Prone positioning attenuates and redistributes ventilator-induced lung injury in dogs. *Crit Care Med* 2000;**28**:295–303.
34 Xin Y, Song G, Cereda M, Kadlecek S, Hamedani H, Jiang Y, Rajaei J, Clapp J, Profka H, Meeder N, Wu J, Tustison NJ, Gee JC, Rizi RR. Semiautomatic segmentation of longitudinal computed tomography images in a rat model of lung injury by surfactant depletion. *J Appl Physiol* 2015;**118**:377–85. https://doi.org/10.1152/japplphysiol.00627.2014.
35 ARDS Definition Task Force, Ranieri VM, Rubenfeld GD, Thompson BT, Ferguson ND, Caldwell E, Fan E, Camporota L, Slutsky AS. Acute respiratory distress syndrome: the Berlin Definition. *JAMA* 2012;**307**:2526–33. https://doi.org/10.1001/jama.2012.5669.
36 Malbouisson LM, Muller JC, Constantin JM, Lu Q, Puybasset L, Rouby JJ, CT Scan ARDS Study Group. Computed tomography assessment of positive end-expiratory pressure-induced alveolar recruitment in patients with acute respiratory distress syndrome. *Am J Respir Crit Care Med* 2001;**163**:1444–50. https://doi.org/10.1164/ajrccm.163.6.2005001.
37 Frank JA, Gutierrez JA, Jones KD, Allen L, Dobbs L, Matthay MA. Low tidal volume reduces epithelial and endothelial injury in acid-injured rat lungs. *Am J Respir Crit Care Med* 2002;**165**:242–9.
38 Mattingley JS, Holets SR, Oeckler RA, Stroetz RW, Buck CF, Hubmayr RD. Sizing the lung of mechanically ventilated patients. *Crit Care Lond Engl* 2011;**15**:R60. https://doi.org/10.1186/cc10034.
39 Terragni PP, Rosboch G, Tealdi A, Corno E, Menaldo E, Davini O, Gandini G, Herrmann P, Mascia L, Quintel M, Slutsky AS, Gattinoni L, Ranieri VM. Tidal hyperinflation during low tidal volume ventilation in acute respiratory distress syndrome. *Am J Respir Crit Care Med* 2007;**175**:160–6. https://doi.org/10.1164/rccm.200607-915OC.
40 González-López A, García-Prieto E, Batalla-Solís E, Amado-Rodríguez L, Avello N, Blanch L, Albaiceta GM. Lung strain and biological response in mechanically ventilated patients. *Intensive Care Med* 2012;**38**:240–7. https://doi.org/10.1007/s00134-011-2403-1.
41 Cressoni M, Cadringher P, Chiurazzi C, Amini M, Gallazzi E, Marino A, Brioni M, Carlesso E, Chiumello D, Quintel M, Bugedo G, Gattinoni L. Lung inhomogeneity in patients with acute respiratory distress syndrome. *Am J Respir Crit Care Med* 2014;**189**:149–58. https://doi.org/10.1164/rccm.201308-1567OC.
42 Serpa Neto A, Cardoso SO, Manetta JA, Pereira VG, Esposito DC, Pasqualucci Mde O, Damasceno MC, Schultz MJ. Association between use of lung-protective ventilation with lower tidal volumes and clinical outcomes among patients without acute respiratory distress

syndrome: a meta-analysis. *JAMA J Am Med Assoc* 2012;**308**:1651–9. https://doi.org/10.1001/jama.2012.13730;
43 Richard JC, Maggiore SM, Jonson B, Mancebo J, Lemaire F, Brochard L. Influence of tidal volume on alveolar recruitment. Respective role of PEEP and a recruitment maneuver. *Am J Respir Crit Care Med* 2001;**163**:1609–13. https://doi.org/10.1164/ajrccm.163.7.2004215.
44 Kallet RH, Luce JM. Detection of patient-ventilator asynchrony during low tidal volume ventilation, using ventilator waveform graphics. *Respir Care* 2002;**47**:183–5.
45 Rubenfeld GD. Confronting the frustrations of negative clinical trials in acute respiratory distress syndrome. *Ann Am Thorac Soc* 2015;**12 Suppl 1**:S58-63. https://doi.org/10.1513/AnnalsATS.201409-414MG.
46 *ARDS: the non-homogeneous lung; facts and hypothesis – ScienceOpen*. n.d. URL: https://www.scienceopen.com/document?vid=6bdb09ff-89e4-4dc4-8c1b-ad58646c489e (Accessed 16 July 2021).
47 Gattinoni L, Caironi P, Cressoni M, Chiumello D, Ranieri VM, Quintel M, Russo S, Patroniti N, Cornejo R, Bugedo G. Lung Recruitment in Patients with the Acute Respiratory Distress Syndrome. *N Engl J Med* 2006;**354**:1775–86. https://doi.org/10.1056/NEJMoa052052.
48 Murphy K, van Ginneken B, Reinhardt JM, Kabus S, Ding K, Deng X, Cao K, Du K, Christensen GE, Garcia V, Vercauteren T, Ayache N, Commowick O, Malandain G, Glocker B, Paragios N, Navab N, Gorbunova V, Sporring J, de Bruijne M, Han X, Heinrich MP, Schnabel JA, Jenkinson M, Lorenz C, Modat M, McClelland JR, Ourselin S, Muenzing SEA, Viergever MA, *et al.* Evaluation of registration methods on thoracic CT: the EMPIRE10 challenge. *IEEE Trans Med Imaging* 2011;**30**:1901–20. https://doi.org/10.1109/TMI.2011.2158349.
49 Galbán CJ, Han MK, Boes JL, Chughtai KA, Meyer CR, Johnson TD, Galbán S, Rehemtulla A, Kazerooni EA, Martinez FJ, Ross BD. Computed tomography–based biomarker provides unique signature for diagnosis of COPD phenotypes and disease progression. *Nat Med* 2012;**18**:1711–5. https://doi.org/10.1038/nm.2971.
50 Cereda M, Xin Y, Meeder N, Zeng J, Jiang Y, Hamedani H, Profka H, Kadlecek S, Clapp J, Deshpande CG, Wu J, Gee JC, Kavanagh BP, Rizi RR. Visualizing the Propagation of Acute Lung Injury. *Anesthesiology* 2016;**124**:121–31. https://doi.org/10.1097/ALN.0000000000000916.
51 Chung JH, Kradin RL, Greene RE, Shepard J-AO, Digumarthy SR. CT predictors of mortality in pathology confirmed ARDS. *Eur Radiol* 2011;**21**:730–7. https://doi.org/10.1007/s00330-010-1979-0.
52 Ichikado K, Muranaka H, Gushima Y, Kotani T, Nader HM, Fujimoto K, Johkoh T, Iwamoto N, Kawamura K, Nagano J, Fukuda K, Hirata N, Yoshinaga T, Ichiyasu H, Tsumura S, Kohrogi H, Kawaguchi A, Yoshioka M, Sakuma T, Suga M. Fibroproliferative changes on high-resolution CT in the acute respiratory distress syndrome predict mortality and ventilator dependency: a prospective observational cohort study. *BMJ Open* 2012;**2**:e000545. https://doi.org/10.1136/bmjopen-2011-000545.
53 Ventilation with Lower Tidal Volumes as Compared with Traditional Tidal Volumes for Acute Lung Injury and the Acute Respiratory Distress Syndrome. *N Engl J Med* 2000;**342**:1301–8. https://doi.org/10.1056/NEJM200005043421801.
54 Gattinoni L, Tognoni G, Pesenti A, Taccone P, Mascheroni D, Labarta V, Malacrida R, Di Giulio P, Fumagalli R, Pelosi P, others. Effect of prone positioning on the survival of patients with acute respiratory failure. *N Engl J Med* 2001;**345**:568–73.
55 Albert RK, Keniston A, Baboi L, Ayzac L, Guérin C. Prone position–induced improvement in gas exchange does not predict improved survival in the acute respiratory distress syndrome. *Am J Respir Crit Care Med* 2014;**189**:494–6.

56 Pelosi P, Brazzi L, Gattinoni L. Prone position in acute respiratory distress syndrome. *Eur Respir J* 2002;**20**:1017–28. https://doi.org/10.1183/09031936.02.00401702.
57 Musch G, Layfield JDH, Harris RS, Melo MFV, Winkler T, Callahan RJ, Fischman AJ, Venegas JG. Topographical distribution of pulmonary perfusion and ventilation, assessed by PET in supine and prone humans. *J Appl Physiol* 2002;**93**:1841–51. https://doi.org/10.1152/japplphysiol.00223.2002.
58 Cornejo RA, Díaz JC, Tobar EA, Bruhn AR, Ramos CA, González RA, Repetto CA, Romero CM, Gálvez LR, Llanos O, Arellano DH, Neira WR, Díaz GA, Zamorano AJ, Pereira GL. Effects of Prone Positioning on Lung Protection in Patients with Acute Respiratory Distress Syndrome. *Am J Respir Crit Care Med* 2013;**188**:440–8. https://doi.org/10.1164/rccm.201207-1279OC.
59 Cereda M, Xin Y, Hamedani H, Bellani G, Kadlecek S, Clapp J, Guerra L, Meeder N, Rajaei J, Tustison NJ, Gee JC, Kavanagh BP, Rizi RR. Tidal changes on CT and progression of ARDS. *Thorax* 2017:thoraxjnl-2016-209833. https://doi.org/10.1136/thoraxjnl-2016-209833.
60 Xin Y, Cereda M, Hamedani H, Siddiqui S, Pourfathi M, Itkin-Ofer M, Turner S, Meeder N, Kadlecek S, Clapp J, Hughes L, Roberts A, Bey Q, Rodriguez A, Drachman N, Duncan I, Profka H, Tustison N, Gee J, Kavanagh BP, Rizi RR. Parametric Response Maps to Measure the Effects of Prone Position in Pigs with Experimental Lung Injury. *B54 Crit. CARE GOLDILOCKS Syndr. - Get. Press. VENT JUST RIGHT ARDS ACUTE Respir. Fail.* American Thoracic Society; 2017. p. A3749–A3749.
61 Xin Y, Cereda M, Hamedani H, Siddiqui S, Pourfathi M, Itkin-Ofer M, Turner S, Meeder N, Kadlecek S, Clapp J, Hughes L, Roberts A, Bey Q, Rodriguez A, Duncan I, Drachman N, Profka H, Tustison N, Gee J, Kavanagh BP, Rizi RR. Parametric Response Mapping Detects Distribution of Abnormal Lung Inflation in Pneumonia and Acid Aspiration. *B54 Crit. CARE GOLDILOCKS Syndr. - Get. Press. VENT JUST RIGHT ARDS ACUTE Respir. Fail.* American Thoracic Society; 2017. p. A3750–A3750.
62 Cereda M, Emami K, Xin Y, Kadlecek S, Kuzma NN, Mongkolwisetwara P, Profka H, Pickup S, Ishii M, Kavanagh BP, Deutschman CS, Rizi RR. Imaging the Interaction of Atelectasis and Overdistension in Surfactant-Depleted Lungs*: *Crit Care Med* 2013;**41**:527–35. https://doi.org/10.1097/CCM.0b013e31826ab1f2.
63 Avants B, Epstein C, Grossman M, Gee J. Symmetric diffeomorphic image registration with cross-correlation: Evaluating automated labeling of elderly and neurodegenerative brain. *Med Image Anal* 2008;**12**:26–41. https://doi.org/10.1016/j.media.2007.06.004.
64 Song G, Tustison N, Avants B, Gee JC. Lung CT image registration using diffeomorphic transformation models. *Med Image Anal Clin Gd Chall* 2010:23–32.
65 Bryan AC. Comments of a devil's advocate. *Am Rev Respir Dis* 1974;**110**:143–4.
66 Blanch L, Mancebo J, Perez M, Martinez M, Mas A, Betbese AJ, Joseph D, Ballús J, Lucangelo U, Bak E. Short-term effects of prone position in critically ill patients with acute respiratory distress syndrome. *Intensive Care Med* 1997;**23**:1033–9.
67 Langer M, Mascheroni D, Marcolin R, Gattinoni L. The Prone Position in ARDS Patients. *Chest* 1988;**94**:103–7. https://doi.org/10.1378/chest.94.1.103.
68 Cereda M, Emami K, Kadlecek S, Xin Y, Mongkolwisetwara P, Profka H, Barulic A, Pickup S, Mansson S, Wollmer P, Ishii M, Deutschman CS, Rizi RR. Quantitative imaging of alveolar recruitment with hyperpolarized gas MRI during mechanical ventilation. *J Appl Physiol* 2011;**110**:499–511. https://doi.org/10.1152/japplphysiol.00841.2010.
69 Cereda M, Xin Y, Hamedani H, Clapp J, Kadlecek S, Meeder N, Zeng J, Profka H, Kavanagh BP, Rizi RR. Mild loss of lung aeration augments stretch in healthy lung regions. *J Appl Physiol* 2016;**120**:444–54. https://doi.org/10.1152/japplphysiol.00734.2015.

70 Chiumello D, Marino A, Brioni M, Cigada I, Menga F, Colombo A, Crimella F, Algieri I, Cressoni M, Carlesso E, Gattinoni L. Lung Recruitment Assessed by Respiratory Mechanics and Computed Tomography in Patients with Acute Respiratory Distress Syndrome. What Is the Relationship? *Am J Respir Crit Care Med* 2016;**193**:1254–63. https://doi.org/10.1164/rccm.201507-1413OC.
71 Galiatsou E, Kostanti E, Svarna E, Kitsakos A, Koulouras V, Efremidis SC, Nakos G. Prone Position Augments Recruitment and Prevents Alveolar Overinflation in Acute Lung Injury. *Am J Respir Crit Care Med* 2006;**174**:187–97. https://doi.org/10.1164/rccm.200506-899OC.
72 Richter T, Bellani G, Harris RS, Melo MFV, Winkler T, Venegas JG, Musch G. Effect of Prone Position on Regional Shunt, Aeration, and Perfusion in Experimental Acute Lung Injury. *Am J Respir Crit Care Med* 2005;**172**:480–7. https://doi.org/10.1164/rccm.200501-004OC.
73 Valenza F, Guglielmi M, Maffioletti M, Tedesco C, Maccagni P, Fossali T, Aletti G, Porro GA, Irace M, Carlesso E, Carboni N, Lazzerini M, Gattinoni L. Prone position delays the progression of ventilator-induced lung injury in rats: Does lung strain distribution play a role?*: *Crit Care Med* 2005;**33**:361–7. https://doi.org/10.1097/01.CCM.0000150660.45376.7C.
74 Broccard AF, Shapiro RS, Schmitz LL, Ravenscraft SA, Marini JJ. Influence of prone position on the extent and distribution of lung injury in a high tidal volume oleic acid model of acute respiratory distress syndrome. *Crit Care Med* n.d.;**25**:16–27.
75 Goligher EC, Kavanagh BP, Rubenfeld GD, Adhikari NKJ, Pinto R, Fan E, Brochard LJ, Granton JT, Mercat A, Marie Richard J-C, Chretien J-M, Jones GL, Cook DJ, Stewart TE, Slutsky AS, Meade MO, Ferguson ND. Oxygenation response to positive end-expiratory pressure predicts mortality in acute respiratory distress syndrome. A secondary analysis of the LOVS and ExPress trials. *Am J Respir Crit Care Med* 2014;**190**:70–6. https://doi.org/10.1164/rccm.201404-0688OC.
76 Wang X-T, Ding X, Zhang H-M, Chen H, Su L-X, Liu D-W, Chinese Critical Ultrasound Study Group (CCUSG). Lung ultrasound can be used to predict the potential of prone positioning and assess prognosis in patients with acute respiratory distress syndrome. *Crit Care Lond Engl* 2016;**20**:385. https://doi.org/10.1186/s13054-016-1558-0.
77 Mauri T, Eronia N, Turrini C, Battistini M, Grasselli G, Rona R, Volta CA, Bellani G, Pesenti A. Bedside assessment of the effects of positive end-expiratory pressure on lung inflation and recruitment by the helium dilution technique and electrical impedance tomography. *Intensive Care Med* 2016;**42**:1576–87. https://doi.org/10.1007/s00134-016-4467-4.
78 Altemeier WA, McKinney S, Krueger M, Glenny RW. Effect of posture on regional gas exchange in pigs. *J Appl Physiol Bethesda Md 1985* 2004;**97**:2104–11. https://doi.org/10.1152/japplphysiol.00072.2004.
79 Gattinoni L, Taccone P, Carlesso E, Marini JJ. Prone position in acute respiratory distress syndrome. Rationale, indications, and limits. *Am J Respir Crit Care Med* 2013;**188**:1286–93. https://doi.org/10.1164/rccm.201308-1532CI.
80 Altemeier WA, McKinney S, Glenny RW. Fractal nature of regional ventilation distribution. *J Appl Physiol* 2000;**88**:1551–7. https://doi.org/10.1152/jappl.2000.88.5.1551.
81 Avants BB, Tustison NJ, Stauffer M, Song G, Wu B, Gee JC. The Insight ToolKit image registration framework. *Front Neuroinformatics* 2014;**8**:44. https://doi.org/10.3389/fninf.2014.00044.
82 Kaczka DW, Cao K, Christensen GE, Bates JHT, Simon BA. Analysis of Regional Mechanics in Canine Lung Injury Using Forced Oscillations and 3D Image Registration. *Ann Biomed Eng* 2011;**39**:1112–24. https://doi.org/10.1007/s10439-010-0214-0.

83 Reinhardt JM, Ding K, Cao K, Christensen GE, Hoffman EA, Bodas SV. Registration-based estimates of local lung tissue expansion compared to xenon CT measures of specific ventilation. *Med Image Anal* 2008;**12**:752–63. https://doi.org/10.1016/j.media.2008.03.007.
84 Xin Y, Cereda M, Hamedani H, Pourfathi M, Siddiqui S, Meeder N, Kadlecek S, Duncan I, Profka H, Rajaei J, Tustison NJ, Gee JC, Kavanagh BP, Rizi RR. Unstable Inflation Causing Injury. Insight from Prone Position and Paired Computed Tomography Scans. *Am J Respir Crit Care Med* 2018;**198**:197–207. https://doi.org/10.1164/rccm.201708-1728OC.
85 Christensen GE, Johnson HJ. Consistent image registration. *IEEE Trans Med Imaging* 2001;**20**:568–82. https://doi.org/10.1109/42.932742.
86 Wandtke JC, Hyde RW, Fahey PJ, Utell MJ, Plewes DB, Goske MJ, Fischer HW. Measurement of lung gas volume and regional density by computed tomography in dogs. *Invest Radiol* 1986;**21**:108–17. https://doi.org/10.1097/00004424-198602000-00005.
87 Ahmad A, Dey L. A k-mean clustering algorithm for mixed numeric and categorical data. *Data Knowl Eng* 2007;**63**:503–27. https://doi.org/10.1016/j.datak.2007.03.016.
88 Selvakumar J, Lakshmi A, Arivoli T. Brain Tumor Segmentation and Its Area Calculation in Brain MR Images Using K-Mean Clustering and Fuzzy C-Mean Algorithm. Presented at the IEEE-International Conference On Advances In Engineering, Science And Management (ICAESM -2012).
89 Ng P, Pun C-M. Skin Color Segmentation by Texture Feature Extraction and K-Mean Clustering. Presented at the 2011 Third International Conference on Computational Intelligence, Communication Systems and Networks.
90 Liu S, Margulies SS, Wilson TA. Deformation of the dog lung in the chest wall. *J Appl Physiol Bethesda Md 1985* 1990;**68**:1979–87. https://doi.org/10.1152/jappl.1990.68.5.1979.
91 Hoffman EA. Effect of body orientation on regional lung expansion: a computed tomographic approach. *J Appl Physiol Bethesda Md 1985* 1985;**59**:468–80. https://doi.org/10.1152/jappl.1985.59.2.468.
92 Lai-Fook SJ, Rodarte JR. Pleural pressure distribution and its relationship to lung volume and interstitial pressure. *J Appl Physiol Bethesda Md 1985* 1991;**70**:967–78. https://doi.org/10.1152/jappl.1991.70.3.967.
93 Krayer S, Rehder K, Vettermann J, Didier EP, Ritman EL. Position and motion of the human diaphragm during anesthesia-paralysis. *Anesthesiology* 1989;**70**:891–8. https://doi.org/10.1097/00000542-198906000-00002.
94 Mure M, Glenny RW, Domino KB, Hlastala MP. Pulmonary gas exchange improves in the prone position with abdominal distension. *Am J Respir Crit Care Med* 1998;**157**:1785–90. https://doi.org/10.1164/ajrccm.157.6.9711104.
95 Santini A, Protti A, Langer T, Comini B, Monti M, Sparacino CC, Dondossola D, Gattinoni L. Prone position ameliorates lung elastance and increases functional residual capacity independently from lung recruitment. *Intensive Care Med Exp* 2015;**3**:17. https://doi.org/10.1186/s40635-015-0055-0.
96 Albert RK, Leasa D, Sanderson M, Robertson HT, Hlastala MP. The prone position improves arterial oxygenation and reduces shunt in oleic-acid-induced acute lung injury. *Am Rev Respir Dis* 1987;**135**:628–33. https://doi.org/10.1164/arrd.1987.135.3.628.
97 Pelosi P, Tubiolo D, Mascheroni D, Vicardi P, Crotti S, Valenza F, Gattinoni L. Effects of the prone position on respiratory mechanics and gas exchange during acute lung injury. *Am J Respir Crit Care Med* 1998;**157**:387–93. https://doi.org/10.1164/ajrccm.157.2.97-04023.
98 Mancebo J, Fernández R, Blanch L, Rialp G, Gordo F, Ferrer M, Rodríguez F, Garro P, Ricart P, Vallverdú I, Gich I, Castaño J, Saura P, Domínguez G, Bonet A, Albert RK. A multicenter trial of prolonged prone ventilation in severe acute respiratory distress syndrome. *Am J Respir Crit Care Med* 2006;**173**:1233–9. https://doi.org/10.1164/rccm.200503-353OC.

99 Pelosi P, Bottino N, Chiumello D, Caironi P, Panigada M, Gamberoni C, Colombo G, Bigatello LM, Gattinoni L. Sigh in Supine and Prone Position during Acute Respiratory Distress Syndrome. *Am J Respir Crit Care Med* 2003;**167**:521–7. https://doi.org/10.1164/rccm.200203-198OC.
100 Kumaresan A, Gerber R, Mueller A, Loring SH, Talmor D. Effects of Prone Positioning on Transpulmonary Pressures and End-expiratory Volumes in Patients without Lung Disease. *Anesthesiol J Am Soc Anesthesiol* 2018;**128**:1187–92. https://doi.org/10.1097/ALN.0000000000002159.
101 Richard JC, Bregeon F, Costes N, Bars DL, Tourvieille C, Lavenne F, Janier M, Bourdin G, Gimenez G, Guerin C. Effects of prone position and positive end-expiratory pressure on lung perfusion and ventilation. *Crit Care Med* 2008;**36**:2373–80. https://doi.org/10.1097/CCM.0b013e31818094a9.
102 Goffi A, Kruisselbrink R, Volpicelli G. The sound of air: point-of-care lung ultrasound in perioperative medicine. *Can J Anaesth J Can Anesth* 2018;**65**:399–416. https://doi.org/10.1007/s12630-018-1062-x.
103 Gattinoni L, Bombino M, Pelosi P, Lissoni A, Pesenti A, Fumagalli R, Tagliabue M. Lung structure and function in different stages of severe adult respiratory distress syndrome. *JAMA* 1994;**271**:1772–9.
104 Matamis D, Lemaire F, Harf A, Brun-Buisson C, Ansquer JC, Atlan G. Total respiratory pressure-volume curves in the adult respiratory distress syndrome. *Chest* 1984;**86**:58–66. https://doi.org/10.1378/chest.86.1.58.
105 Guérin C, Beuret P, Constantin JM, Bellani G, Garcia-Olivares P, Roca O, Meertens JH, Maia PA, Becher T, Peterson J, Larsson A, Gurjar M, Hajjej Z, Kovari F, Assiri AH, Mainas E, Hasan MS, Morocho-Tutillo DR, Baboi L, Chrétien JM, François G, Ayzac L, Chen L, Brochard L, Mercat A, investigators of the APRONET Study Group, the REVA Network, the Réseau recherche de la Société Française d'Anesthésie-Réanimation (SFAR-recherche) and the ESICM Trials Group. A prospective international observational prevalence study on prone positioning of ARDS patients: the APRONET (ARDS Prone Position Network) study. *Intensive Care Med* 2018;**44**:22–37. https://doi.org/10.1007/s00134-017-4996-5.
106 Grasso S, Mascia L, Del Turco M, Malacarne P, Giunta F, Brochard L, Slutsky AS, Marco Ranieri V. Effects of recruiting maneuvers in patients with acute respiratory distress syndrome ventilated with protective ventilatory strategy. *Anesthesiology* 2002;**96**:795–802. https://doi.org/10.1097/00000542-200204000-00005.
107 Xin Y, Cereda M, Hamedani H, Martin KT, Tustison NJ, Pourfathi M, Kadlecek S, Siddiqui S, Amzajerdian F, Connell M, Abate N, Kajanaku A, Duncan I, Gee JC, Rizi RR. Positional Therapy and Regional Pulmonary Ventilation: High-resolution Alignment of Prone and Supine Computed Tomography Images in a Large Animal Model. *Anesthesiology* 2020;**133**:1093–105. https://doi.org/10.1097/ALN.0000000000003509.
108 Gerard SE, Herrmann J, Kaczka DW, Musch G, Fernandez-Bustamante A, Reinhardt JM. Multi-resolution convolutional neural networks for fully automated segmentation of acutely injured lungs in multiple species. *Med Image Anal* 2020;**60**:101592. https://doi.org/10.1016/j.media.2019.101592.
109 Patroniti N, Bellani G, Manfio A, Maggioni E, Giuffrida A, Foti G, Pesenti A. Lung volume in mechanically ventilated patients: measurement by simplified helium dilution compared to quantitative CT scan. *Intensive Care Med* 2004;**30**:282–9. https://doi.org/10.1007/s00134-003-2109-0.
110 Fukuda Y, Ishizaki M, Masuda Y, Kimura G, Kawanami O, Masugi Y. The role of intraalveolar fibrosis in the process of pulmonary structural remodeling in patients with diffuse alveolar damage. *Am J Pathol* 1987;**126**:171–82.

111 Costa EL, Lima RG, Amato MB. Electrical impedance tomography. *Curr Opin Crit Care* 2009;**15**:18–24. https://doi.org/10.1097/MCC.0b013e3283220e8c.
112 *Introduction to Mixed Modelling: Beyond Regression and Analysis of Variance | Wiley*. Wiley.Com. n.d. URL: https://www.wiley.com/en-us/Introduction+to+Mixed+Modelling%3A+Beyond+Regression+and+Analysis+of+Variance-p-9780470035962 (Accessed 13 October 2020).
113 Bates D, Mächler M, Bolker B, Walker S. Fitting Linear Mixed-Effects Models Using lme4. *J Stat Softw* 2015;**67**:1–48. https://doi.org/10.18637/jss.v067.i01.
114 Allen GB, Leclair T, Cloutier M, Thompson-Figueroa J, Bates JHT. The response to recruitment worsens with progression of lung injury and fibrin accumulation in a mouse model of acid aspiration. *Am J Physiol-Lung Cell Mol Physiol* 2007;**292**:L1580–9. https://doi.org/10.1152/ajplung.00483.2006.
115 Protti A, Chiumello D, Cressoni M, Carlesso E, Mietto C, Berto V, Lazzerini M, Quintel M, Gattinoni L. Relationship between gas exchange response to prone position and lung recruitability during acute respiratory failure. *Intensive Care Med* 2009;**35**:1011–7. https://doi.org/10.1007/s00134-009-1411-x.
116 Gattinoni L, Vagginelli F, Carlesso E, Taccone P, Conte V, Chiumello D, Valenza F, Caironi P, Pesenti A, Prone-Supine Study Group. Decrease in PaCO2 with prone position is predictive of improved outcome in acute respiratory distress syndrome. *Crit Care Med* 2003;**31**:2727–33. https://doi.org/10.1097/01.CCM.0000098032.34052.F9.
117 Musch G, Harris RS, Vidal Melo MF, O'Neill KR, Layfield JDH, Winkler T, Venegas JG. Mechanism by Which a Sustained Inflation Can Worsen Oxygenation in Acute Lung Injury. *Anesthesiology* 2004;**100**:323–30. https://doi.org/10.1097/00000542-200402000-00022.
118 Chesnutt AN, Matthay MA, Tibayan FA, Clark JG. Early detection of type III procollagen peptide in acute lung injury. Pathogenetic and prognostic significance. *Am J Respir Crit Care Med* 1997;**156**:840–5. https://doi.org/10.1164/ajrccm.156.3.9701124.
119 Curley GF, Contreras M, Higgins B, O'Kane C, McAuley DF, O'Toole D, Laffey JG. Evolution of the Inflammatory and Fibroproliferative Responses during Resolution and Repair after Ventilator-induced Lung Injury in the Rat. *Anesthesiology* 2011;**115**:1022–32. https://doi.org/10.1097/ALN.0b013e31823422c9.
120 Gaver DP, Nieman GF, Gatto LA, Cereda M, Habashi NM, Bates JHT. The POOR Get POORer: A Hypothesis for the Pathogenesis of Ventilator-induced Lung Injury. *Am J Respir Crit Care Med* 2020;**202**:1081–7. https://doi.org/10.1164/rccm.202002-0453CP.
121 Li X, Scales DC, Kavanagh BP. Unproven and Expensive before Proven and Cheap: Extracorporeal Membrane Oxygenation versus Prone Position in Acute Respiratory Distress Syndrome. *Am J Respir Crit Care Med* 2018;**197**:991–3. https://doi.org/10.1164/rccm.201711-2216CP.
122 Klaiman T, Silvestri JA, Srinivasan T, Szymanski S, Tran T, Oredeko F, Sjoding MW, Fuchs BD, Maillie S, Jablonski J, Lane-Fall MB, Kerlin MP. Improving Prone Positioning for Severe Acute Respiratory Distress Syndrome during the COVID-19 Pandemic. An Implementation-Mapping Approach. *Ann Am Thorac Soc* 2021;**18**:300–7. https://doi.org/10.1513/AnnalsATS.202005-571OC.
123 De Jong A, Molinari N, Sebbane M, Prades A, Futier E, Jung B, Chanques G, Jaber S. Feasibility and effectiveness of prone position in morbidly obese patients with ARDS: a case-control clinical study. *Chest* 2013;**143**:1554–61. https://doi.org/10.1378/chest.12-2115.
124 Grasselli G, Pesenti A, Cecconi M. Critical Care Utilization for the COVID-19 Outbreak in Lombardy, Italy: Early Experience and Forecast During an Emergency Response. *JAMA* 2020;**323**:1545. https://doi.org/10.1001/jama.2020.4031.

125 Ball L, Robba C, Maiello L, Herrmann J, Gerard SE, Xin Y, Battaglini D, Brunetti I, Minetti G, Seitun S, Vena A, Giacobbe DR, Bassetti M, Rocco PRM, Cereda M, Castellan L, Patroniti N, Pelosi P, Ball L, Robba C, Maiello L, Battaglini D, Brunetti I, Minetti G, Seitun S, Vena A, Giacobbe DR, Bassetti M, Castellan L, Patroniti N, *et al.* Computed tomography assessment of PEEP-induced alveolar recruitment in patients with severe COVID-19 pneumonia. *Crit Care* 2021;**25**:81. https://doi.org/10.1186/s13054-021-03477-w.
126 Huppert LA, Matthay MA, Ware LB. Pathogenesis of Acute Respiratory Distress Syndrome. *Semin Respir Crit Care Med* 2019;**40**:31–9. https://doi.org/10.1055/s-0039-1683996.
127 West JB. Invited review: pulmonary capillary stress failure. *J Appl Physiol Bethesda Md 1985* 2000;**89**:2483-2489;discussion 2497. https://doi.org/10.1152/jappl.2000.89.6.2483.
128 Gattinoni L, Pesenti A. The concept of 'baby lung'. *Intensive Care Med* 2005;**31**:776–84. https://doi.org/10.1007/s00134-005-2627-z.
129 Rix U, Hantschel O, Dürnberger G, Remsing Rix LL, Planyavsky M, Fernbach NV, Kaupe I, Bennett KL, Valent P, Colinge J, Köcher T, Superti-Furga G. Chemical proteomic profiles of the BCR-ABL inhibitors imatinib, nilotinib, and dasatinib reveal novel kinase and nonkinase targets. *Blood* 2007;**110**:4055–63. https://doi.org/10.1182/blood-2007-07-102061.
130 Waller CF. Imatinib mesylate. *Recent Results Cancer Res Fortschritte Krebsforsch Progres Dans Rech Sur Cancer* 2010;**184**:3–20. https://doi.org/10.1007/978-3-642-01222-8_1.
131 Stephens RS, Johnston L, Servinsky L, Kim BS, Damarla M. The tyrosine kinase inhibitor imatinib prevents lung injury and death after intravenous LPS in mice. *Physiol Rep* 2015;**3**:. https://doi.org/10.14814/phy2.12589.
132 Wolf AM, Wolf D, Rumpold H, Ludwiczek S, Enrich B, Gastl G, Weiss G, Tilg H. The kinase inhibitor imatinib mesylate inhibits TNF-{alpha} production in vitro and prevents TNF-dependent acute hepatic inflammation. *Proc Natl Acad Sci U S A* 2005;**102**:13622–7. https://doi.org/10.1073/pnas.0501758102.
133 Matute-Bello G, Frevert CW, Martin TR. Animal models of acute lung injury. *Am J Physiol - Lung Cell Mol Physiol* 2008;**295**:L379–99. https://doi.org/10.1152/ajplung.00010.2008.
134 Letsiou E, Rizzo AN, Sammani S, Naureckas P, Jacobson JR, Garcia JGN, Dudek SM. Differential and opposing effects of imatinib on LPS- and ventilator-induced lung injury. *Am J Physiol-Lung Cell Mol Physiol* 2014;**308**:L259–69. https://doi.org/10.1152/ajplung.00323.2014.
135 Matthay MA, McAuley DF, Ware LB. Clinical trials in acute respiratory distress syndrome: challenges and opportunities. *Lancet Respir Med* 2017;**5**:524–34. https://doi.org/10.1016/S2213-2600(17)30188-1.
136 Beitler JR, Thompson BT, Baron RM, Bastarache JA, Denlinger LC, Esserman L, Gong MN, LaVange LM, Lewis RJ, Marshall JC, Martin TR, McAuley DF, Meyer NJ, Moss M, Reineck LA, Rubin E, Schmidt EP, Standiford TJ, Ware LB, Wong HR, Aggarwal NR, Calfee CS. Advancing precision medicine for acute respiratory distress syndrome. *Lancet Respir Med* 2021. https://doi.org/10.1016/S2213-2600(21)00157-0.
137 Horie S, McNicholas B, Rezoagli E, Pham T, Curley G, McAuley D, O'Kane C, Nichol A, dos Santos C, Rocco PRM, Bellani G, Laffey JG. Emerging pharmacological therapies for ARDS: COVID-19 and beyond. *Intensive Care Med* 2020;**46**:2265–83. https://doi.org/10.1007/s00134-020-06141-z.
138 Xin Y, Cereda M, Martin K t., Humayun S, Duncan I, Profka H, Kadlecek S, Rizi R r. Tyrosine Kinase Inhibitor Imatinib Alleviates the Progression of Ventilator-Induced Lung Injury. *TP4 TP004 ARDS SEPSIS Transplant. Mech. Stud.* American Thoracic Society; 2021. p. A1301–A1301.
139 Pourfathi M, Xin Y, Rosalino M, Cereda M, Kadlecek S, Duncan I, Profka H, Hamedani H, Siddiqui S, Ruppert K, Chatterjee S, Rizi RR. Pulmonary pyruvate metabolism as an index of

inflammation and injury in a rat model of acute respiratory distress syndrome. *NMR Biomed* 2020;**33**:e4380. https://doi.org/10.1002/nbm.4380.
140 Efron B. Logistic Regression, Survival Analysis, and the Kaplan-Meier Curve. *J Am Stat Assoc* 1988;**83**:414–25. https://doi.org/10.1080/01621459.1988.10478612.
141 Dudek SM, Chiang ET, Camp SM, Guo Y, Zhao J, Brown ME, Singleton PA, Wang L, Desai A, Arce FT, Lal R, Van Eyk JE, Imam SZ, Garcia JGN. Abl Tyrosine Kinase Phosphorylates Nonmuscle Myosin Light Chain Kinase to Regulate Endothelial Barrier Function. *Mol Biol Cell* 2010;**21**:4042–56. https://doi.org/10.1091/mbc.e09-10-0876.
142 Henzler D, Hochhausen N, Chankalal R, Xu Z, Whynot SC, Slutsky AS, Zhang H. Physiologic and Biologic Characteristics of Three Experimental Models of Acute Lung Injury in Rats. *Anesth Analg* 2011;**112**:1139–46. https://doi.org/10.1213/ANE.0b013e3182104dac.
143 Glassman PM, Myerson JW, Ferguson LT, Kiseleva RY, Shuvaev VV, Brenner JS, Muzykantov VR. Targeting drug delivery in the vascular system: Focus on endothelium. *Adv Drug Deliv Rev* 2020;**157**:96–117. https://doi.org/10.1016/j.addr.2020.06.013.
144 *A Study to Investigate the Effects of Imatinib on Pulmonary Vascular Dysfunction in a Human Model of Lung Injury - Full Text View - ClinicalTrials.gov*. n.d. URL: https://clinicaltrials.gov/ct2/show/NCT03328117 (Accessed 6 November 2019).
145 Aman DJ. *A Randomised, Double-blind, Placebo-controlled Study to Investigate the Safety and Efficacy of Intravenous Imatinib Mesylate (Impentri®) in Subjects With Acute Respiratory Distress Syndrome Induced by COVID-19*. clinicaltrials.gov; 2021.
146 *Randomized Double-Blind Placebo-Controlled Trial on the Safety and Efficacy of Imatinib for Hospitalized Adults With COVID-19*. clinicaltrials.gov; 2020.
147 Alexandria University. *Imatinib for the Treatment of SARS-COV-2 Induced Pneumonia: A Pilot Study*. clinicaltrials.gov; 2020.
148 Fuld MK, Halaweish AF, Haynes SE, Divekar AA, Guo J, Hoffman EA. Pulmonary perfused blood volume with dual-energy CT as surrogate for pulmonary perfusion assessed with dynamic multidetector CT. *Radiology* 2013;**267**:747–56.
149 Kay FU, Beraldo MA, Nakamura MAM, De Santis Santiago R, Torsani V, Gomes S, Roldan R, Tucci MR, Abbara S, Amato MBP, Amaro E. Quantitative Dual-Energy Computed Tomography Predicts Regional Perfusion Heterogeneity in a Model of Acute Lung Injury: *J Comput Assist Tomogr* 2018;**42**:866–72. https://doi.org/10.1097/RCT.0000000000000815.
150 Patel BV, Arachchillage DJ, Ridge CA, Bianchi P, Doyle JF, Garfield B, Ledot S, Morgan C, Passariello M, Price S, Singh S, Thakuria L, Trenfield S, Trimlett R, Weaver C, Wort SJ, Xu T, Padley SPG, Devaraj A, Desai SR. Pulmonary Angiopathy in Severe COVID-19: Physiologic, Imaging, and Hematologic Observations. *Am J Respir Crit Care Med* 2020;**202**:690–9. https://doi.org/10.1164/rccm.202004-1412OC.
151 Laubach VE, Sharma AK. Mechanisms of Lung Ischemia-Reperfusion Injury. *Curr Opin Organ Transplant* 2016;**21**:246–52. https://doi.org/10.1097/MOT.0000000000000304.
152 den Hengst WA, Gielis JF, Lin JY, Van Schil PE, De Windt LJ, Moens AL. Lung ischemia-reperfusion injury: a molecular and clinical view on a complex pathophysiological process. *Am J Physiol Heart Circ Physiol* 2010;**299**:H1283-1299. https://doi.org/10.1152/ajpheart.00251.2010.
153 Porteous MK, Diamond JM, Christie JD. Primary graft dysfunction: lessons learned about the first 72 hours after lung transplantation. *Curr Opin Organ Transplant* 2015;**20**:506–14. https://doi.org/10.1097/MOT.0000000000000232.
154 Tanaka S, Chen-Yoshikawa TF, Kajiwara M, Menju T, Ohata K, Takahashi M, Kondo T, Hijiya K, Motoyama H, Aoyama A, Masuda S, Date H. Protective Effects of Imatinib on

Ischemia/Reperfusion Injury in Rat Lung. *Ann Thorac Surg* 2016;**102**:1717–24. https://doi.org/10.1016/j.athoracsur.2016.05.037.
155 Magruder JT, Grimm JC, Crawford TC, Johnston L, Santhanam L, Stephens RS, Berkowitz DE, Shah AS, Bush EL, Damarla M, Damico RL, Hassoun PM, Kim BS. Imatinib Is Protective Against Ischemia-Reperfusion Injury in an Ex Vivo Rabbit Model of Lung Injury. *Ann Thorac Surg* 2018;**105**:950–6. https://doi.org/10.1016/j.athoracsur.2017.10.002.